Artur Rafael Servo Nunes Duarte Saramago

Licenciado em Ciências da Engenharia Química e Bioquímica

Tablets Manufacturing – Direct Scale-up from Lab to Manufacturing facilities

Dissertação para obtenção do Grau de Mestre em Engenharia Química e Bioquímica, pela Universidade Nova de Lisboa, Faculdade de Ciências e Tecnologia

Orientador: Cláudia Consuelo Vieira Reis Leite Moura
Senior Scientist, Hovione Farmaciencia SA

Co-orientador: Ana Isabel Nobre Martins Aguiar de Oliveira Ricardo
Professora Catedrática, Departamento de Química, FCT NOVA

Júri

Presidente: Rui Manuel Freitas Oliveira, Professor Associado com Agregação, Departamento de Química, FCT NOVA

Arguente: Mário Fernando José Eusébio, Professor Auxiliar, Departamento de Química, FCT NOVA

Vogal: Cláudia Consuelo Vieira Reis Leite Moura, Senior Scientist, Hovione Farmaciencia SA

FACULDADE DE CIÊNCIAS E TECNOLOGIA
UNIVERSIDADE NOVA DE LISBOA

Dezembro, 2020

Tablets Manufacturing – Direct Scale-up from Lab to Manufacturing facilities

“There will be obstacles. There will be doubters. There will be mistakes. But with hard work, there are no limits.”

-MP

Acknowledgements

First, I would like to thank Hovione for providing me this opportunity and also all the scientific environment needed to accomplish this journey. I want to express my special admiration for my mentor in this journey, Cláudia Moura, who always provided me the tools for a sense of scientific and critical thinking. To professor doctor Ana Aguiar Ricardo, for providing me guidelines at the light of her continuous experience in teaching.

A huge thank you to all the people that were directly involved in my work, and gave me the necessary equipment tutorials to proceed with my work plan, Calixto, Pedro and Miguel. A special mention to the other laboratory technicians who shared their experience, know-how and good manufacturing practices with me, André, Ricardo, Eloy and Norberto. To all of the scientists who came across my pathway and inspired me to look from other perspectives to my work. Also, to all of the Master and PhD students that helped me during my period at the lab.

To FCT – UNL, for building into me the necessary knowledge to face this challenge and all the teachers that captivated me from their distinct way of teaching and inspired me to always think one step further.

I want to thank my father, mother and brother, for always believing in my potential, for all the sacrifices they made for me and for always instilling me the best values.

An extraordinary thank you to Rute, for her love and unstoppably & continuous support throughout the last three years, not only during this journey but also for bringing out the best version in me. Although she went through the same challenge, remained always supportive through her love and attention.

I would like to leave a special mention to Diogo, for instill me the taste for swimming and being also one of my biggest references when it comes to life decisions and personal growth. Also to my roommates during my academic life, that were always there to take me a good laugh every day, Hugo, Mário and Fábio.

Thank you to all my childhood friends, Carolina, Teresa and especially to Esteves who although not present in body but always mentally accompanies me. To all my long lasting school friendships, Afonso, Bea, Bia, Carolina, Cláudia, Delfim, Floris, Herberto, Inês, Joe, Kika, Maria, Mariana, Rosarinho and Rita.

A word of appreciation for all the swim coaches that I had the pleasure to grew up and learn from, António, Ana, Bruno, Catarina and specially Tiago to continuously writing me swimming and conditioning plans so that I kept myself active throughout my academic life. I want to also thank my swim mates, especially Bruno, Duarte, Hugo, João Pedro, João Carlos, Lonh, Miguel, Tomás and Zé.

Abstract

HPMCAS and PVPVA, typically selected polymers for amorphous solid dispersions (ASD) production, were incorporated into a standard dry granulation formulation. The solid dispersions were manufactured via spray drying (SD), followed by intragranular blending, roller compaction (RC) (compaction and milling) (MF) or slugging and milling (LAB), extragranular blending, and tableting. The goal was establish a lean scale-up methodology by comparing materials from different process routes.

An RC model, based on Johanson's rolling theory, for predicting the intragranular phase solid fraction (SF) at gap, was validated and calibrated from compaction simulator data. By comparing these predictions with SF at gap estimations via throughput from each trial, the average deviation was 8.0%.

Using different toolings and dwell time, the Lab slugging was not able to mimic the manufacturing facilities (MF) ribbons elastic recovery. Even when using historical project data with lower SD dispersion load.

The milling step was successfully simulated obtaining granules with similar size distributions from different sites. Concerning, RC parameters, at higher force and tighter gap larger granules were obtained due to higher at gap SF, also, MF granules presented a higher fine content which may owe to fines bypassing the gap. Using average Hausner Ratio from different process routes as flowability metric, the granules yielded results within dry granulation flowability categories (1.25 and 1.34 for PVPVA and HPMCAS, respectively).

Tableting profiles were generated and regardless of the RC parameters, PVPVA tablets, showed better tableting characteristics and 2.3 times less elastic recovery, comparing to HPMCAS. Specifically, for RC force 5 kN/cm and gap 3 mm, MF, Lab plus MF and Lab tablets, yielded Tensile Strength (TS) at 100 MPa equal to 4.09; 3.59; 3.97 for PVPVA and 1.40; 1.46; for HPMCAS; and TS at SF of 0.80 equal to 2.32; 2.04; 2.00 for PVPVA and 1.32, 1.31 for HPMCAS.

Keywords: Roller Compaction; Dry Granulation scale-up; Tableting; Amorphous Solid Dispersions

Resumo

Incorporou-se HPMCAS e PVPVA, polímeros tipicamente selecionados para a produção de dispersões sólidas por *spray drying* (SDD), numa formulação padrão de *dry granulation*. Estas SDD foram fabricadas via spray *drying* (SD), seguido de mistura intragranular, *roller compaction* (RC) (compactação e granulação) ou *slugging* e granulação (LAB), mistura extragranular e *tableting*. O objetivo foi estabelecer uma metodologia económica de *scale-up*, comparando materiais de diferentes vias processuais.

Um modelo RC, baseado na teoria de Johanson, para prever a *Solid Fraction (SF) at gap*, foi validado, calibrado com dados do simulador de compactação. Comparando esimativas de *Solid Fraction (SF) at gap* através do rendimento de cada trial com as previsões do modelo, obteve-se um desvio médio de 8,0%.

Variando o jogo de punções e tempo de compactação, a etapa de *slugging* em laboratório não reproduziu a expansão elástica das *ribbons* da fábrica (MF), mesmo utilizando dados históricos de projeto com carga de dispersão SD mais baixa.

Em relação à granulação, a etapa foi simulada com sucesso, obtendo-se grânulos com distribuições de tamanho semelhantes, nas diferentes vias processuais. No que concerne os parâmetros RC, uma força maior e fresta mais estreita foram obtidos grânulos maiores devido ao maior na folga SF. Adicionalmente, os grânulos da fábrica apresentaram um maior teor em finos que pode ser devido a fugas através da fresta. Usando *Hausner Ratio* médio, como métrica de escoamento, e comparando diferentes vias processuais, obteve-se, para os grânulos, resultados dentro de categorias de escoamento para *dry granulation* (1,25 e 1,34 para PVPVA e HPMCAS, respectivamente).

Gerou-se os perfis de *tableting* e, independentemente dos parâmetros de RC, os comprimidos de PVPVA apresentaram melhores características de compactação e 2,3 vezes menos recuperação elástica, em comparação com HPMCAS. Especificamente, para força a 5 kN/cm e fresta de 3 mm durante RC, MF, Lab mais MF e Lab, resultou numa *Tensile Strength* (TS) a 100 MPa de 4,09; 3,59; 3,97 para PVPVA e 1,40; 1,46; para HPMCAS; e TS (a SF de 0,80) igual a 2,32; 2.04; 2,00 para PVPVA e 1,32, 1,31 para HPMCAS.

Palavras-chave: Compactação por Rolos; Escalonamento de granulação seca; Produção de comprimidos; Dispersões Sólidas Amorfas

List of Contents

List of Figures

List of Tables

List of Acronyms

API	Active Pharmaceutical Ingredient
ASD	Amorphous Solid Dispersion
CTC	Compressibility Tabletability Compactability
DG	Dry Granulation
DoE	Design of experiments
FFC	Flow Function Coefficient
GMP	Good Manufacturing Practices
HPMCAS	HydroxyPropyl MethylCellulose Acetate Succinate
MF	Manufacturing Facilities
PSD	Particle Size Distribution
PVPVA	PolyVinylPyrrolidone-Vinyl Acetate Copolymer
RC	Roller Compaction
SCF	Specific Compaction Force
SD	Spray Drying
SDD	Spray Dried Dispersion
SEM	Scanning Electron Microscopy
SF	Solid Fraction
SF in die	Solid Fraction during compaction simulator compression
SF out of die	Solid Fraction after compaction simulator and tablets/slugs being allowed to expand
SF at gap	Solid Fraction during Roller Compactor compression
SF out of gap	Solid Fraction after Roller Compaction and ribbons being allowed to expand
SF F=0	Solid Fraction calculated when the force from the punches is released

TS	Tensile Strength
USP	United States Pharmacopoeia
WG	Wet Granulation

1

Introduction

1.1. Motivation

The present work aims to have a lean material sparing approach for laboratory development to enable a direct scale-up of the blending, Roller Compaction (RC) and tableting steps to the manufacturing facilities (MF). This methodology will expedite the process development and scale-up to the MF and increase the right-first time batches requiring minimal/no trials at lab scale expanding the MF building availability for other incoming projects, while reducing costs, materials and time that are specially critical in early-stage programs. The main goal was to assess the scalability of traditional laboratory slugging and milling steps (LAB), versus dry granulation (by RC at MF) and propose a lean scale-up methodology. These steps were therefore, further studied.

1.2. Thesis outline

This thesis is divided into four chapters. The first chapter includes a theoretical background covering the main topics in dry granulation and tableting as well as the main achievements in scale-up from LAB to RC state of the art.

Chapter two covers all the selected materials and employed methods throughout this work.

Chapter three covers all the results and discussion grouped in different studies developed with this thesis. Figure 1.1 is a schematic representation of the different workflows and studies performed. Each arrow color represents an independent workflow tableting route while the arrow outline color, when applicable, describes which study belongs to that steps.

Study 1: RC model validation – The aim of this study was to validate the RC model developed at Hovione[1]. This consists in using in die intragranular blend data obtained at the laboratory compaction simulator STYL'One NANO by MedelPharm. The RC model was calibrated for both formulations (PVPVA and HPMCAS. By taking the intra-blend's properties at the lab, (tensile strengths, compaction pressures and in die densities) and specifying the RC design parameters to be used at scale (Rolls width, diameter and speed) the model was calibrated and able to predict, through Johanson model, the mass flow rate and ribbon SF at gap for specific RC forces and gap between rolls.

Study 2: Slugging conditions and tooling assessment – What tooling and compaction conditions should be adopted in lab to produce ribbon-representative slugs? This stage consisted in slugging using different toolings and dwell times to understand how they can impact the slugs elastic recovery from the compaction simulator, to assess which tooling and conditions mimic (if any) the ribbons elastic recovery obtained from MF.

Study 3: Milling assessment – How are the granules' properties (particle size distribution, bulk and tap density) affected by the RC/slugging parameters and milling process? The goal was to benchmark the milling step conducted at MF and Lab by selecting different conditions and assessing the impact on the granules size distribution and flowability.

Study 4: Tableting RC parameters impact – How RC and milling affects the tableting profiles? The tablets compactability, tabletability and compressibility (CTC) profiles from the different process routes and conditions are compared.

Study 5: Pilot-scale tableting process capability – Study of the feeding and turret speed parameters on the pilot-scale rotary press to understand the operational space while maximizing throughput, as well as to compare the tablets compactability profile obtained at MF versus Lab.

The fourth chapter presents all the conclusions and future work considered important.

At the end of this thesis, the appendixes found necessary to supplement all the work and data generated.

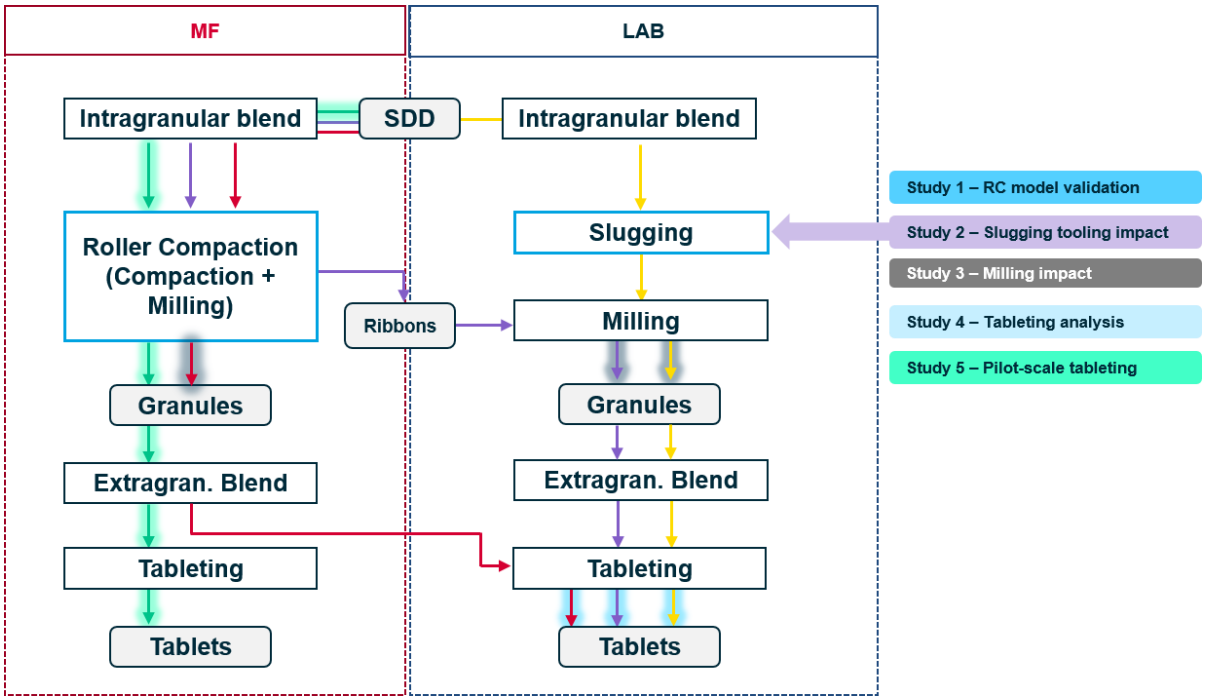

Figure 1.1 – Schematic representation of the workflow routes (arrows fill) and studies performed (arrows outline).

1.3. Thesis Background – Oral dosage forms

Nowadays, tablets are the preferred choice when it comes to oral drug delivery dosage forms, representing, approximately, 39% of the new therapeutic approvals by FDA, in 2019.[2] This may be explained by their ease of administration, patient compliance, good drug content uniformity (CU) and improved bioavailability, when compared to other dosage forms.[3] Additionally, oral dosage forms alone (here counted as tablets and capsules), represented approximately half of the new drug approvals in the last three years (Figure 1.2).

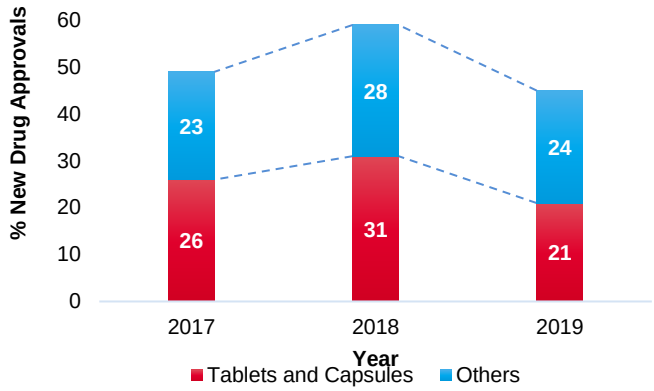

Figure 1.2 - New Drug Approvals. [2][4][5]

Orally administered dosage forms often face solubility issues concerning gastrointestinal (GI) absorption of drug content. In data up to 2016, class II (poor solubility, high permeability) of the Biopharmaceutics Classification System (BCS) represented 30% of the marketed products. It is also estimated that, currently, 70-90% of the drugs in the pipeline display solubility issues.[6] This owes to larger average molecular weights, higher melting temperatures and the fact that potential therapeutic candidates are chosen based on their ability to bind to cell receptors, often involving hydrophobic interactions, which makes lipophilic drugs mostly adopted for development.[7][8]

The main approaches to improve solubility, are chemical modifications (e.g., formation of salts)[9], physical modifications (cyclodextrin complexation[10], self-emulsifying drug delivery systems[11], nanocrystals[12], cocrystals[13]), manufacture of amorphous or polymorphic forms of drug[14] and amorphous solid dispersions (ASD) [8][15].

1.3.1. Solubility enhancement via ASD

ASD have been gaining more attention over the years since at the amorphous state there is no energy requirement to break the crystal lattice structure, allowing the API (Active Pharmaceutical Ingredient) molecules to interact with solvent and thus becoming solubilized.[16] Nevertheless, the amorphous form is a metastable state, meaning that the drug will recrystallize over time (Figure 1.3), so the challenge will be sustaining the amorphous state as long as possible. With API-Polymer systems as ASD, recrystallization is delayed by surrounding the API within a polymeric matrix, reducing its molecular mobility and hence inhibiting the nucleation and crystal growth rates.

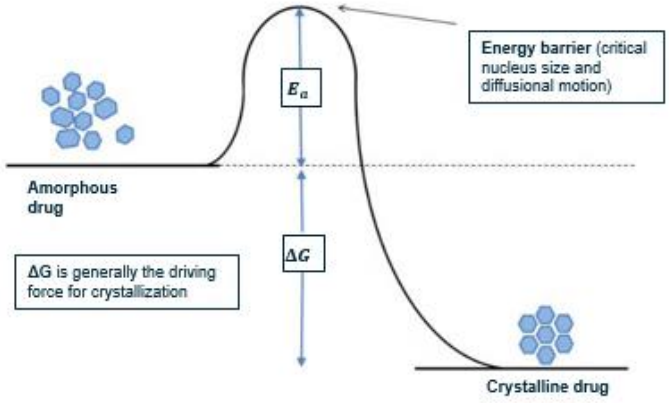

Figure 1.3 – Amorphous to crystalline form transition. Adapted from [8].

Compared to the amorphous drug alone, the addition of a polymer will provide a more stable phase, through drug-polymer inter-molecular interactions (e.g. hydrogen bonding), reduced drug's mobility and chemical potential and providing physical barriers to the recrystallization process (local viscosity). This stabilization will allow for longer periods of storage without the occurrence of recrystallization.[8][16].

1.3.1.1. *The spring and parachute effect*

Forming an ASD brings an unstable supersaturated solution, since the API is in its amorphous form – the spring – and sustains super saturation by stabilization from the polymer – the parachute – which will prevent solvent-mediated crystallization during the period available for absorption in the gastrointestinal lumen and thus drug's bioavailability is maximized (*i.e.* the fraction of the oral administered drug that reaches the circulatory system), with recrystallization predominantly occurring only after permeation through the intestinal mucosa.[17]

1.3.2. **ASDs Manufacturing**

Energy must be provided for the crystalline-to-amorphous transition to occur. ASD are mainly manufactured by melting or solvent evaporation based processes, typically Hot Melt Extrusion (HME) or Spray Drying (SD), respectively. Both are well established continuous processes among the pharmaceutical industry.[16][18][19] To select a suitable technique, insight is needed on API properties. One key aspect, in both processes is an additional downstream step. This will be a milling/pelletization and a secondary drying, for HME and SD, respectively.[18] Most importantly, both processes are scalable.[8]

1.3.2.1. ***Spray Drying***

Although SD technology is widely used nowadays in the pharmaceutical industry, it was first mentioned in 1872 for the food industry. Currently, this technology is employed in diverse industries such as food industry (e.g. coffee, milk); cosmetics (e.g. face powder, lipsticks), textiles (e.g. dyestuffs), ceramics, polymers and the pharmaceutical industry.[20][21]

In the pharmaceutical framework, SD has been widely explored as the main particle engineering technology or even as a complementary drying technology for powders manufacturing. Applications for spray dried dispersions (SDD) include oral dosages forms, through ASDs or coated nanoparticles for API bioavailability enhancement (aspirin, paracetamol, vitamins, supplements and antibiotics), and inhalation due to the ability of producing fine particles.[20]

Spray drying consists in the drying of a liquid feedstock which can be a solution, suspension, emulsion, or paste, containing low to high solids content. The feed is delivered by pumping and then dispersed through an atomizer (nozzle) that disperses the liquid into small droplets [55]. In the drying chamber, the generated droplets contact with a hot gas stream, leading to solvent evaporation, under controlled conditions. The formed particles are then carried by the drying gas and collected in a cyclone [55]. Figure 1.4 presents a schematic diagram of a standard SD apparatus and the main process parameters.

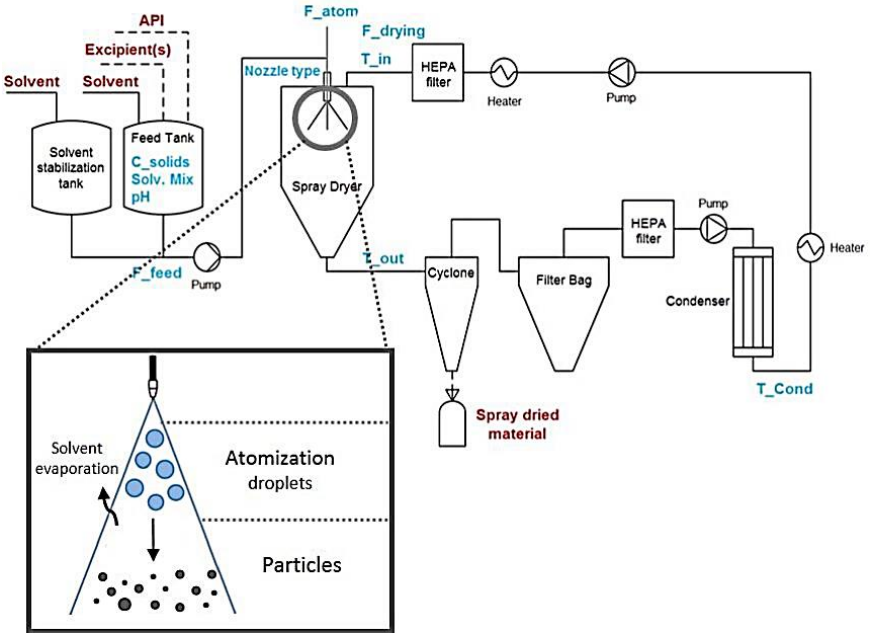

Figure 1.4 –Schematic diagram of a standard SD apparatus and the main process parameters.

Process parameters are challenged to meet the final product properties such as particle size distribution (PSD), bulk density, morphology and residual water and solvents' content. [22][23][24] SD possesses a fast-drying capability, as consequence of high surface area droplets which enables drying of some thermolabile drugs as a result of its short exposure period to high processing temperatures denominated evaporative cooling.[25] Also, it enables the control of particle size and density. The drawback may be the need to find a volatile organic solvent in which the API and the polymer, in case of an ASD, must be soluble and stable.[18][19] The main advantages are summarized in Table 1.1.

The SD process can be carried out in a closed or open cycle, by recirculating or not the drying gas, respectively, which should be assessed according to the required scale.

Another important factor linked to some of the critical process variables is the nozzle type. Typically, the main commercial nozzles available are: two-fluid (internal or external mixing)[26], pressure, rotary and ultrasonic. [22][27]

Table 1.1 – Spray Drying main process advantages and disadvantages.[19]

Main Advantages	Disadvantages
• Single step and rapid process; • Simple operation; • Able to operate in continuous mode; • Easily scalable: methodology and equipment available; • Flexible process: fine control over powder / particle properties: PS, morphology, density, residual moisture/solvents content; • Suitable for the production of crystalline or amorphous materials; • Production of micro and nanoparticles. • Able to produce thermolabile and sensitive molecules (e.g. proteins); • Wide variety of nozzles available with different operating principles (pneumatic, pressure, rotary, and ultrasonic); • Safe; • High process yield; • Well established in the Pharmaceutical Industry; • Know-how: fundamental operating principles of the particle formation well understood; • Spray dried commercial products available on the market.	• Use of solvents (post-processing may be required); • High energy process - expensive • Amorphous content may be undesirable • Thermal stress for some biomolecules (required to evaporate solvents); • Mechanical / shear stress (nozzle): may not be suitable for some sensitive biomolecules. • Low density materials that result in poor flowability.

1.3.3. Excipients

Besides surrounding the API for ASD manufacturing, as discussed above in section 1.3.2 the polymer also plays an important role by improving bioavailability or providing mechanical properties to the formulation, such as acting like a binder or/and a filler. For the effect, some of the most used stabilizing polymers are vinyl-pyrrolidone-based polymers that include poly (vinyl

pyrrolidone) (PVP) and poly (vinyl pyrrolidone)-poly (vinyl acetate) copolymer (PVPVA); cellulose-based polymers such as hydroxypropyl methylcellulose (HPMC) and hydroxyl propyl methylcellulose acetate-succinate (HPMCAS); and polymers that contain acidic groups ionizable only at high pH, targeting the small intestine, such as methacrylate-based enteric coating polymer systems (Eudragits)[8], [16][19].

Spray dried HPMCAS polymer and PVPVA copolymer were used in this thesis which are representative of typical ASDs spray dried powders. HPMCAS, is an enteric polymer with different available grades, according to the pH range at which it dissolves (L – low, M – medium or H – high) and to its predominant particle size (F – cohesive fine powder or G – free flowing granules).[28] PVPVA copolymer is non-enteric, also used as a tablet binder, and as part of the matrix used in controlled-release formulations. It provides good adhesion, elasticity, and hardness, and can be used as a moisture barrier.[28]

Other than the polymer selected for ASD manufacturing, excipients play specific roles in a tablet formulation whether by improving flowability (glidant), reducing sticking to material (lubricant), promoting particle disaggregation and/or swelling when in contact with water (disintegrant), holding the formulation together (binder) or increasing the bulk density in order to provide a practical size for powder compression (filler). The right formulation will enable to target the desired tablets physical performance such as its friability, disintegration time, dissolution time and its bioavailability as a drug delivery system.[29] These are critical aspects when manufacturing tablets from ASD. Table 1.2 presents the typical range for the particular excipients selected in this thesis. Among each of these excipients class there are a wide range of available grades.

Table 1.2 – Recommended excipients range.[28][30]

Excipient	Role	Recommended range % (w/w)	Working principle
Microcrystalline Cellulose	Diluent	20–90	Make up the bulk of the solid dosage form for dosage size compliance.
Monohydrated Lactose	Binder/Diluent	N/A	Improves flowability by conferring cohesive properties to the powder to the desired granule size.
Croscarmellose Sodium	Disintegrant	0.5–5.0	Hygroscopic materials that cause swelling thus enhancing tablet disintegration.
Fumed Silica	Glidant	0.1–0.5	Improves flowability by reducing friction between particles.
Magnesium Stearate	Lubricant	0.5-1.0	Forms a thin film between the powder and the compacting surface that avoids sticking to it.

1.4. Tablets Manufacturing Methods

Once the ASD is manufactured, usually it presents poor flowability,[31] like the majority of pharmaceutical powders [32], due to low particle size and bulk density. Particularly, if the particles are smaller than 100 µm, forces due to surface interactions become more significant than gravity forces and, therefore, hinder powder flowability.[33] Some factors like particle size, particle shape, particle size distribution, surface area, surface energy, electrostatics[34], moisture content and solid-state structure[35] have all been showed to influence flowability. This leads to building a tablet formulation, through the most suitable tableting method (Figure 1.5), that is able to overcome this flowability issues while achieving optimal bioavailability.

In tablets manufacturing, powders' poor flowability may lead to inconsistent die filling and hopper emptying as well as inefficient powder blending. These issues contribute to wider weight variations and/or inconsistent drug content uniformity. [33][35] Delivering uniform dosages to patients may be challenging for some poorly flowing formulations through direct compression. When this happens, granulation processes (wet or dry) overcome flowability issues that ASD may bring through particle size and density increase. Here, granules are used as intermediaries (between powder and tablets) for blending with excipients prior to tablet compression/capsule filling, ideally ranging from 0.2 to 0.5 mm in particle size.[36] As the granulation process unfolds, the material Solid Fraction (SF) also increases from powders to further granules and, finally, to tablets.

Dry granulation is a continuous process with the advantage to be able to work with heat or moisture sensitive drugs while reducing costs compared to wet granulation. Wet granulation is more complex, requiring more specialized equipment and time than dry granulation and may present stability issues when dealing with thermolabile and moisture sensitive API, since a liquid is added to form wet granules that are subsequently dried (more specifically with ASD's where phase separation may occur, and, therefore, not being suitable to deal with SDDs).[37] Table 1.3 shows the main process advantages and disadvantages between dry and wet granulation.

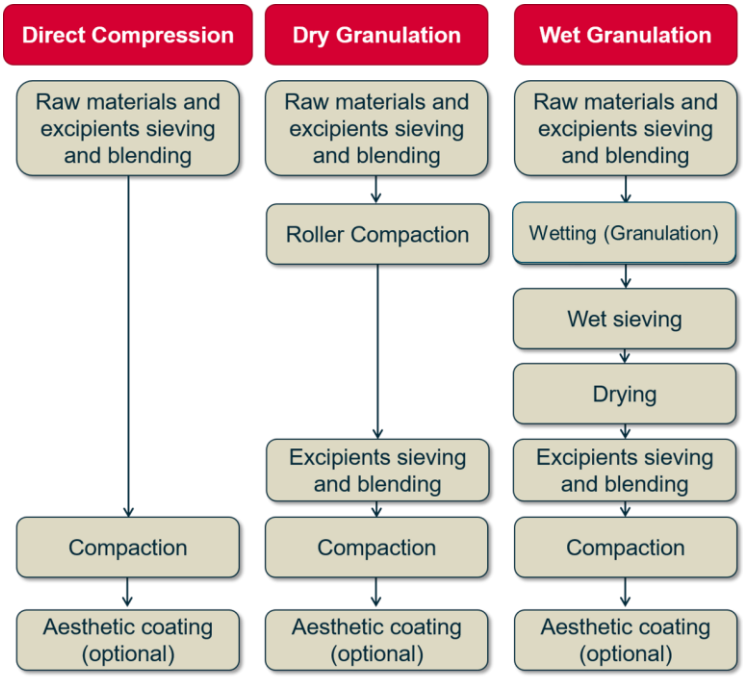

Figure 1.5– Tablets' manufacturing methods. Adapted from [38].

Table 1.3 – Dry granulation and wet granulation processes comparison.

Dry Granulation		Wet Granulation	
Advantages	**Disadvantages / Challenges**	**Advantages**	**Disadvantages**
• Enhances the flow and density[39] for poorly flowing powders that are sensitive to heat or moisture content.[40][41] • It can work with higher drug loads, in cases the API is poorly flowable; • Improves content uniformity and prevents segregation, since it presents two blending stages, comparing to direct compression method; [42] • Can be a continuous process; • Runs at small to moderate densification speeds; • Requires small GMP area; • A relatively large mass throughput; • Applicable to compounds sensitive to heat or hydrolysis, • Handles poor flowable powder; • Reduced costs compared to wet granulation since requires low amounts of energy as there is no need to evaporate granulation liquids;[43] [42] • Without the use of heat or solvents.[44] • Good control of process parameters; • Reduces dust generation (reducing fines content).[45]	• The API is subjected to great stresses during milling and roller compaction;[46] • Equipment cost; • Fines generation during Roller compaction and milling;[35] • Requires high amounts of excipient for the same dosage hence allows lower drug loadings comparing to wet granulation.[47] • Loss of compaction of the material as it passes through the rolls and its effect on the final blend compactability.[48]	• Improves blend uniformity, flowability and Compactability;[49]	• Likely to induce phase transitions (such as polymorphic conversion, hydration/dehydration, salt/parent conversion or salt/salt exchange, cocrystal/ parent conversion or cocrystal/cocrystal exchange, and vitrification/crystallization); • Physical and chemical stability may be affected; [50] • High residual solvents;[51] • Not suitable for ASD manufacturing as API polymer phase separation may occur.

1.4.1. **Direct Compression**

Direct compression is a time saving and reduced costs method when compared to other granulation methods since there are no intermediate powder physical modification steps. However, due to the reduction in steps involved in direct compression, when dealing with high drug contents, a higher excipient quantity will be required compared to wet/dry granulation to provide a suitable direct compression process with an acceptable flowability. This results in heavier tablets which might not be compliant with patients. Therefore, it is crucial to select direct compression excipients that correlate well with high dose APIs in order to maximize the patient acceptance with the dosage form. [52]

Eventually, what will lead to the decision of a powder to be directly compressed into tablets, is that it must possess low segregation tendency, good flowability and high compactability [32] (*i.e.* capacity to form new bonding areas). This is not impossible, although the great majority of pharmaceutical powders do not possess these properties, hence the need for a granulation step. Nevertheless, a series of new excipients with enhanced flowability properties has arisen in the recent years to enable direct compression.

1.4.2. **Wet Granulation**

Particle size enlargement and improved flowability, especially to feed the tablet press, can also be enhanced through the wet granulation process. During this intragranular blending step, a liquid binder is added to form granules from the small powder particles, allowing particle bonding.

The mixture is then granulated (wet) and subsequently dried to remove the moisture content. When compared directly to dry granulation the main drawback of wet granulation is the addition of a liquid binder, usually water, that further needs to be dried.[53] This approach combines the active ingredient with one or more of the other components and is frequently carried out as a wet process in a fluidized bed.

When it comes to dealing with ASDs, wet granulation may be disadvantageous since the wetting step can promote segregation of the ASD (API-Polymer matrix) and therefore, recrystallizing the API hindering its solubility in bio relevant media.

Additionally, the resultant wet mass requires to be dried and milled to generate a product that can then be tableted/encapsulated are time consuming steps increasing additional costs.[41]

1.4.3. Dry Granulation / Roller Compaction

1.4.3.1. *Working mechanism and design*

Roller compaction (RC) has appeared to replace the traditional slugging and milling steps by introducing a single machine that performs both compaction (compacts powders into ribbons) and milling (ribbons to granules). RC is gaining attention since it is a continuous process suitable for heat/moisture sensitive drugs particle size enlargement process to improve flowability and thus optimize the final tablets content uniformity.[45] Furthermore, dry granulation represents less costs when compared to wet granulation.

Before the compaction starts, the powder, previously blended, is introduced into the hopper mounted on the top as seen in Figure 1.6. The resulting blend is then fed, through two feeding augers, to the two rolls between which the powder is densified into ribbons. The RC unit is typically composed by the feeder system (feeds the powder to the rolls), the compaction unit (where compaction and ribbon forming takes place) and a milling unit (for the resulting ribbons from the previous region into granules).

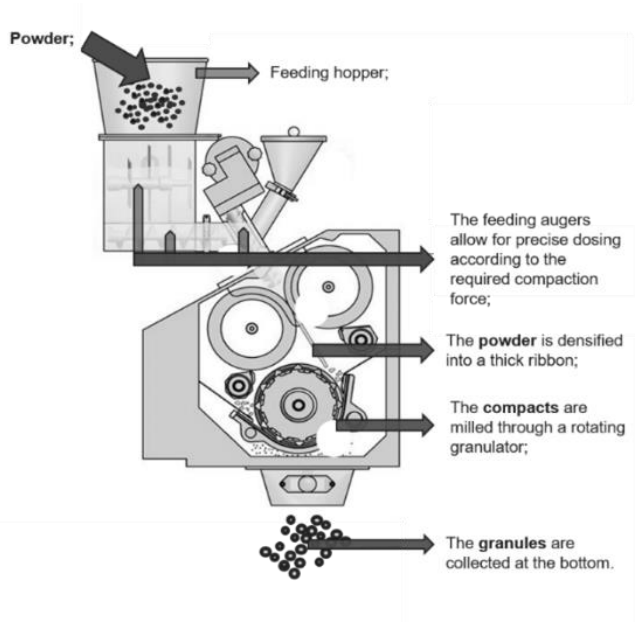

Figure 1.6 – Roller compaction and design scheme.

In more detail: the compaction process can be divided into three different zones (Figure 2.2); first, the feeding zone. The process of powder transportation from the feeder/hopper to the rolls determines the degree of homogeneity of the powder in the compaction zone which in turn

will affect the ribbons' density distribution.[54] At the feeding zone, particle rearrangement takes place with low stresses being applied, here the rolls speed is higher than the powder's. When the powder speed equals the rolls' linear speed, the powder particles stop "sliding" at the rolls and the compaction zone is achieved, described by the nip angle (α). Here, the powder is subjected to a maximum pressure Pm as it is compacted through plastic flow, brittle fracture, and most usually a combination of the two, into ribbons by establishing new bonding areas. After the minimum rolls gap width is passed, stresses are relieved and a third zone – extrusion zone – is achieved. Here, depending on the material properties, the compacts undergo a certain amount of elastic recovery.[45] [55]Typically, brittle deforming materials present negligible elastic recovery (Monohydrated lactose) whereas plastic deforming materials present higher elastic behavior (Microcrystalline Cellulose) – more strain rate sensitive.

Both maximum pressure and roll densification time dictate compact density. As compaction time decreases (shorter densification time) (*i.e.* by increasing roll speed), the minimum pressure required to achieve compacts at the target SF at gap increases. However, for high strain rate sensible materials, higher compaction speeds, result in wider elastic recovery, than at low compression speeds. That is, by providing a longer densification time, particles are offered more time to rearrange by establishing new bonding areas.

Additionally, there is an upper pressure limit for friable materials or elastic materials prone to delamination issues. [56][57]

After the compacting process, the ribbons are subsequently milled into granules, by a rotating granulator, and collected at the bottom of the equipment. These granules are headed to a mixing stage with excipients (extra granular blend) prior to being compressed into tablets.

1.4.3.2. ***RC Main Parameters***

The most impacting parameters in the final tablet properties will be the gap between the two rolls as well as the compaction force. Other parameters like, Feeder screw's speed and design, roll speed, mill speed, mill screen size, type of sealing system and roll surface can also can have impact. The rolls surface can be either flat or knurled, being that former prevents material sticking to the roles, reducing the amount of lubricant needed[35] and the latter is most typically selected as it promotes material flow at the slipping region. As for the rolls sealing system, it is

very crucial to avoid fines bypassing the gap and collecting non compacted material which consequently decreases compacted material yield. For Gerteis Mini-Pactor, it can be in the form of cheek plates or rimmed roll assembly (Figure 1.7). It has been shown through experimental and model data that when using a Mini-Pactor and microcrystalline cellulose the cheek plate system provides a more uniform ribbon SF distribution across the rolls width while rimmed roll assembly provides more porous ribbons at the edges.[58]

The ribbons' SF has been reported to be independent of the roll's width when scaling up the rolls' width and maintaining the same RC parameters including fixed roll diameter.[59]

Lactose and Microcrystalline Cellulose powder mixtures have demonstrated that with increasing compaction force, the ribbons' SF also increases up to a certain force until the SF reaches a high limit at higher forces, where it no longer decreases the compact's porosity. Conversely, for larger gaps, at fixed specific compaction froce, it has been shown that SF decreases, since with increasing gap, the same force needs to be applied to a higher amount of powder.[60]

It has been reported that , when using Mannitol as feeding material (brittle behavior[61]) in *Gerteis MINI-PACTOR*®, the rolls speed of 2 and 4 RPM were found to play a negligible impact on the ribbons SF results. On the same study, it was also observed that the sealing system type (cheek plates or rimmed roll) was a significant factor affecting the ribbon SF. Cheek plate sealing system resulted in the densest ribbons, when smooth rolls were used. The type of rolls surface pattern was less significant compared to the effect of the sealing system. The combination of rimmed roll sealing and knurled rolls resulted in comparable ribbon SF to those obtained by combining cheek plate sealing and smooth rolls. [54]

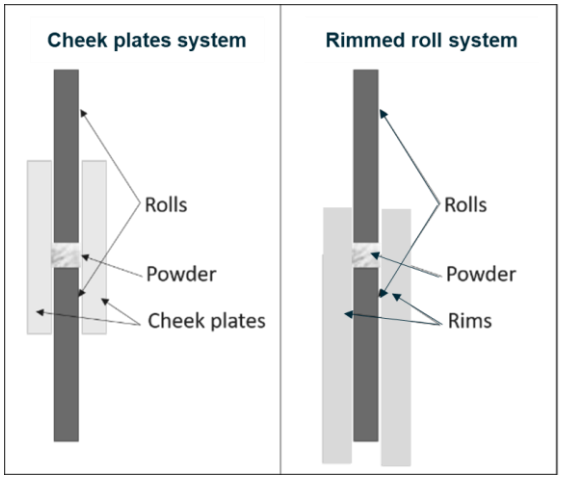

Figure 1.7 – GERTEIS Mini-Pactor sealing systems.

1.4.4. **Powder Rheology: Setting the bar between DC and DG**

Through proper analytical characterization it is possible to gain insight about the powder flowability which combined with the API material (micronized API, ASD) may indicate the best process: dry granulation, wet granulation or direct compression (e.g. when powders possess intrinsic cohesive properties direct compression may be suitable). Some of the widely used rheological tests, described in the literature, to assess flowability are: angle of repose, flow-through-an-orifice, ring shear cell[62], FT4 powder rheometer[41] and bulk and tap density (providing Hausner Ratio (HR) or Carr's compressibility index (CI) as seen in Equation 1.1).[33][63][64] Carr's index can provide indirect measurements of size and shape, surface area, moisture content, and cohesiveness of materials since all of these can influence the observed compressibility index.[65]

$$CI = \frac{\rho_b - \rho_t}{\rho_b} \qquad HR = \frac{\rho_b}{\rho_t}$$

Equation 1.1 – Carr's compressibility index and Hausner ratio calculation.

Where, ρ_b is the density before compaction and ρ_t after compacting the powder in g/mL. Besides these two indicators being simple to obtain, they can be performed with just a few grams of material input, which potentiates their wide use. According to the obtained values of these two indexes, flowability can be qualified, according to Table 1.4.

Table 1.4 – Hausner Ratio or Carr's compressibility index flow characterization.[65]

Carr's Index (%)	Flow Quality	Hausner Ratio	Angle of Repose
≤10	Excellent	1.00-1.11	25-30
11-15	Good	1.12-1.18	31-35
16-20	Fair	1.19-1.25	36-40
21-25	Passable	1.26-1.34	41-45
26-31	Poor	1.35-1.45	46-55
32-37	Very Poor	1.46-1.59	56-65
>38	Very, very poor	> 1.60	>66

Angle of repose is a relatively simple to perform test, although it possesses high variability since it is not an intrinsic property of the powder. It consists in placing a centered funnel above a base with a low retaining edge. The funnel height above the cone is recommended to be varied 2-4 cm as the powder flows from the funnel and the pile is formed. This method shall only be used if a symmetrical cone of powder is observed. The angle of repose is further calculated through the height of the pile formed (h) and the base's diameter or radius (d) as presented below in Equation 1.2.

Some concerns should arrive when using this method such as: the peak of the cone can be distorted from the powder falling from above – this is minimized by slowly building the cone;

the nature of the base upon which the powder is poured may influence the angle measurement - this can be fixed by forming a powder layer base, this is where the base edge becomes important.

$$\tan(\alpha) = \frac{h}{\frac{1}{2}d}$$

Equation 1.2 – Angle of repose formula.

Although particle size distribution (*e.g.* by sieve-shaker) doesn't give a direct measure of flow, it can be used to assess fines content in powders/granules.

In order to gather complete information regarding the flowability of a powder, the best approach is to combine various measurements. However, some of the methodologies highlighted above are destructive as well as requiring high material input, which is not always available.

One reported widely used approach for classifying flowability is Carr's characterization system. It is based on four flowability tests, namely: angle of repose, angle of spatula, Carr's compressibility index and uniformity coefficient (retention of 2 grams of powder material, on the top screen, of a nest of 250,150 and 74 µm screens above a bottom pan, the nest is then vibrated for 20-120 seconds. Each 0.1g on the 74, 150 and 250 µm equals to one, three and five points, respectively).[66]

Although this approach can provide a consistent flowability assessment in the pharmaceutical industry[33], complementary tests should be performed such as Ring shear cell.

Ring Shear Cell: This test can provide useful information regarding powder flowability such as the unconfined yield strength, powder flow function and angle of internal friction. This method has de advantage of being precise, predictive and may be non-destructive.

The most common method of treating shear data is the Mohr circle analysis (Figure 1.8). The intersections of the Mohr circles are drawn in such a way that they are tangent to the yield locus. These circles represent the total forces on the powder bed at the point of shear for any direction. The unconfined yield strength at an associated major principle consolidation force is obtained from the drawing the 1st Mohr Circle, drawn tangent to the yield locus and passes on the axes origin from of the shear versus load forces plot. This parameter provides the maximum principal stress acting on a free surface required to cause failure. The 2nd circle is drawn in a way that it is simultaneously tangent to the yield locus and its center corresponds to the point of maximum

shear and zero normal applied forces. The intersection with the x-axis provides the principal normal stress which is the maximum perpendicular force that the powder can be consolidated before it changes volume.[33] By plotting the unconfined yield strength by the principal normal stress, flow function coefficient is obtained.

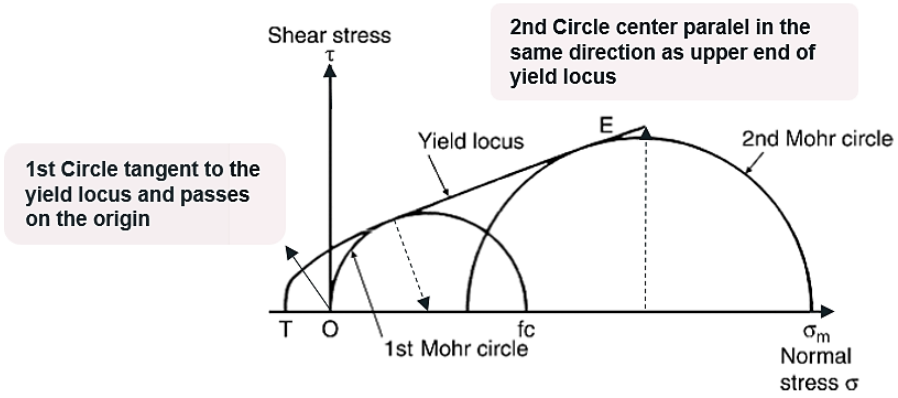

Figure 1.8 – Mohr circles analysis scheme.

The flow function coefficient (FFC) at a given consolidating stress can be referenced against established flowability categories (Table 1.5). A FFC greater than 3 is a sufficient value for predictable and reproducible gravimetric feeding in continuous direct compression systems[34] and may set the bar between DC and DG.

Typically, in order for a blend to be suitable for continuous direct compression, it must hold at least “Good” flowability indexes provided from the rheology tests.

Table 1.5 – Flowability categories according to the flow function coefficient. [65]

Flow function coefficient	Flow category
>1	Very cohesive
>2	Cohesive
>4	Easy flowing
>10	Free flowing

1.5. RC scale-up: State of the art

Most RC scale-up papers available mainly refer to equipment transfer (i.e. RC from different manufacturers or scale-up within the same manufacturer, whether it be equipment or process parameters). Few papers focus on scale-up from a LAB compaction simulator to MF RC methodology to predict the throughput, ribbons and granules properties. This approach seems to allow more material and costs savings, although die compaction and roller compaction stress paths are reported to be clearly different, with roller compaction exhibiting higher shear than die compaction, which increases the challenge of simulating roller compaction through confined die uniaxial compaction process. [55]

Among the proposed models for roller compaction process simulation, some of the most important are the slab model [67] where elastic unloading at the roll exit is ignored; Johanson Model [68][69]; Cunningham[55], thin layer model [43], as well as enhanced approaches based on the previous models[1][48][47].

This thesis focuses on a scale-up methodology from LAB compaction simulation to MF roller compaction process while aiming to saving time and material. Compaction simulators are equipped with sensors for measuring online compression force and displacement measurements, being key to obtain tablets with the desired SF whether in or out of die. Oppositely, RC technology usually does not provide this flexibility, since the process is different (Figure 1.1), making scale-up from lab compaction simulator to MF RC more challenging.[48] Some efforts in this topic were made and are summarized below.

Simulation of roller compaction using a laboratory scale compaction simulator (2004)[39]

Zinchuk suggested a sine wave function like time-displacement profile to mimic the RC process using compaction simulator. The following equation was proposed:

$$\boldsymbol{D = Rsin(wt)}$$

Equation 1.3 – Proposed punch time displacement profile to mimic RC process.

Where D is upper and lower punches displacement in mm, w is the rolls rotating speed in s^{-1} and t is the time in s. The maximum value for this function corresponds to R, suggesting that this parameter can be inputted to simulate the RC process minimum rolls gap. When the punches

start touching the powder it simulates the RC densification phase (nip angle to gap) (Equation 1.3).

This study's validation was done by plotting SF and ribbons' tensile strength of the simulated versus real RC ribbons. In that work it was determined that the ribblets (short term for ribbons + tablets) surface pattern was irrelevant in terms of scale-up curve (Tensile strength versus Solid fraction).[39]

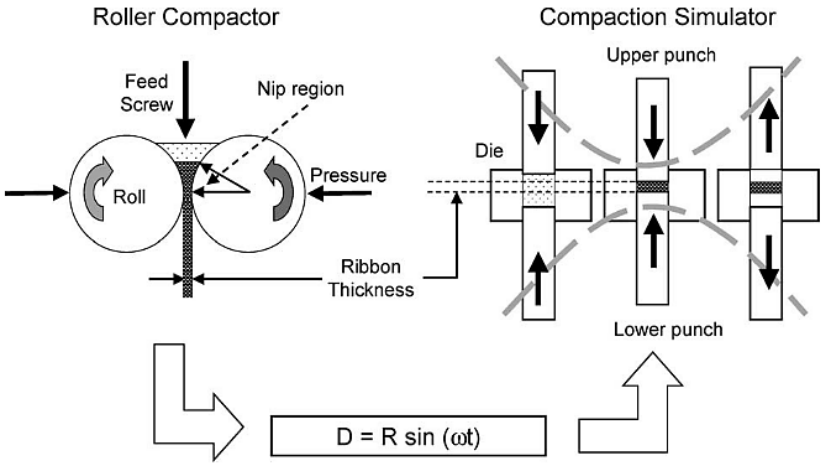

Figure 1.9 – Proposed roller compaction rotation mimicking by compaction simulator.[39]

Roller compaction/Dry granulation: Use of the thin layer model for predicting densities and forces during roller compaction (2010)[43]

The thin layer model assumes that the powder's deformation during tableting can be transferred to the RC process, as long as the tableting process is carried out with sufficient accuracy, which should not be a problem when using a compaction simulator. It is assumed that between the nip angle and the gap (densification zone) the powder is divided in thin layers of constant mass and fixed thickness, h and width, w and varying length, l_i (Figure 1.10). The first and longest layer has the length corresponding to the distance between the rolls at the nip angle (l_{nip}) and the shortest length is obtained at the gap (l_{gap}).

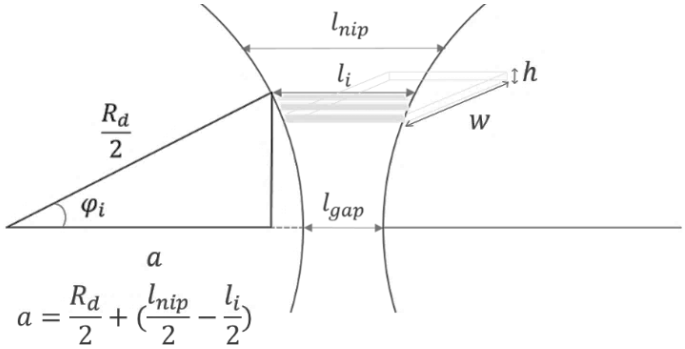

Figure 1.10 - Thin layer model schematic representation.

With decreasing length each layer's density increases. The rolling angle of each layer can be calculated by the Equation 1.4.

$$\cos(\varphi_i) = 1 + \frac{l_{nip} - l_i}{R_d}$$

Equation 1.4 – Rolling angle of each layer (thin layer model).

The force to the rolls by each layer at the densification phase (F_{DP}) is calculated according to:

$$F_{DP} = \frac{1}{w} \sum_{i=0}^{n} w.h.p_i$$

Equation 1.5 – Specific compaction force applied during densification phase.

The elastic expansion is estimated from tableting in a uniaxial compaction simulator, by performing a second compression for a given die filling right after the first compression. The elastic recovery equation is obtained by normalizing the pressure from the second compression cycle from the pressure correspondent to the maximum density of the first compression cycle. On the other hand, at-density is plotted normalizing by the maximum density achieved in the first compression. This yields a polynomial fit between both standardized applied compaction pressure and in die density. Using this approach the force due to elastic recovery F_{ER} can be calculated and summed to the force during the densification phase resulting in the total specific compaction force.

$$F_{total} = F_{DP} + F_{ER}$$

Equation 1.6 - Total force in RC process.

Hybrid modeling of roll compaction processes with the STYL'One Evolution (2019)[60]

In 2016, a hybrid modeling approach was proposed linking mechanical RC mimicking through uniaxial compression and mathematical modeling to convert the applied compaction pressure into a computed SCF, using the thin layer model explained above, – the same as the force per roll' width applied in the RC process. For the effect, ribbons were manufactured across a pre-established specific compaction force range, at two different gaps, then the same SCF range is mimicked in lab by compaction simulation using a flat rectangular 20x10 mm tooling to represent ribbons. The same sinewave punch displacement as proposed by Zinchuk[39] was used.

It was concluded that when plotting the results as SCF vs SF (at-gap) results for the RC process and compaction simulator can be correlated by an equipment dependent and material independent parameter, the constant Kp – same constant was yielded by testing two different formulations and two different constants. A drawback here is the need for previous RC trials to yield the Kp constant and possibly further RC trials corrected with Kp to confirm the corrected SCF validity. [60]

Roller Compaction Scale-Up Made Simple: An Approximate Analytical Solution to Johanson's Rolling Theory (2020)[1]

In 2020, a roller compactor scale-up methodology, developed at Hovione, established a new dimensionless number for scale-up or RC equipment transfer, the Midoux number, which relates the densification factor (DF) (dependent on nip angle (α) and at gap density (ρ_0)) with process parameters (rolls force and gap), geometric parameters (roll diameter and width) and material properties (σ_0 and K_M). One of the advantages of this approach is yielding accurate ribbon density predictions at gap even when calibrating material properties from uniaxial die compression, which is the case of this thesis.[1]

The Midoux parameter was achieved, through analytical approximations, derived from a set of equations, from Johanson's model, that are solved iteratively using the fixed-point method. Similarly, to thin-layer model the need for rheology constants input is eliminated which is advantageous since material characterization can be time consuming.

$$\begin{cases} \boldsymbol{\sigma_0 = \frac{2F}{LD}\sqrt{(\frac{2K}{\pi S/D})}} \\ \boldsymbol{DF^K = \frac{\sigma_0}{\sigma_{ref}}} \end{cases}$$

Equation 1.7 - Densification factor and analytical approximation to maximum roll pressure.

$$\boldsymbol{Mi = \frac{2F}{LD\sigma_{ref}}\sqrt{\frac{2K}{\pi S/D}} = DF^K}$$

Equation 1.8 - Midoux number.

Where, σ_0 is the maximum pressure, F and S are rolls force and gap, respectively, L and D are the rolls width and diameter, respectively, and K is a material dependent constant. By combining the two equations above, Midoux number is obtained, and it can be concluded that by maintaining $\frac{F}{LD}\sqrt{\frac{1}{S/D}}$ constant, equipment transfer or scale-up can be successfully achieved.

1.6. Tableting Step

The tablet compression mechanism can be divided into four main steps; i) the powders/granules are fed into the die through a feeding shoe. Inside this feeding system, there might be a set of paddles rotating, to increase flowability to the die. At this step, the powder/granules already must possess good flowability, low segregation tendency and high Compactability, as previously stated.

The powders'/granules' weight is adjusted trough the filling height and then a scrapper removes excess powder/granules above the die surface; ii) A Pre-compaction step can occur, before main Compaction. This step allows for particle rearrangement and bonding as well as for air entrapped to be released from the powder preventing tableting defects such as capping for concave punches; iii) Compaction, in which the tablet achieves the desired compression thickness (generally controlled from the distance between punches); iv) when both upper and lower punches retrieve decompression takes place, where compacts suffer elastic recovery. Further tablet ejection occurs from the lower punch. Generally, viscoelastic recovery takes place after this step (*i.e.* the tablet expands leading to a porosity increase/SF decrease);

Regardless the manufacturing method, DC, DG or WG, the tableting step is common to the three previously described methods. During the tableting step tablets are formed and should have acquired by now the target physical (integrity and dissolution) and mechanical properties (elastic, plastic, brittle behavior).

At production scale, rotary tablet presses are usually employed for tablets manufacturing. They consist of a rotary table with a set of upper and lower punches and dies where the powder runs from the hopper, through a feed frame composed by metering wheels, into the dies in a large steel plate rotating with the same speed as the punches head. This method promotes a uniform fill of the die and therefore a more accurate tablet weight.

1.6.1. **Viscoelastic and elastic recovery**

The expansion of a compacted material can be divided in two different stages, an almost rather immediate elastic recovery after compaction that has a large effect on the density/SF and a time dependent slow recovery (viscoelastic recovery) resulting in lower SF decrease (Figure 2.6), which is considered to be completed at least 24 h after compact formation, depending on the formulation.[43] Based on the materials viscoelastic and elastic recovery formulation enhancement is assessed.

1.6.1.1. *Elastic recovery estimation*

By using in die data from only one compression-decompression cycle up to a relatively high pressure, it is possible to obtain compressibility profiles (*i.e.* SF vs. compaction pressure) across a pressure range up to the maximum pressure experimented.[70]

This method has two assumptions: first being that, the amount of elastic deformation that occurs during compression phase is equivalent to the elastic recovery upon decompression phase. By assuming this, it is possible to correct the SF from elastic recovery using the equation below, to qualify plastic and elastic deformation ratio.

$$\boldsymbol{SF_{c/d} = SF_c - \left(SF_d - SF_d(0)\right)}$$

Equation 1.9 – Solid Fraction corrected from elastic recovery.[70]

Where, SF_c is the solid fraction during compression phase at pressure P, SF_d is the solid fraction at decompression phase, at same pressure P, and $SF_d(0)$ is the solid fraction at the end of decompression phase, when pressure applied is zero.

The second assumption is that the extent of viscoelastic recovery occurring post ejection is relatively independent of the maximum applied pressure.[70] (*i.e.* tablets compacted at different pressures, will present the same viscoelastic recovery after fully expanded, which is a time dependent process).

Elastic recovery is reported to be directly proportional to capping tendencies in tableting.[71]

1.6.1.2. *Viscoelastic recovery estimation*

More recently[72], the previous method was improved and, by adding a second tablet compacted at a relatively low pressure, it became possible to evaluate the viscoelastic recovery as a linear function of compaction pressure, instead of assuming a constant value, independent of pressure, as in the previous model. By applying this, SF, previously corrected from elastic recovery, can be further corrected from viscoelastic recovery.

To estimate viscoelastic recovery, two parameters are required, the tablet's SF when the force is released and the thickness out of die, which in this thesis was measured 4 minutes after

the tablet was ejected from the die. Subtracting these two parameters provides viscoelastic recovery, a time dependent phenomenon (Equation 1.10).

$$\boldsymbol{SF_{corrected} = SF_{c/d} - \Delta SF(P)}$$

Equation 1.10 - Solid fraction corrected from elastic and viscoelastic recovery.[72]

Where, $\Delta SF(P)$ corresponds to the pressure dependent viscoelastic recovery linear function that occurs post ejection.

Additionally, by measuring the two compacts (low and high pressure) tensile strength, it is possible to generate a Compactability profile, between the maximum and minimum compaction pressures experimented by fitting Ryshkewitch-Duckworth equation.[72] This approach reveals to be very useful since it is material sparing and time reducing as full in die and out of die compressibility profiles can be obtained by producing only two tablets.

This method provides an effective time saving tool, for instance, when adopting a DoE approach and various CTC profiles have to be generated for each of the trials. Using this approach, compacting only 2 tablets, one at low and the other at a high compaction pressure, can provide a complete out of die CTC, allowing material and time savings.

Typically, SF is simply measured out of die and expansion that occurs both during decompression and after ejection is not took in account. Using the approach stated above, SF reduction due to elastic and viscoelastic recovery is an important tool that may be used to compare different materials mechanical properties.

1.6.2. **Compaction force and time profile**

Compaction force-time profiles during compaction simulation can provide information regarding the plastic and elastic deformation of a certain drug, excipients, or formulations.

On a rotary tablet press, the force-time curves are divided into a compression, a dwell time, and a decompression phase (Figure 1.11).[32]

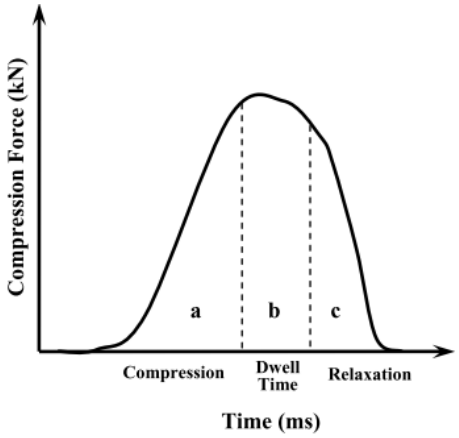

Figure 1.11 – Rotary press force-time profile phases.[32]

The areas under each stage can be a useful tool for describing phase specific material behavior type (plastic or brittle), besides compactability, compressibility and tabletability profiles that can also provide additional information regarding this.

The area under the compression phase will be thinner for high density powders (*e.g.*, dicalcium phosphate dihydrate) and larger for those with low density (*e.g.*, microcrystalline cellulose) *i.e.* for a same time point, higher compaction forces are achieved for a denser than for a less dense material.[32]

As the punches approach the minimum in die thickness, the velocity approaches zero and the relaxation within the compacted bed leads to a force decrease even though the compression thickness is not achieved yet.[43]

Once the compression thickness is achieved (*i.e.* dwell time phase is achieved), plastic materials show a decrease in force due to stress relaxation, whereas, in brittle materials a force plateau is more likely to be observed (dicalcium phosphate, crystalline lactose). During this phase, drawing a horizontal line from start to end points, can be used to measure the plasticity of a powder.

Another important parameter is the difference between the time when maximum compaction force and maximum in die density (compression thickness) are achieved (t_{diff}). The occurrence of the maximum force before the minimum volume is achieved is attributed to relaxation of plastic flow (Figure 1.12). The duration of t_{diff} depends on the ability of the compacted powder to relieve stress and thus is an indicator of plastic deformation behavior. This value will be higher, the sooner stress is relieved by plastic flow. Contrarily, for a brittle material, t_{diff} is expected to

be shorter, at the limit if not once the compression thickness/dwell time phase is reached. The occurrence of tableting problems at high production speeds may be attributed to the decrease in the plastic flow which may be indicated by a lower t_{diff}.

Hiestand came with the Brittle fracture index (BFP) which varies from 0 to 1, and showed that materials that are known to cap (higher BFP) showed slow stress relaxation after a maximum compaction force was achieved whereas plastic deforming materials (lower BFP) such as microcrystalline cellulose and spray dried lactose presented a quicker stress relaxation by plastic deformation.[73] Therefore, for brittle materials, stress relief (elastic behavior relaxation) does not depend strongly on the application rate of stress (dwell time may play a negligible impact on stress relaxation).[32]

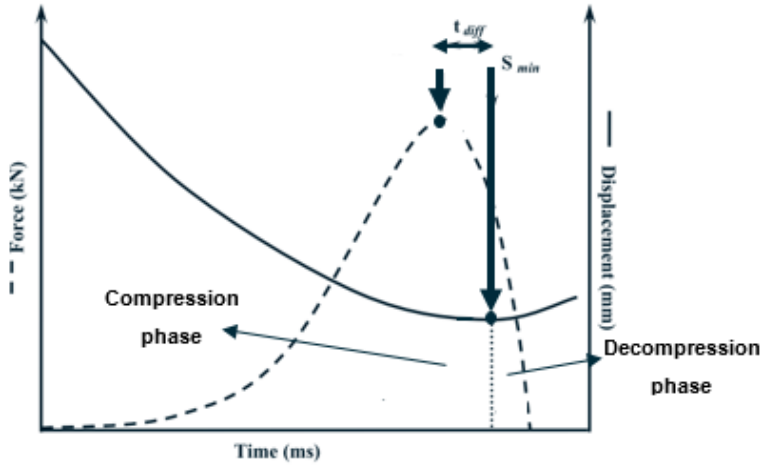

Figure 1.12 – Compaction force and punch displacement versus time profiles. (adapted from [32])

1.6.3. Compaction force and punch displacement profile and dwell time

Besides force times profiles, force and (punch) displacement profiles are an essential tool that also provides information regarding the specimen compaction behavior. The work performed during tableting can be defined as the area under the force-displacement curve. Hence, for a specific target compression thickness, the higher the work load the lower is material's compressibility.

As observed in Figure 1.13, the steeper the decompression phase curve is, until the force reaches zero, the lower elastic recovery material's tendency (area under decompression curve). Conversely, for elastic materials, the area under decompression curve will be larger.

When compaction occurs in a tablet press, powders experience complex stresses that cause particle rearrangement, plastic deformation and fragmentation. During this process, brittle materials consolidate mainly by fragmentation while plastic materials deform by plastic flow.

The compaction of brittle materials is less likely to be time dependent since fragmentation is rapidly achieved.[74] In general, an extended dwell time, will provide a longer period for material rearrangement and consolidation, absorbing elastic strain, which allows to reduce elastic recovery when the compaction force is released.[32]

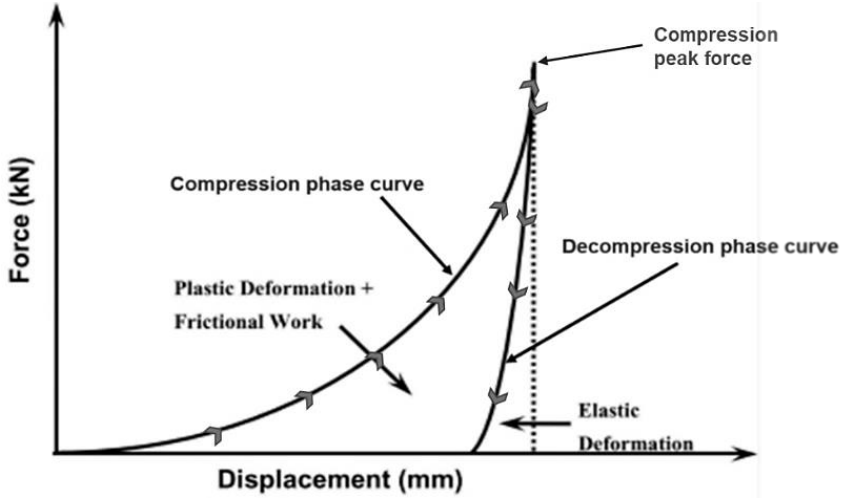

Figure 1.13 – Force-displacement curve in a compaction process. (adapted from [32])

Dwell times play a very important role in tableting and can be defined as the period of time during which the distance between upper and lower punch remains at its minimum. Others, define dwell time as the period above which the force applied is higher than 90% of its maximum value.[75]

Longer dwell times will absorb more of the elastic strain by forming new bonding areas as consequence of a better powder consolidation. Equation 1.11 shows dwell time calculation for a rotary press.

$$D_t = 1000\frac{60}{\pi n D}d_{hf}$$

Equation 1.11 – Dwell time calculation.[76]

Where, D_t is the dwell time in milliseconds, n corresponds to the turret speed in rpm, D is the tablet press pitch in millimeters and d_{hf} the diameter of punch head flat in mm.

For a specific compaction pressure, lower dwell times will produce less robust tablets down to a point where it increases the risk of failures such as capping or lamination[32], especially in large scale production where higher turret speeds are desired to maximize productivity.

1.6.4. **Assessing tablet properties**

Tablets properties such as SF, compaction force/pressure and tensile strength can be assessed through tabletability, compressibility and compactability analysis.

Compressibility (Heckel equation [77]) is the ability that a material has to undergo a reduction in its volume as a function of the applied pressure/force - It describes a relationship between SF and compaction pressure. A compressible powder consolidates even at low forces; Compressibility profiles can be estimated using Heckel equation (Equation 1.12) which assumes that the process of volume reduction during compression follows a first order kinetic profile. Although it was proposed almost 60 years ago, it continues to be the most used powder compaction equation to assess plastic deformation.[78]

$$\ln\left(\frac{1}{1-S_F}\right) = kP + A \qquad k = \frac{1}{P_y}$$

Equation 1.12 – Heckel Equation.[77]

Where: SF is the solid fraction obtained by dividing apparent density by true density; P is the pressure exerted by the punch; A is the degree of packing at low pressures as a result of the rearrangement that takes place before interparticle bonding becomes significant and k is the reciprocal of P_y. The latter will be higher for brittle materials and lower for plastic materials.[79]

According to Heckel, non-linearity at low pressures may be explained by particle rearrangement processes in powder and general behavior as individual particles rather than a coherent mass.[77] Additionally, deviations from linearity are also observed at high compaction pressures due to elastic deformation.[80] Typically, a in die Heckel analysis can be divided into three regions, a particle rearrangement governed region, a linear region and third region ruled by elastic deformation.[81]

One source of deviation when deriving the yield pressure value from Heckel profiles, is the approach to which K is derived. This is owes to although it is accepted that yield pressure is derived from the gradient of a linear slope, Heckel plots are not uniformly linear throughout the linear region.[80]

There are other models also used for compressibility studies, such as Kuentz-Leuenberger[82] and Kawakita's[83] (Equation 1.13) equations.

$$\boldsymbol{C = \frac{\Delta V}{V} = \frac{abP}{1 + bP}}$$

Equation 1.13 – Kawakita's equation.[83]

Where C is the degree of volume reduction at compression pressure P; a and b are the Kawakita parameters; $\Delta V = V(0) - V$ is the magnitude of volume reduction with $V(0)$ and V being the initial and under pressure P powder volumes, respectively; a may be interpreted as measure of the maximal engineering strain of the granule bed. [84] The Kawakita's equation b parameter provides info regarding the minimum critical pressure for a tablet to be formed.[85]

Compactability (Ryshkewitch-Duckworth, Equation 1.14 [86]) evaluates the tendency to produce tablets with sufficient strength under the effect of densification. It describes a relationship between tensile strength and SF (or porosity). Tensile strength is the maximum tensile stress that the tablet can tolerate before breaks radially.[87] It decreases exponentially with increasing porosity.[88] Although the equation was proposed more than 50 years ago, it is still currently used to estimate Compactability profiles and an essential tool for tableting process scale-up.[72]

For common pharmaceutical excipients, presenting different compaction properties, the Compactability profile was shown to be speed independent, i.e. the relationship between tensile strength and solid fraction (or porosity) remains constant for a range of dwell times. This speed independency can be explained by the internal structure of the tablet (porosity, structure and interparticle bonding) at a given SF remaining the same, regardless of the compaction speed used. [74][89]

Therefore, Compactability analysis, can be used as an effective scale-up parameter and therefore is independent of the tooling used, *i.e.* for predicting tablets' strength at high speed production.

$$T_S = T_0 \exp(-k_b \varepsilon)$$

Equation 1.14 – Ryshkewitch-Duckworth equation.[86]

Where T_0 the tensile at zero porosity in MPa; ε is the tablet's porosity; and k_b is a constant.

Tabletability (Power equation proposed in [79]) (Equation 1.15) is the capacity of a powder/granule to be compacted into a tablet of a specified strength under the effect of compaction pressure. It is used as a measure of effectiveness of the applied pressure in increasing the tablet's tensile strength. Thus, it is plotted by tensile strength and compaction pressure. [32][88]

In a study including more than one hundred materials, a relationship between tensile strength and compression pressure was found (tabletability).

$$T_S = \frac{T_0}{P_0^{\frac{kb}{K}}} P^{\frac{k_b}{K}} = dP^g$$

Equation 1.15 – Power equation for tabletability.[79]

Where d represents the tabletability capacity at different pressures and g is a pressure sensitivity index, higher g values correlate into easier compressed powders at high pressures.

For $d > 0.5$, at low pressures, powders can easily be compressed into tablets with Tensile Strength higher than 2 MPa. If $d < 0.002$, compaction cannot provide tablets with Tensile Strength higher than 2 MPa even at high compression pressures.

For intermediate *d* values (*i.e.* $0.002 < d < 0.5$) tabletability is divided into 3 categories. Category A (acceptable tabletability (TS> 2MPa) at low to middle pressure range (50-100 MPa) while presenting good tabletability at mid to high pressure (100-150 MPa)), B (acceptable tabletability only at middle to high pressure (100-200 MPa)) and C (Unacceptable tabletability over the full pressure range).[79]

2

Materials and Methods

This chapter focus on the materials and all equipment used for the dry granulation process as well as for the powders and compacts analytical characterization.

Figure 2.1 – Main dry granulation steps. Critical to scale-up stages highlighted in black.

2.1. Materials

Two typical spray dried placebo formulations were manufactured to mimic a typical ASD spray dried formulation. The first comprised Hydroxypropyl Methylcellulose Acetate Succinate (HPMCAS), an enteric polymer and the second formulation, Poly (1-vinylpyrrolidone-co-Vinyl Acetate) (Copovidone) (PVPVA Copolymer), non-enteric, also used as a tablet binder.

The excipients used were microcrystalline cellulose (Avicel PH-102 by FMC biopolymer), monohydrated lactose (Tablettose® 80 by Meggle Pharma), fumed silica (Cab-O-Sil®, by Cabot Corporation), croscarmellose sodium (Ac-Di-Sol® by FMC Biopolymer) and magnesium stearate

(by Merck). The blended weight percentages for intragranular and Extra-granular phases are displayed in Table 2.1.

Table 2.1 –Selected formulations.

Blend Phase	Components	% (w/w)	Bulk Density (g/mL)	Nominal Particle Size (μm)
Intra-granular	Spray Dried Dispersion (HPMCAS or PVPVA)	50.00	HPMCAS: 0.16 PVPVA: 0.35	HPMCAS: 44.53 PVPVA: 25.00
	Microcrystalline Cellulose	11.75	0.28-0.33	100
	Monohydrated Lactose	10.00	0.6	80
	Croscarmellose Sodium	2.50	0.4-0.5	50
	Fumed Silica	0.50	<0.06	<1
	Magnesium Stearate	0.25	N/A	<20
Subtotal (Intragranular Blend)		75.00		
Extra-granular	Microcrystalline Cellulose	11.75		
	Monohydrated Lactose	10.00		
	Croscarmellose Sodium	2.50		
	Fumed Silica	0.50		
	Magnesium Stearate	0.25		
Total (Extragranular blend)		100.00		

2.2. SF estimation

2.2.1. **Tablet density**

The tablet density was calculated according to its weight and volume, measured immediately after manufacturing, and according to the die specific area and in-die or out of die thickness, respectively, as seen below. Where m_{tablet} is the tablet's weight in mg; V_{tablet} is the tablet volume in mm^3.

$$\boldsymbol{\rho_{tablet} = \frac{m_{tablet}}{V_{tablet}}}$$

Equation 2.1 – Tablet density estimation.

When a convex tooling was used, the tablet's volume calculation was subdivided in wall's and cups' volume, as displayed below in Equation 2.2.

$$\boldsymbol{V_{tablet} = 2 \times V_{cup} + V_{wall} = 2 \times V_{cup} + A_{die} \times h_{wall}}$$

Equation 2.2 – Convex Tablet volume calculation.

Where, V_{cup} is the cup volume, in mm^3; V_{wall} is the tablet's wall volume, in mm^3; A_{die} is the die specific area in mm^2, and h_{wall} is the wall's height in mm. Regarding cup volumes, it was provided by the tooling's supplier.

2.2.2. True density estimation and determination

In this thesis, true density was performed by helium pycnometery in Micromeritics Accupyc 1340 II. All measurements were done in duplicate, aiming to and achieving <2.00 % variability. Eight samples were analyzed in a total of sixteen runs, where 1-2 g per sample was required for measurement. The goal was to assess the difference between SDD, SDD plus intragranular blend phase and SDD plus extragranular blend phase true density, *i.e.* how the excipients adding influenced the blend's absolute density. For the Extra-granular phase, only the lowest and highest density runs were selected.

Table 2.2 – Testing parameters used in True Density determination for each sample run.

Parameter	Value
Cup size	3.5 cm3
Number of purges	5
Purge pressure	19.5 psig
Number of runs	10
Run fill pressure	19.5 psig
Equilibration rate	0.02 psig
Run precision	Yes
Percentage full scale	**0.05%**

After obtaining true density, SF can be calculated according to Equation 2.3, where ρ_{true} is the tablet's true density in mg/mm^3. The true density results are displayed in Appendix A – True Density .

$$SF = \frac{\rho_{tablet}}{\rho_{true}}$$

Equation 2.3 – Solid fraction estimation.

2.3. Blending

LAB: The intra granular and extra granular blends were all mixed in a TURBULA® T2F, System Schatz. In both blends the conditions were the same. First, all the excipients, except magnesium stearate, were individually sieved (30 mesh) before added to a HDPE bottle and agitated for 10 minutes at 32 revolutions per minute. The magnesium stearate was further weighed, sieved and added to the formulation, followed by 4 minutes agitation at 32 revolutions per minute.

MF: The intra granular and extra granular blends were all mixed in a 5 L Bohle blender using the same sieving and blending procedure performed at the lab.

2.4. Roller Compaction

The used roller compactor was a MINI-PACTOR® (Gerteis Maschinen Processengineering AG, Switzerland), a pilot-scale roller compactor composed by three units: a feeding, compaction and milling stage.

2.4.1. **Theoretical considerations**

The RC model[1] was used to estimate the mass flow rate and SF at gap of each trial, through in die data calibration from compaction simulator. By estimating the throughputs one can have an idea of how long each test should run in order to collect enough material for further testing and data generation in lab.

Knowing each trial's mass yield, further SF at gap for each trial was estimated using the equations in Table 2.3. However, the time period adopted in the calculations only accounted when

the force and gap values were stationary, at the desired trial values, (*i.e.* the parameters' stabilization time was not taken in account in the SF at-gap estimations, as this should not play a crucial impact on the total collecting times).

The next step was nip angle (α) determination for each trial, to attain the correspondent densification times. For this, it is assumed that densification occurs only between the nip angle and the gap, compaction zone in Figure 2.2, *i.e.* when the nip height is achieved ($0.5R_D sin(\alpha)$).[43] The nip angle depends on the densification factor (DF), which in turn depends on at gap and nip angle densities. As a simplification, the nip angle density was replaced by the granules tap density, which should not provide a significant deviation.

Estimations for densification times were further adopted as dwell times during slugging in the compaction simulator tests using the extended dwell time profile, (Sinewave-like profiles are not available in the STYL'One NANO Allix software, the reason why not selected) This is a way of simulating the continuous RC process using a batch approach in the lab.

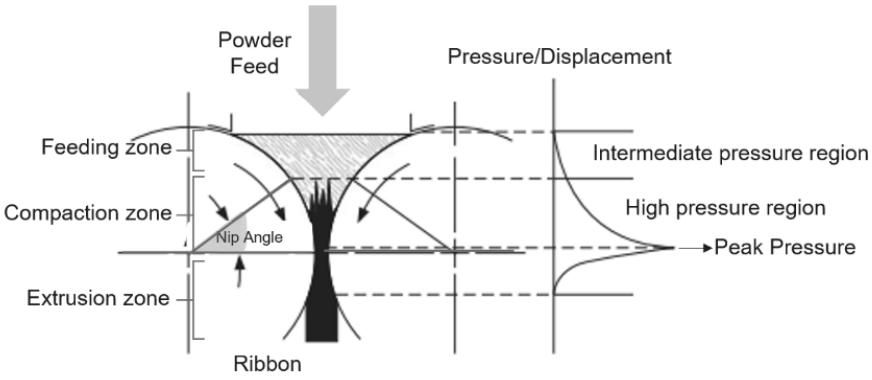

Figure 2.2 – RC process (adapted from [57]).

Table 2.3 –Equations used for throughput and process outputs estimation.

Parameter	Unities	Symbol	Value/Equation
Rolls' width	m	R_w	0.025
Distance between rolls	m	R_g	variable
At-gap Area	m^2	$A_{at\ gap}$	$A_{at\ gap} = R_W R_G$
Rolls' speed	rpm	R_s	2
Rolls' diameter	m	R_d	0.25
Rolls' speed	m/s	u	$u = \frac{R_S(\pi R_D)}{60}$
Mass throughput	kg/s	$\dot{m}$	variable
Powder's true density	kg/m^3	ρ_{true}	variable
SF at gap	-	$SF_{at\ gap}$	$SF_{at\ gap} = \frac{\dot{m}}{A_{at\ gap} u \rho_{true}}$
Nip Angle [1]	rad	α	$\alpha = \arccos\left(\frac{R_G + R_D + \sqrt{(R_G + R_D)^2 - 4R_G\ DF\ R_D}}{2R_D}\right)$ where, $DF = at\ gap\ \rho\ /\ tap\ \rho$
Densification time	ms	D_t	$D_t = \frac{1000\alpha}{\frac{R_S}{60} 2\pi}$

2.4.2. **Plan of experiments and run parameters**

A design of experiments was used to assess the influence of specific compaction force and minimum distance between rolls and compare to the granules obtained from the laboratory milling process. Three levels of specific compaction force and minimum distance between rolls were used: 3, 5 and 7 kN/cm and 2, 3 and 4 mm, respectively (Figure 2.3).

The trials were conducted in ascending throughput order to be as material sparing as possible between runs. Since there are two formulations, the aim was repeat the amount of experiments for both, however, for HPMCAS based formulation, there was not enough material, and only trial #1, #2 and #5 were performed. Ideally, a scale should have been mounted at the bottom area to only collect the desired material amount and avoid over collected material in early runs.

All the runs were carried out at 50 rotations per minute milling speed using the star type rotor. For PVPVA, all the planned DoE trials were successfully completed and two additional runs were performed, trial #6 (5 kN/cm specific compaction force, 3 mm minimum distance between rolls and 70 RPM milling speed) and trial #7 (7 kN/cm specific compaction force, 6 mm minimum distance between rolls and 50 RPM milling speed).

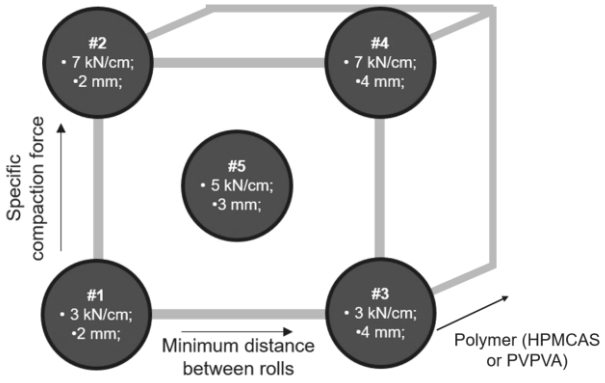

Figure 2.3 – Roller Compactor plan of experiments.

The equipment was used to yield all the ribbons and granules from the manufacturing facilities. Between each run, the rolls were manually activated to clean the equipment from fines and possible stuck materials from previous run, in order to prepare from the next one.

Table 2.4 – Roller compactor fixed parameters.

Parameter	Settings
Rolls	Knurled
Sealing system	Cheek plate
Agitator (rpm)	10
Tamp/feed ratio (%)	165
Mill angle (º)	250º Clock-wise/125ºCounter Clock-wise
Screen opening (mm)	1
Mesh wire type	Squared
Mill type	Star rotor

2.5. Milling – Slugs and Ribbons

The Frewitt is a laboratory scale milling unit which was used to mill the resulting ribbons from the manufacturing facilities as well as the slugs made in laboratory. The compacts were milled by using the OscilloWitt head (Figure 2.4).

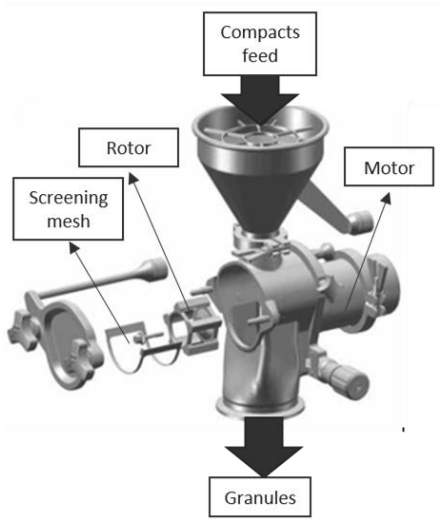

Figure 2.4 – OscilloWitt Head assembly for milling compacts.

A design of experiments was performed to assess the influence of milling speed and feed rate and compare to the granules obtained from the Mini-Pactor. Three milling linear speeds and feeding timings were selected: 100, 650 and 1200 mm/s and feed all compacts at once, every 3 seconds and every 6 seconds, respectively as displayed in Figure 2.5. This design of experiments was only carried out, for both polymers, for the ribbons obtained from RC trial 3 (5 kN/cm and 3 mm). The target mill speed is performed at 650 mm/s since is mimics the same tip speed of the RC rolls.

In the bottom of the rotor, the resulting granules were sieved through a 1 mm squared opening screen. The distance between the sieve and the rotor was kept under 1 mm in every run performed, by supplier recommendation.

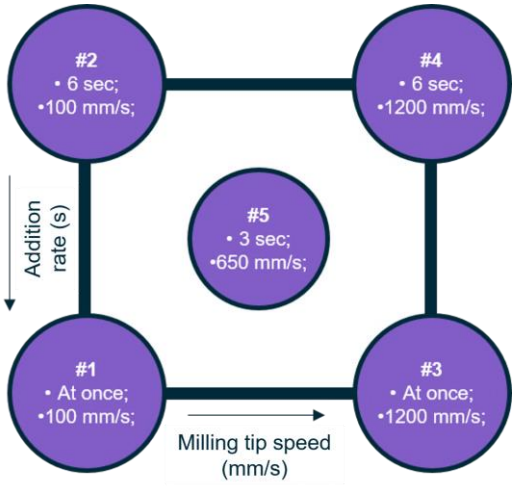

Figure 2.5 – Frewitt design of experiments.

2.6. Overall ribbon imaging with scale

2.6.1. Scanning Electron Microscopy

The morphology of the ribbons was analyzed by a scanning electron microscope (SEM) Phenom Pro-X equipment. A fraction of the HPMCAS and PVPVA ribbon was attached to a double-sided carbon adhesive tape. The samples were imaged using SEM with an accelerating voltage of between 5 and 10 kV.

2.6.2. Morphology

Ribbon measurements were performed in a particle analyzer system (Morphologi G3 Essentials, Malvern Instruments Ltd, UK). An amplification of 5 times was used.

2.7. Compaction simulator – STYL'One Nano

The STYL'One Nano, by *Medel-Pharm*, is a uniaxial compaction simulator that was used to manufacture both intra and Extra-granular formulation slugs and tablets. Different toolings were assembled during this work: 24 mm round beveled (~1 g slugs), 16x10 mm ellipsoidal concave (~600 mg slugs), 10 mm round flat (~300 mg slugs), 19.5 mm (~600 mg slugs) and 7 mm round concave (~125 mg tablets). During all the experiments, the powder was always fed to the die by hand.

One of the advantages of the compaction simulator, compared to the RC process, is that is able to accurately calculate the SF in die, through in die compression thickness live measuring. These SF in die is analogous to the RC SF at gap (Figure 2.6). Furthermore, during compaction at lab, no fines escape the die, meaning that all the filled into the die powder is compacted into a compacted material, which opposes to the RC process, which may have fines bypassing the compaction area.

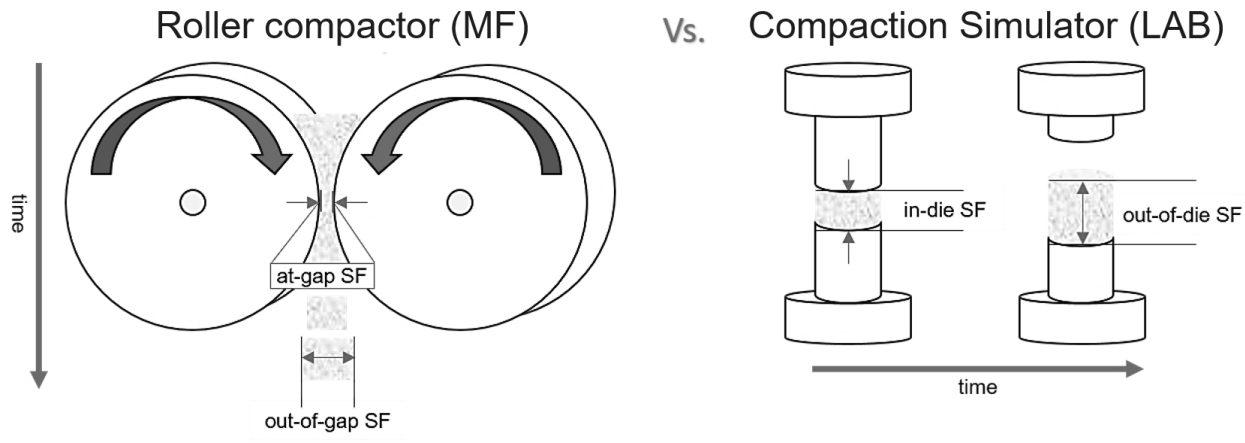

Figure 2.6 – Viscoelastic Recovery visual representation.

2.7.1. **Weight adjustment**

First of all, prior to starting producing compacts, it is essential to adjust the filling depth to achieve the desired weight. This process, is done through iterations, where a first tablet was produced and at an initial bed filling depth, the weight was measured in a equipment-independent measuring scale and input to the software is given. The software then iterates the best filling depth. To achieve the desired weight, two tablets were produced at the start of each batch.

2.7.2. **Maximum force achievable**

Following the weight adjustment, a maximum force test was performed to evaluate the minimum achievable compression thickness (i.e. maximum compaction pressure) that each powder batch was able to undergo. This run was useful in order to establish the starting point for the CTC curve data generation.

2.7.3. **CTC curve data generation**

For this step, four compacts were manufactured at 6 different compression thicknesses starting as near as possible of the minimum thickness (obtained previously through the learning step) possible. For the following tablets, 0.2 mm were added to the compression thickness at decreasing SF order. All the tablets were compacted at the same dwell time by selecting the "small rotary press at 30 rotations per minute" option – this feature aims to reproduce the dwell time that tablets are subjected as if they were being produced in a rotary press at 30 rpm.

Tablets weight, lower punch main compression pressure, thickness when force is released, minimum punch thickness, dwell time and out of die thickness (measured 4 minutes after being compressed) were collected for the produced tablets. The hardness from 2 of the 3 compacts of each compression thickness were measured in an Erweka TBH 325 (with 3-40 N adjustable measuring sensitivity) to measure the hardness and thickness (measured by a caliper) to subsequently calculate the tensile strength according to the tooling (TS calculations in detail in section 2.11 below).

2.7.4. **Target to Solid Fraction in die**

With the intent to reproduce slugs at the same ribbons solid fraction "at-gap", the required thickness (t), in mm, was calculated according to the tablet desired weight (m_{tablet}), in mg; the die area (A_{die}), in mm^2; the powder's true density (ρ_{true}), in g/mL to reach the desired Solid Fraction (SF_{target}) (Equation 2.4).

$$\boldsymbol{t = \frac{m_{tablet}}{A_{die}\rho_{true}SF_{target}}}$$

Equation 2.4 – Target thickness for a desired SF at gap.

However, for the simulator to be able to produce tablets with exactly the target thickness, a learning step needs to be done, which consists at producing 3 tablets each at a different thickness near the target thickness. This procedure allows the equipment to plot a small linear regression in order to know the target thickness value that must be inputted to "trick" the simulator and produce a tablet with exactly the desired in die thickness.

In case a shaped tooling is assembled (*i.e.* non-flat punch) one very important note is cup volumes and height must be inputted. Nevertheless, the compression thickness the software retrieves, after a compaction cycle is performed, does not account for the cup heights being that it must be added to the obtained compression thickness to obtain in die SF (software version: July 2020).

2.8. Ribbons' viscoelastic recovery

Since the majority of the ribbons were fractured, it was impracticable to measure their volume in order to calculate the apparent density with acceptable accuracy. The main advantage of Geopyc by Micromeritics is the ability of obtaining envelope volume of irregular shaped compact's surface. (Figure 2.7) This is possible through DryFlo, small lubricated beads that shape to the material surface. For each run, at the Geopyc, ribbons were sampled to obtain a sample mass of, approximately 2 g, the recommended for this analysis.

At each run, first, a blank data run was performed to measure the volume of the sample chamber only filled with DryFlo bed. The bed was compacted up to a certain force through a plunger, performing ten measuring cycles. Then, the sample chamber-plunger assembly was removed and the sample was placed inside the chamber. The run was set to start and the Geopyc performs another ten cycles, this time for envelope volume measurement, by returning the average and standard deviation values. The apparent density can be, consequently, obtained according to Equation 2.5.

$$\rho_{env} = \frac{m_{sample}}{V_{env}} = \frac{m_{sample}}{(V_{sample+dryflo} - V_{dryflo})}$$

Equation 2.5 – Envelope density calculated from sample's weight and envelope volume measured on GeoPyc.

To assess the impact of both elastic and viscoelastic recovery, SF out of gap was measured for the ribbons, in order to compare it with the previous estimated SF at gap. With these two constants, ribbons' elastic recovery was obtained, according to Equation 2.6. Note that, the viscoelastic recovery already accounts for the fast elastic recovery that occurs immediately after ribbons pass the RC gap.

$$Viscolastic\ Recovery = SF_{at\ gap} - SF_{out\ of\ gap} = SF_{at\ gap} - \frac{\rho_{env}}{\rho_{true}}$$

Equation 2.6 – Viscoelastic recovery and out-of-gap solid fraction.

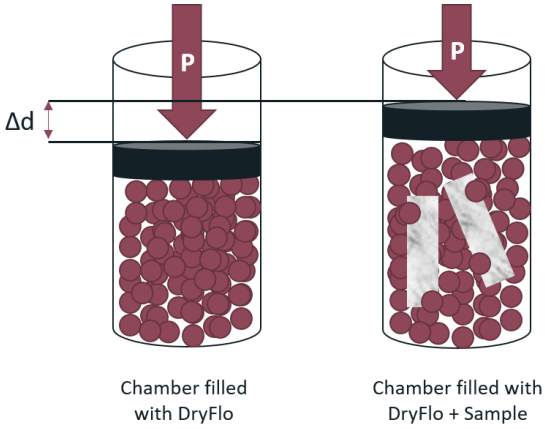

Figure 2.7 – Displacement method for measuring envelope density.

2.9. Granules analysis

The resulting granules from: lab slugs, MF ribbons (granulated in LAB) and MF ribbons (granulated in MF) were all characterized by Bulk and Tap Density (BD/TD) and particle size distribution by sieve shaker.

2.9.1. Size distribution by sieve-shaker

Six sieve openings were used in each run, 1000, 710, 500, 355, 125 and 63 µm. First, each sieve and the collecting pan were individually tared, then the sample, previously weighed, was placed on the top (coarsest sieve). The sieves' nest was agitated for a 5 minutes period followed by individual careful removal for weighing.

The sample's weight at each sieve was obtained by subtracting the sieve plus sample minus the tared sieve weights. The same procedure for the collecting pan. The process was repeated until the endpoint criteria, according to USP[90] are met. This is, **a)** when the weight of the sieves did not change by more than 5% or 0.1 g, from the previous weight, on the same sieve and **b)** if less than 5% of the total sample weight was on a single sieve, the endpoint for that sieve was increased to a weight change of not more than 20% of the previous weight on that sieve.

Upon the analysis, total sample recovered mass was obtained by subtracting the tared sieve weights from the sieve plus sample weights where, total losses must not exceed 5%. Also, the sample weight on a single sieve, must not exceed 50% of the total sample weight.

The endpoint criteria were met after five runs of 5 minutes at 30 seconds agitation period at 1.5 mm amplitude. For further experiments, 20 minutes runs, 30 seconds agitation period at 1.5 mm amplitude.

2.9.2. **Compressibility Index and Hausner Ratio**

The Carr's compressibility index or Hausner Ratio was only performed for granules containing the intragranular blend phase, from milling in lab and MF.

The bulk density was measured inside a previously tared 10 mL measuring cylinder, using a plastic funnel and a small piece of tracing paper placed from the top to ~2/3 of the cylinder volume scale. The sample was smoothly poured through the funnel and the bulk volume was noted. Then, the measured cylinder plus sample was weighed to obtain bulk density according to Equation 2.7. Where, $m_{cylinder+sample}$ is the total weight of the cylinder and sample, $m_{cylinder}$ is the cylinder's weight, in grams, and V_{bulk} is the powder's bulk volume, in mL.

$$\boldsymbol{BD = \frac{m_{sample}}{V_{bulk}} = \frac{m_{cylinder+sample} - m_{cylinder}}{V_{bulk}}}$$

Equation 2.7 – Bulk density.

The tap density was obtained in a SOTAX TD1. The measuring cylinder containing the sample was carefully placed on the tester. The run was set to start and 10 taps were done, the volume was noted, 490 taps follow (500 total taps), volume noted, and then 750 (1250 total taps) where the tap volume (V_{tap}) was obtained. All taps at an average of 249 taps/min.

$$\boldsymbol{TD = \frac{m_{sample}}{V_{tap}}}$$

Equation 2.8 – Tap Density.

2.10. Pilot plant rotary tablet press trials

The tablets, at the MF, were produced using a Korsch XL100 Pro rotary press. When running the machine, before the powder reaches the die, it flows through a paddle metering wheel that has rotating paddles with adjustable speed – designated feeder speed here afterwards – that will consequently feed the powder to the dies. The dies are located on a rotating turret that also has controllable speed, impacting the dwell time applied by the punches.

The aim of this trials was to conduct a parameters' study in order to assess the turret and feeder speed impact on the tablets weight variability and compactability, friability and disintegration time. Two sets of toolings were used, 7 mm round convex for 125 mg tablets and 16x10 mm ellipsoidal convex for 800 mg tablets. Four different paddle and feeder speeds were planned for each trial. The process conditions tested are summarized below in Table 2.5.

The die filling height was adjusted manually to achieve target tablet weight 125 and 800 mg for the 7 and 16x10 mm toolings, respectively. The pre-compression force used was 15% of the main compaction force. The compacting pressure was kept at 8 (±1) kN (kiloNewton) and 24 (±3) kN for 7 and 16x10 mm, respectively. Outside this compaction forces ranges, the tablet press would reject the manufactured specimens.

To assess the feeding conditions impact, it was planned to sample from each trial 20 and 10 tablets to measure, weight, thickness and hardness at MF and lab, respectively; 10 tablets were sent for friability analysis; and 6 tablets were used for disintegration testing.

Table 2.5 – Initial plan for rotary tablet press planned trials.

Assembled tooling	**125 mg – 7 mm round convex tablets**	**800 mg – 16x10 mm oval convex tablets**	
Compaction force (kN)	8	24	
Turret Speed (RPM)	**Estimated dwell time (ms)**		**Feeder Speed (RPM)**
20	56.6	129.5	5 20 40 60
40	28.3	64.7	5 20 40 60
60	18.9	43.2	60 40 20 5

2.10.1. **Tablets weight variation**

Inconsistent powder or granulate density, particle size distribution and poor flowability are common sources of weight variation during compression. Variations between in tablets dose and weight must be reduced to a minimum. The uniformity of weight is an in-process test parameter, to ensure consistency of dosage units during compression. 20 tablets, from each trial, were collected and weighed individually. Then, the average weight was calculated and further weight variation from the limits was assessed according to European Pharmacopoeia[91] (Table 2.6).The tablets passed the USP test if no more than 2 tablets were outside the percentage limit and if no tablet differs by more than 2 times the percentage limit.

Table 2.6 – Weight variation test.[91]

Pharmaceutical form	Average weight	Percentage deviation
Tablets (uncoated and film-coated)	80 mg or less	10.0
	More than 80 mg and less than 250 mg	7.5
	250 mg or more	5.0

2.11. Tablets tensile strength

An ERWEKA TBH 325 was used to measure tablets' hardness through crushing strength. Further tablets tensile strength was obtained with hardness and morphology parameters, depending on the tablet's shape (Table 2.7). When round flat or oval convex tablets were manufactured Tensile Strength (TS) was calculated as displayed below, respectively and according to USP.[92] These equations are an approximation, since they assume that all the stresses are evenly distributed through all the tablet's volume during hardness test.

Table 2.7 – Selected tooling shape.

Tablet shape	Oval with convex cup	Round flat with no cup	Round with convex cup
Top View			
Side View			
TS formula	$\frac{2}{3}\left(\frac{10H}{\pi D^2\left(2.84\frac{t}{D}-0.126\frac{t}{W}+3.15\frac{W}{D}+0.01\right)}\right)$	$\frac{2H}{\pi Dt}$	$\left(\frac{10H}{\pi D^2\left(2.84\frac{t}{D}-0.126\frac{t}{W}+3.15\frac{W}{D}+0.01\right)}\right)$

Where H is the breaking force in N; D is the tablets' diameter and semi-minor axis length for round and elongated tablets, respectively in mm; t is the tablet's thickness overall thickness (wall height plus cups height) in mm; and W is the wall height for convex shaped tablets.

2.12. Friability

2.12.1. **Lab tablets friability**

In order to obtain the friability, all tablets were individually weighed before and after being introduced in the rotating drum, at 25 revolutions per minute during 4 minutes for a total of 100 rotations. The equipment allowed to simultaneously use a drum on each side, rotating simultaneously, each containing tablets from a different blend. Each blend contained tablets compacted at six different compaction forces, with *n=2* (total twelve tablets per rotating drum).

The total weight loss was calculated according to Equation 2.9. The criteria for passing the test was set at 1.00 % weight loss per individual tablet, ideally it is informally acceptable < 0.5%. Where, m_{before} is the initial mass and m_{after} is the mass of the eroded compact.

$$\%F = \frac{m_{before} - m_{after}}{m_{before}} \times 100$$

Equation 2.9 – Individual tablet friability calculation.

2.12.2. **MF tablets friability**

The friability test was conducted in a compendial apparatus and according to the USP <1216> monograph.[93] Regarding the 125 mg tablets, compacts were sampled to a total of 6.5 g in weight and further re-weighed after rotating 100 times at 25 revolutions per minute, the weight loss was obtained according to Equation 2.9. Whereas for 800 mg tablets, since individual weight was over 650 mg, the USP method describes to sample and weigh 10 specimens.

2.13. Disintegration

2.13.1. **Lab tablets disintegration**

The disintegration tests were conducted in an ERWEKA ZT320 Series apparatus. Two 1 L cylindrical beakers were filled with de-ionized water and heated up to 36.5$\pm$0.5 ºC. When the temperature was set, three tablets were placed per basket-rack assembly, one tablet per tube, total six tablets per test. Each blend contained tablets compacted at six different pressures, with n=2. Every time tablets from a single blend were tested, the water medium was removed, renewed and heated to the target temperature.

The timer started when the basket-rack assembly was lowered and, for each test tube, the time was stopped when no material was observed above the mesh wire at the bottom of each test tube.

The tablets that did not pass the friability test, were not tested in the disintegration apparatus.

As observed below in Table 2.8, for uncoated tablets there is not a general consensus between pharmacopoeias.

Table 2.8 – Disintegration test specifications.[94]

Dosage form	USP General chapter	USP Dietary Supplements Chapter	European and British Pharmacopoeia	Japanese Pharmacopoeia
Uncoated tablets	Using water or specified medium. Disks used if proscribed by the individual monograph	Using water or specified mediums with a 30-min time limit. Disks used if proscribed by the individual monograph	Using water as the medium. 15 minute time limit. Disks are used.	Using water or specified medium and a 30-min time limit unless otherwise specified. Disks used if proscribed by the individual monograph.

2.13.2. **MF tablets disintegration**

From each rotary press trial, six specimens were selected for disintegration and the time was recorded for the first and last specimen. The results were registered as a mean for each test.

3

Results and Discussion

The main objective of this thesis was to enable direct dry granulation and tableting scale-up from lab to manufacturing facilities when a future tableting project arrives to save material, time and reduce costs.

As discussed above, when a project arrives, on a first approach, at the laboratory, the CTC is performed followed by tablets manufactured at different SF/TS's and further friability, disintegration and dissolution testing (and bio relevant dissolution when applicable) allows the selection of the desired manufacturing SF.

However, typically, there is no analysis on the slugging dwell time impact (which should be as representative as the future RC GMP batch trial to be performed) nor the tooling used for slugging. This thesis identified that the elastic recovery was independent of the used tooling and that for the 10 mm flat round tooling, the dwell time played negligible impact on the elastic recovery, for the PVPVA formulation.

For scale-up to be successful and based on the results below it was concluded that ribbons' SF out of gap should be as similar as slugs' SF out of die. This will guarantee LAB and MF tablets similarly tabletable/compactable, therefore reducing the need for preliminary trials. However, although the SF at gap and in die can be estimated, the correlation between SF at gap/in die versus SF out of gap/die behavior, between lab and MF, is yet to be studied.

The next studies show some remarks related to and identified as imperative for a Dry Granulation process scale-up. At the end of this chapter a methodology is proposed for upcoming projects for material, time and costs savings.

3.1. Study 1: RC Model Validation

3.1.1. RC Model Calibration

Usually, when a project launches, on a first approach, CTC data is generated to gain insight on the powder/granules tableting properties. In this thesis, a 10 mm flat round punch tooling was used for each formulation to gather blend specific input for model calibration. For the effect, n = 3 tablets were produced, at six different compression thicknesses (total 18 tablets per formulation).

The corresponding in die density (calculated using the thickness in die), tensile strength and compaction peak pressure data were inputted to the RC model that outputs two Johansson's model constants (k_M and c_M) (Equation 3.1). These constants, formulation dependent and tooling independent, were used to estimate the RC trials throughput and SF at gap based on the process parameters (Rolls' force, gap and speed).

$$\ln(\boldsymbol{P}) = \boldsymbol{K_M} \ln(\boldsymbol{\rho_{in\ die}}) + \boldsymbol{C_M}$$

Equation 3.1 – Johanson constitutive law.[1]

The results were fitted using an exponential relationship for the compactability profiles with a minimum correlation coefficient (R^2) of 0.99 indicating the excellent reproducibility of the measurements in die for model calibration (Figure 3.1).

Only the compactability and compressibility profiles are distinct when comparing in die versus out of die measurements, since the tabletability profile does not rely on the powder's density.

Comparing both polymers at the intra-granular phase, for a given solid fraction at gap, PVPVA provides more robust tablets. Also, combining the in die with out of die data, one can assess the difference between the polymers more significantly in terms of mechanical behavior as HPMCAS reveals a more elastic behavior compared to PVPVA in the compressibility plot be-

low. This emphasized the use of in die Heckel that requires less time and it's of easy data collection. The results demonstrate that both in and out of die, a linear region in terms of compressibility is achieved, due to the pressure ranges applied.[81]

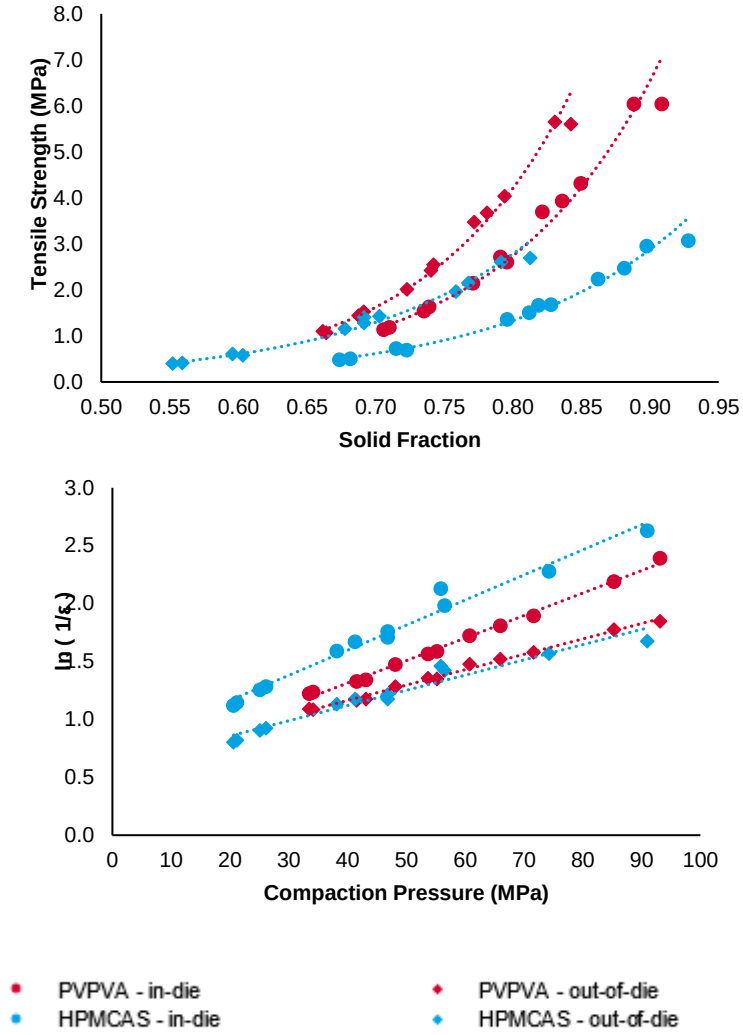

Figure 3.1 – Compactability and compressibility data used for RC model die calibration using tooling 10 mm flat round.

3.1.2. **SF predictions**

After the model was calibrated using in die parameters, it was used to predict the mass throughput, and SF at gap of each trial. For PVPVA, two different toolings were used to generate data for model calibration, 10 mm and 19.5 mm round flat punches. For HPMCAS, only the 10 mm was used, due to material quantity unavailability.

The predicted mass throughputs revealed to be a useful tool to draw an idea of how long each run should take, to avoid unnecessary material collecting. With this in mind, further ribbons and granules were manufactured during the established times.

To assess deviation from the model, SF at gap for each trial was estimated. These values were obtained according to the mass yield of each RC trial, as shown in (Table 2.3). One important aspect when estimating the SF at gap was the area at gap, ($A_{at\ gap}$), used in the calculations. The rolls gap, R_G, set-point is obtained based on the minimum distance between rolls (Figure 3.2). Since the assembled, rolls in this work, were knurled, the area available at the densification zone is not constant and the indentation's depth cannot be ignored. Using microscopy, the ribbons shape profile was analyzed as displayed below in Figure 3.3. It can be seen that the distance between indentations at the minor axis is ~1.202 mm, and that the indentation width and depth are ~0.354 mm and 0.300 mm (which matched with info sent by the RC supplier) respectively. With this measures obtained as seen in Figure 3.2 and Figure 3.3, the area at gap can be corrected according to the weighted average of the rolls profile across a certain cross section (Equation 3.2). This approach is only valid knurled rolls. Regarding smooth rolls, maintain the current strategy and calculation, only by multiplying rolls' width by rolls' gap set point at steady state. An additional suggestion may be the addition for a tag in the RC model to select roll the surface smooth and knurled and change the calculations accordingly.

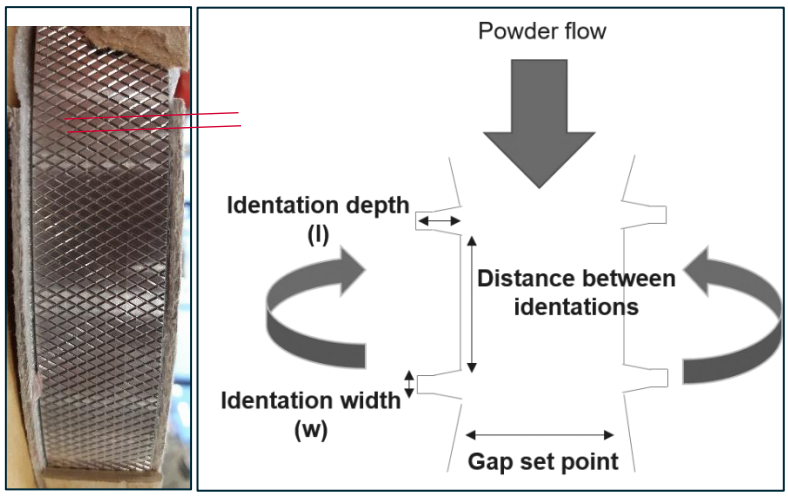

Figure 3.2 – Knurled rolls front and side view.

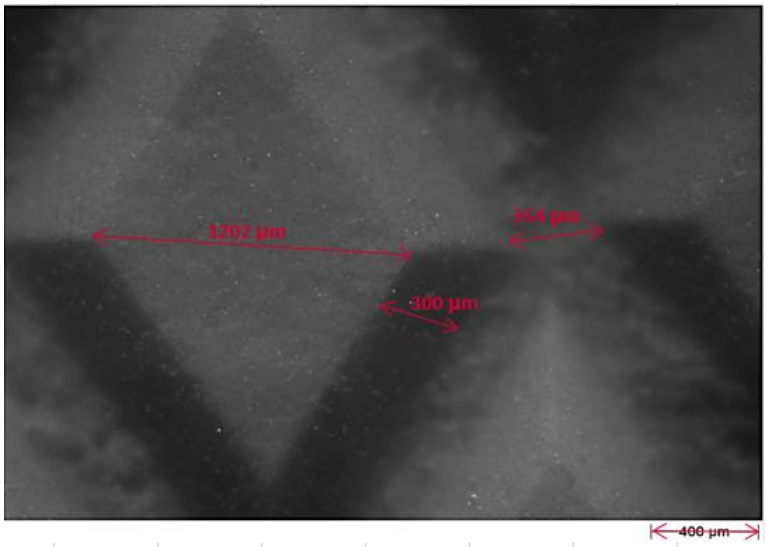

Figure 3.3 – Ribbons morphology analysis for ribbons shape profile.

$$A_{at\ gap\ corrected} = 0.58R_wR_G + 0.16R_w(R_G - 0.3 \times 2) + (1 - 0.58 - 0.16)R_w\left(R_G + \frac{0.3}{2} \times 2\right)$$

Equation 3.2 – Area at gap corrected from indentation's depth.

Where:

$A_{at\ gap\ corrected}$: Corrected densification area from each roll's indentations

R_G: Rolls' gap in mm

R_W: Rolls' width in mm

With the intent of understanding how the area at gap estimation impacts solid fraction, it was compared the previous at gap area estimation method (only according to roll's width and gap) with the corrected area method after measuring ribbons through microscopy (Figure 3.3).

According to Figure 3.4, comparing the historical area at gap estimation method, with the newly corrected area at gap displayed above, the model's relative deviation to estimated SF at gap is reduced. This corrected area will play a larger impact as the rolls gap set-point is reduced.

Regarding the corrected estimated versus model predicted SF values (Figure 3.4), the wider deviations are for HPMCAS first trial. All the process inputs and outputs and material outputs are displayed in Table 3.1. Overall, the model overestimated the SF at gap. There are two possible explanations for this; first, fines are bypassing the rolls gap and not being compacted

due to the current sealing system, so it was considered that all the collected material was being compacted when it was not. Secondly, the time used for calculations did not account for the set points stabilization, (it was assumed a shorter run time than the actual). Consequently, both these explanations lead to SF overestimation compared to model predictions.

Exceptions are: HPMCAS first trial (2 mm and 3 kN/cm), and PVPVA six trial (4 mm and 7 kN/cm). There is no clear explanation for this SF being underestimated by the model. Possible explanation may be the provided mass yield for these tests being wrong.

First the gap was adjusted and only then the force achieves the set point, so the material that was being collected prior to set point should have a solid fraction lower than the target SF.

Solid fraction estimation via throughput is simple, however, assumptions requiring approach to estimate SF at gap. Since the prior to gap and force set-point time was not took in account since the mass throughput was not constant, this leads to solid fraction overestimation, as stated above. Nevertheless, it may yield accurate precisions estimations if the run extent is higher, *i.e.* the stabilization time is shorter than the parameters set-point time length.

Unexpectedly, considering the trials performed, no general trend was observed between considered collecting time and deviation between the estimated and model SF at gap. It should have been expected a negative trend, *i.e.* higher deviation associated to shorter collecting times.

Another important note to add is to only start collecting material immediately after the desired parameters set-point values are achieved, in order to avoid collect ribbons/granules that are not inside specification.

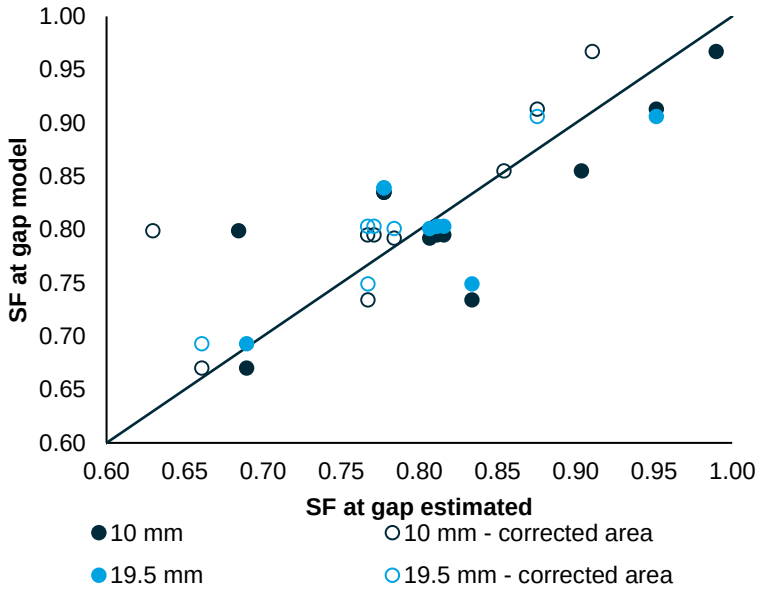

Figure 3.4 – Roller Compactor Model Validation.

Table 3.1 – Gerteis Mini-Pactor process parameters and outputs.

		Formulation	PVPVA							HPMCAS		
RC Inputs	**Symbol**	**Unities/Trial no.**	**#1**	**#2**	**#3**	**#4**	**#5**	**#6**	**#7**	**#1**	**#2**	**#3**
Specific Compaction Force	R_f	kN/cm	3	7	5	5	3	7	7	3	7	5
Rolls Gap Width	R_g	mm	2	2	3	3	4	4	6	2	2	3
Corrected Area at gap	$A_{at\ gap\ corr}$	mm^2	54.3	54.3	79.3	79.3	104.3	104.3	154.3	54.3	54.3	79.3
Rolls Speed	R_s	rpm	2									
Rolls linear speed	u	mm/s	26.2	26.2	26.2	26.2	26.2	26.2	26.2	26.2	26.2	26.2
Mill Speed	M_s	rpm	50	50	50	70	50	50	50	50	50	50
		mm/s	654	654	654	916	654	654	654	654	654	654
Material Inputs												
Powder's tap density	ρ_{tap}	g/mL	0.59	0.62	0.59	0.60	0.56	0.59	0.60	0.47	0.56	0.56
Powder's true density	ρ_{true}	g/mL				1.31					1.37	
Collecting time	t	s	351	323	246	243	220	193	126	146	100	166
Mass yield	m	kg	0.502	0.527	0.513	0.510	0.520	0.515	0.523	0.179	0.178	0.404

Material Outputs												
Mass throughput	$\dot{m}$	g/min	85.8	97.9	125.2	125.9	141.9	160.0	249.0	73.7	106.5	145.9
Solid Fraction at-gap estimated	$SF_{at\ gap\ estimated}$	-	0.767	0.875	0.767	0.771	0.661	0.745	0.784	0.630	0.911	0.854
Solid Fraction at-gap model (calibrated from 10 mm flat slugs)	$SF_{at\ gap\ model}$	-	0.726	0.900	0.785	0.785	0.665	0.824	0.783	0.798	0.967	0.855
Solid Fraction at-gap model (calibrated from 19.5 mm flat slugs)	$SF_{at\ gap\ model}$	-	0.749	0.906	0.803	0.803	0.693	0.839	0.801	-	-	-
Solid Fraction out-of-gap	$SF_{out\ of\ gap}$	-	0.592	0.689	0.598	0.607	0.542	0.649	0.626	0.477	0.666	0.505
Nip angle	α	deg	6.4	7.0	7.8	7.7	7.9	8.6	11.1	6.9	8.4	9.6
Densification time	D_t	ms	536	582	648	644	657	718	927	575	702	804
Densification height	D_h	mm	14.0	15.2	16.9	16.8	17.2	18.7	24.1	15.0	18.3	20.9
Densification pressure		MPa	21.4	46.0	29.6	29.8	17.5	37.4	29.0	20.0	38.2	23.9

3.2. Study 2: Slugging vs RC – Elastic Recovery assessment

The main goal was to manufacture slugs using toolings with different surface areas and dwell times (only done for 10 mm flat round tooling) and determine if any resembles ribbons elastic recovery range, obtained from the tested RC conditions, when targeting slugs in die SF to achieve the same ribbons SF at gap. To simulate the RC slow densification process, both extended dwell times a 3 RPM simulated rotary press profiles were tested in compaction simulation at lab.

The aim was to assess which tooling yielded a more representative ribbon elastic recovery (Figure 3.5). Initially, the plan was to manufacture slugs targeting to the estimated SF at gap for at least the high, central and the low SF RC conditions, but since there was not enough material available, it was only performed for RC trial 3 (5 kN/cm and 3 mm), for both formulations.

Figure 3.5 - Slugs manufacturing methodology.

For the ribbons, the elastic recovery immediately after being manufactured and sampled could not be calculated, so only the viscoelastic recovery was obtained through envelope volume, 2 months after manufacture. This allowed to obtain the ribbons SF out of gap.

Comparing both polymers in Figure 3.6 and Figure 3.7, the HPMCAS formulation has a larger elastic behavior both in ribbons and tablets. Also, for both formulations, the elastic recovery tends to independent of the slugs compaction area and dwell time. An exception are 10 mm flat slugs manufactured at 3 RPM which produced a slightly higher viscoelastic recovery when compared to 3 RPM dwell time for the same tooling.

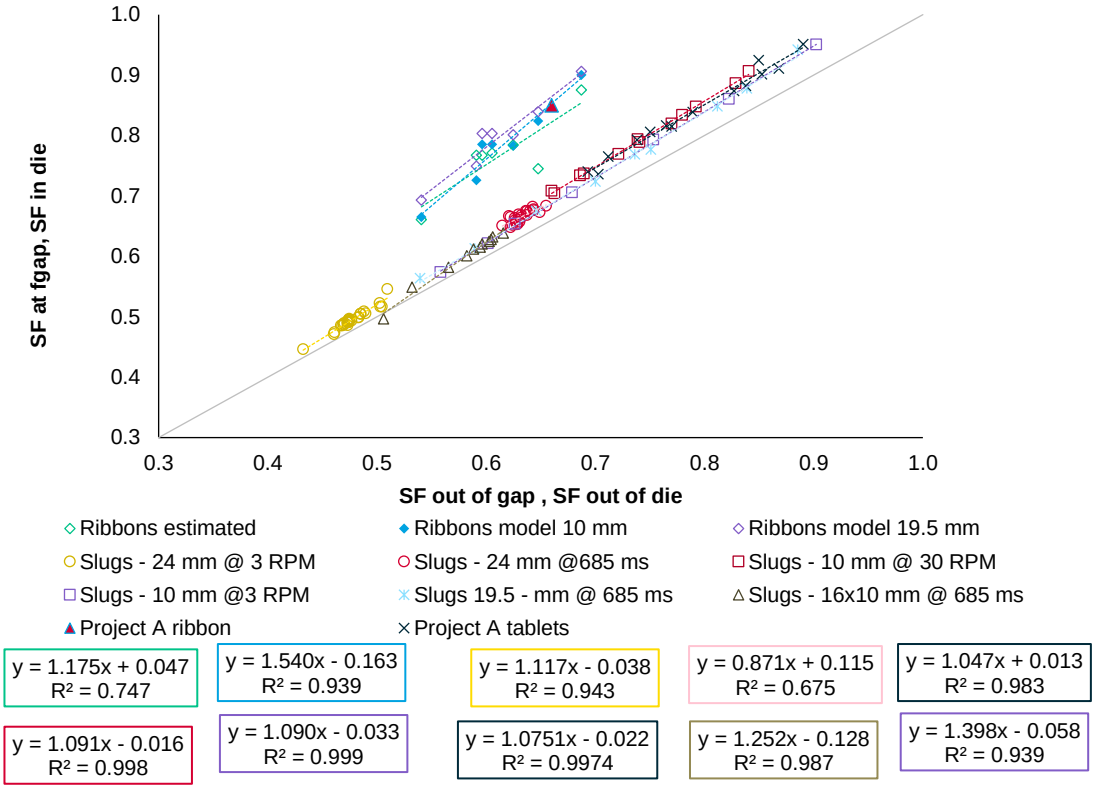

Figure 3.6 – PVPVA – Viscoelastic recovery, corrected from elastic recovery, assessment using different toolings.

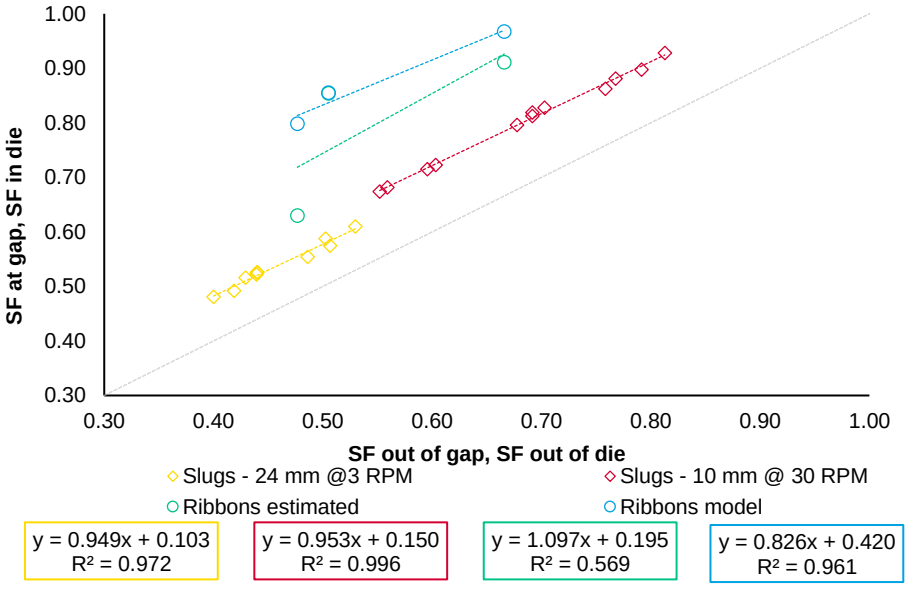

Figure 3.7 – HPMCAS – Viscoelastic recovery assessment using different toolings.

Different tooling areas, dwell times and SF were tested and no tooling presented a representative ribbon elastic recovery (Table 3.3). Taking into account the formulation used (Table 2.1), a high solid dispersion fraction (>60% in weight/weight) can be found in the intra-granular phase, present during the slugging phase. Provided this, the lab versus manufacturing data was compared to a previous project (Project A) that incorporated PVPVA SDD dispersion, however, in a lower weight percentage (8% in weight/weight) and also blended with the same excipients adopted in this thesis. The results were obtained and further compared with the data in this thesis. Unexpectedly, the same elastic recovery gap between slugs and ribbons was found. There might be four possible explanations for the deviation between ribbons and slugs;

• First being that, as stated above, ribbons viscoelastic recovery was measured two months after they were manufactured. Although ribbons were stored inside sealed High-Density-Poly-Ethylene bag, which in turn were inside a sealed aluminum bag to avoid moisture absorption, during the storing period there might have been some viscoelastic recovery, however not significant to provide a wider deviation from slugs;

• Second being that ribbons envelope density (out of gap SF) was miscalculated; to confirm this, two 1000 mg slugs were produced and allowed to expand for 5 minutes, thickness out of die were then measured via caliper for both of it. The slugs were placed inside Geopyc to obtain envelope density. Slugs' SF out of gap by envelope volume was estimated via Equation 2.5 whereas SF out of gap by caliper was obtained via Equation 2.3. Although the results are not precisely equal (Table 3.2), the difference was not able to explain the difference between ribbons and slugs elastic behavior;

• A third hypothesis was that the rolls cheek plates sealing system could be malfunctioning, allowing for fines bypassing the gap as presented ahead in *3.3.1 – RC trials - Granules analysis*. This leads to a SF overestimation since there was collected fines that were not being compacted. This was supported by the model predicted SF at gap values, that are lower than the estimated values, except for the first trial in each formulation for the reason already discussed in 3.1.2 – SF predictions;

• Fourth and final possible explanation was the tooling shape, as ribbons are rectangular shaped compacts, a rectangular tooling acquisition should be considered. This was already experimentally reported in the literature, obtaining accurate results by comparing tensile strength and solid fraction of simulated flat and serrated faced punch ribbons versus real ribbons manufactured using serrated rolls.[39]

Table 3.2 - SF out of gap envelope vs caliper comparison.

SF out of gap	Slug #1	Slug #2
Via caliper	0.449	0.451
Via caliper – average	0.450	
Via envelope volume	0.448	

Taken in account the possible explanations above, ideally in the future, a ribbon representative tooling should be found. With this in mind, in an upcoming project campaign, first a SF operating range must be established, by plotting SF in die (via software output) and SF out of die (via caliper). Further optimal SF out of die for slugging should be selected, as explained in 0 –

. This approach would automatically allow to adopt a RC SF at gap equal to the previously selected lab optimal SF in die (correspondent to the optimal SF out of die).

Ultimately, a tooling that has a parallel slope, *i.e.* a fixed elastic recovery gap, between slugs and ribbons, could be chosen, guarantying a fixed difference between SF at gap and SF in die although this is formulation dependent.

Table 3.3 – Elastic recovery assessment for PVPVA and HPMCAS intragranular blend.

Tooling	Dwell time (ms) – time-displacement profile	Compact area (mm^2)
24 mm flat round	(1200-1600) – 3 RPM simulated rotary press	452
Ribbons	685 – extended dwell time	275-350
16x10 mm oval convex	685 – extended dwell time	126
10 mm flat round	1200 – 3 RPM simulated rotary press	79
19.5 mm flat round	685 – extended dwell time	298

3.3. Study 3: Milling assessment

The milling is divided in two sets of results, first, the granules analysis yielded from different RC trials, whether by milling at LAB or MF (all at 650 mm/s, except for trial 4: 916 mm/s) and, second, assess the impact of feeding parameters at the Frewitt using the OscilloWitt head.

These studies are intended to characterize granules', from different RC trials, flowability and size distribution, through Bulk/Tap Density and sieve-shaker, respectively.

All milling trials had process yield higher than 90 %. Losses were due to fines that got stuck in a gap between the screen mesh and the OscilloWitt wall. Additionally, during the milling process, the operator cannot see the process, and, therefore, it was difficult to predict when all the compacts are milled, ending up with a couple of agglomerates still attached to the rotor, when the process was stopped. The probability of this can be reduced by allowing a longer milling period. This means that nearly all the resulting granules from milling, prior to sieving, had diameters below 1 mm (selected mesh opening for all trials), and, therefore the selected mesh revealed to be a suitable choice.

Before all the trials, the distance between the screen mesh and the rotor was set to below 1 mm, as recommended in the supplier's manual guide.

3.3.1. RC trials - Granules analysis

3.3.1.1. *PSD by sieve-shaker*

One of the main goals was to compare the granules obtained from milling in the laboratory (Frewitt) versus in the production (Mini-Pactor). A clear difference between HPMCAS and PVPVA formulations was observed.

PVPVA: In the following graphics, milling was compared at the MF and lab for each RC trial performed. The RC DoE central point was added in each graphic for comparison.

The results display that RC granules present a higher fines content than the lab granules. This may be due to a sealing equipment part malfunctioning at the MF RC that owing to his continuous use, allows for fines to bypass the rolls ending up being inappropriately collected in the final granules.

At fixed force, a larger gap increases fines content, for the reason that a larger gap results in a lower SF, which is in agreement with observed in [43]. When fixing the force, at 3 or 7 kN/cm – Figure 3.8 (a) and (b) – this trend was more pronounced when the compaction force was higher, as a result of a linear relation between force and solid fraction, yielding larger granules at 7 kN/cm. This may be an indicator of low loss by compaction for the reason that increasing the force still affects the size distribution. Otherwise, increasing the RC force would not produce larger granules as a cause of loss by compaction.

Additionally, between fixed 2 and 4 mm rolls gap – Figure 3.8 (c) and (d) – size distribution seems to be more affected by the rolls' force when a tighter gap was selected.

Unexpectedly, for the central points (3 mm and 5 kN/cm), the three production routes, present identical size distributions, nevertheless, the RC granules present higher fines content comparing to Lab granules.

HPMCAS: Regarding HPMCAS, the same trend was observed, for 2 mm gap increasing the compaction force yielded larger granules. For the Slugging plus Milling at lab for trial 3, there was very low quantity available, as this may be accountable for the significantly higher fines content than the other trials.

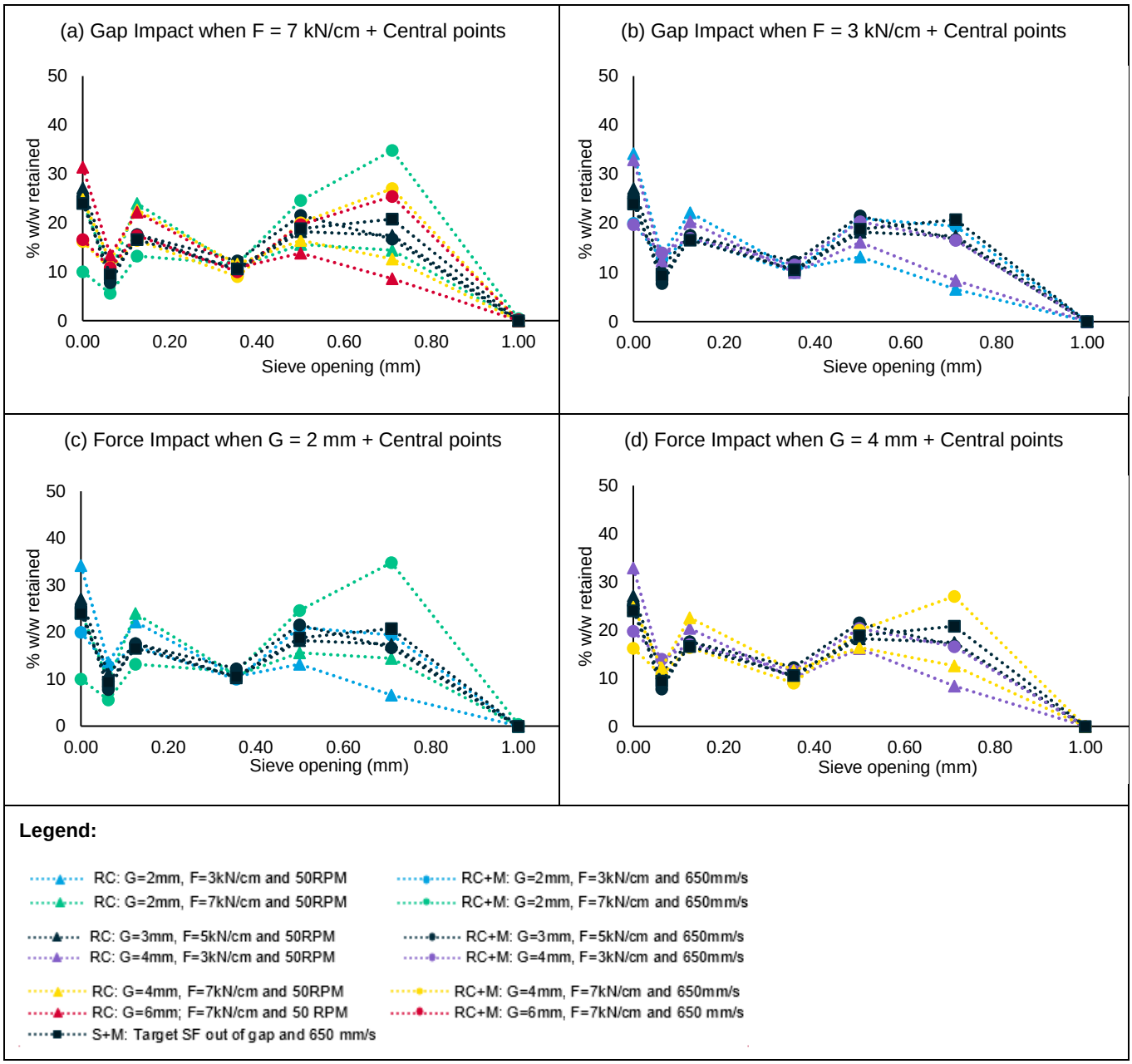

Figure 3.8 – Size distribution results for PVPVA.

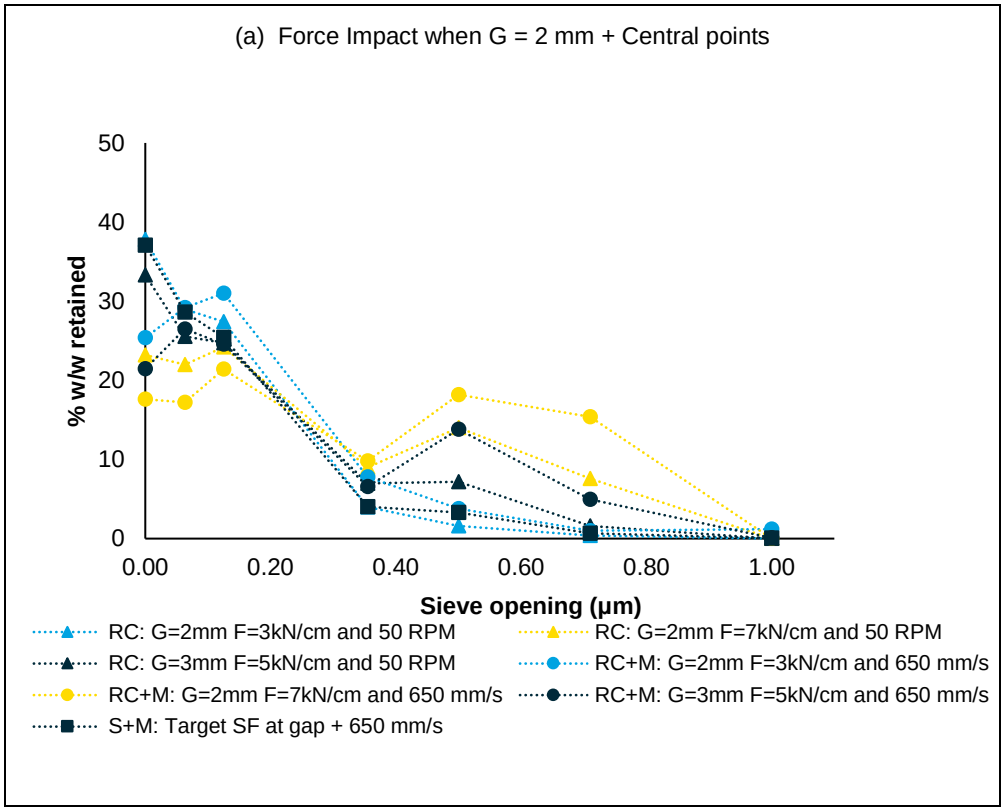

Figure 3.9 – Size distribution results for HPMCAS.

3.3.1.2. ***Bulk and tap density***

The results in Figure 3.10, are related to granules from MF and LAB containing the intra-granular blend phase formulation, where each tone represents a flowability category according to USP, as stated above in section 1.4.4.

The bulk and tap density are used to assess flow properties through obtain Carr's compressibility index as well as Hausner ratio (section 1.4.4). For PVPVA, in general, the Hausner ratio seems to be located between 1.12 and 1.30 representing flow properties between the "passable" and "good" regimes, as already expected for dry granulation. On the other hand, for HPMCAS, there seems to be a wider flowability range and for a shorter number of trials. Overall, both formulation do not present suitable direct compression characteristics.

Amongst the trials carried, the 4 mm and 7 kN/cm (SF at gap estimated: 0.66) and 2 mm and 7 kN/cm (SF at gap estimated: 0.88), demonstrate the better flowing granules, for PVPVA

and HPMCAS, respectively. Despite for HPMCAS trial 6 was not performed, PVPVA trial 2 displays the better flowing properties after trial 6.

For HPMCAS, the lab granules, from trial 3, appear to have a very poor flowability, this strongly may owe to the significantly high fines content as assessed in the size distribution in Figure 3.12. As for the milling impact, for both polymers trial 1 (2 mm and 3 kN/cm) represents the narrower difference between lab and MF, for this there is no clear explanation.

Concerning the parameters range tested, the flowability seems no to be significantly impacted by the rolls force nor gap selected (Figure 3.10). Nonetheless, Bulk and Tap Density measurement is a high variable test, when there is a need to be material sparing, as slightly higher fines content in the measuring cylinder can play impact the result.

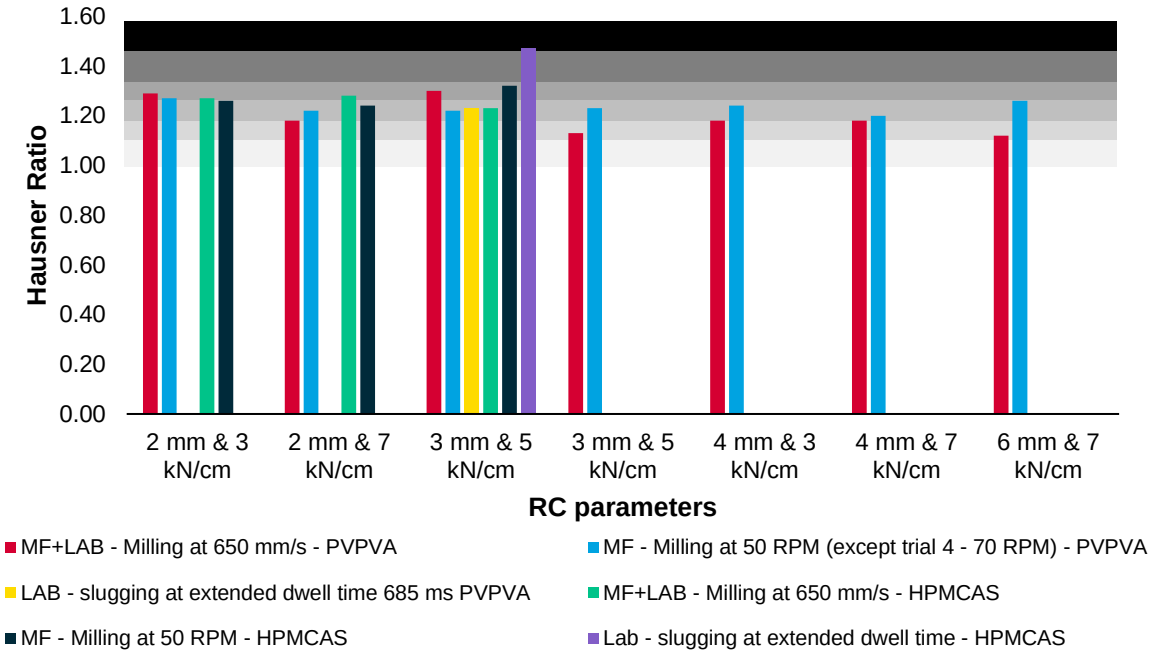

Figure 3.10 – RC DoE granules flow properties for PVPVA and HPMCAS.

3.3.2. **Frewitt trials – Granules analysis**

The RC trial 3 ribbons were milled at four different conditions at the Frewitt milling unit with the purpose to assess any impact on the granules. Additionally, slugs were manufactured aiming to reproduce RC trial 3 Solid fraction, the results are in Table 3.4.

Table 3.4 – Average target Solid Fraction results using compaction simulator.

Average / Formulation	HPMCAS	PVPVA
RC: Force 5 kN/cm and Gap 3 mm		
SF at gap	0.85	0.77
SF out of gap	0.51	0.60
Target out of gap		
SF in die	Not enough material	0.67
SF out of die		0.63
Target at gap		
Biased SF in die	0.90	0.78
SF in die	0.54	0.49
SF out of die	0.46	0.48

3.3.2.1. ***PSD by sieve-shaker***

A clear difference between each polymer's size distributions can be distinguished, as PVPVA granules tend to be larger than HPMCAS.

Changing the milling tip speed and the feeding rate at Lab did not significantly affect the granules size distribution for PVPVA, except when the milling speed was 1200 mm/s and the ribbons were fed every 6 seconds, which yielded less fines content On the other hand, for the HPMCAS formulation, feeding the compacts all at once and at 1200 mm/s milling speed that yielded the size distribution with the higher fines content. Comparing 50 and 70 RPM milling speed at MF, the results display that the size distribution is negligibly affected by this change.

For PVPVA, Figure 3.11 shows that granules originated from slugs "targeted at SF at gap" presented substantially higher fines content. However, this result was biased due to a software

bug derived from compression thickness (in-die thickness). When manufacturing slugs targeting to the ribbons SF at gap, the compression thickness outputted was thought to already include the lower and upper cup height from the 24 mm diameter round beveled tooling used. However, the software was retrieving in-die thickness taking into account only the slugs' wall height. The bug was further fixed, by the supplier, in an updated *Allix* software version. In this work, not having accounted for the cups' height in the at-die thickness, to calculate the SF in die, this resulted in an average 0.78 slugs SF at gap (which alone deviated from the desired SF at gap 0.79) when, actually, it was 0.49, as presented in Table 3.4. This, therefore, resulted in fragile compacts and may explain the higher fines content, in the sieve-shaker results, when comparing to the slugs targeted at SF out of gap that resulted in fairly similar size distributions.

Caution should be taken in SF in die calculations. To avoid future errors like this, all the tooling supplier measurements must be accurately introduced when assembling a set of punches for the first time, which will, therefore, allow SF in die to be precisely calculated.

Regarding HPMCAS (Figure 3.12), although the slugs were manufactured targeting to ribbons' SF at gap, the slugs and ribbons granules presented a very similar size distribution. This owes to the slugs' measured SF out of die not significantly varied from ribbons' SF out of gap, as can be seen in Table 3.4.

Most importantly, for both formulations, the results suggest that by intermittently feeding slugs every 3 seconds and using a milling tip speed that aims to replicate the MF RC process, yields granules with similar size distributions. In this thesis, a 50 RPM milling speed was adopted at the MF, which by using the Lab milling machine rotor's diameter can be converted into milling tip speed.

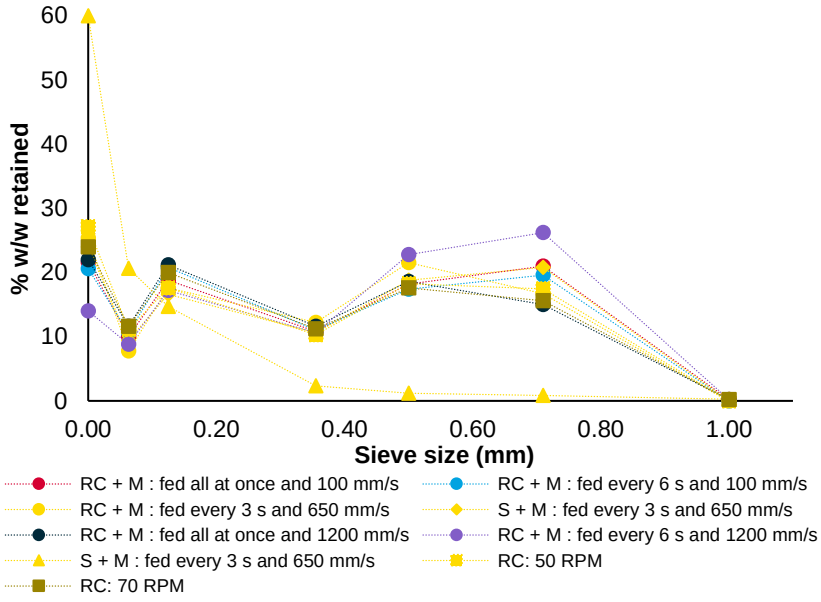

Figure 3.11 – Milling parameters impact for PVPVA formulation. Where, RC+M denotes ribbons formed by RC and milled at LAB; S+M denotes Slugging and Milling performed at LAB at; RC denotes ribbons and milling performed at MF.

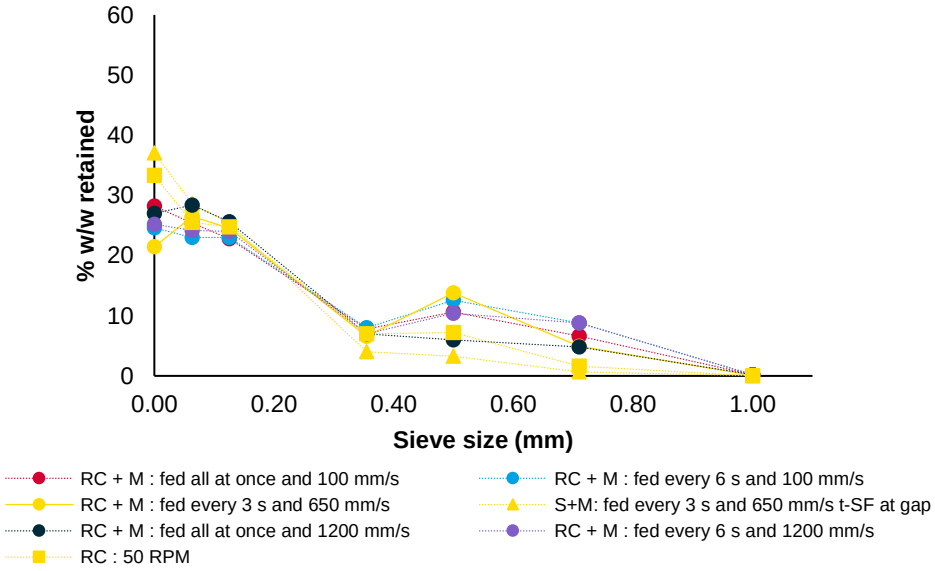

Figure 3.12 – Milling parameters impact for HPMCAS formulation. Where, RC+M denotes ribbons formed by RC and milled at LAB; S+M denotes Slugging and Milling performed at LAB at; and RC denotes ribbons and milling performed at MF.

3.3.2.2. *Bulk and Tap Density*

The same variability range in flow properties as in RC DoE (section 3.3.1) was observed since the Bulk and Tap Density has various variability sources such as the speed at which the powder was poured into the measuring cylinder.

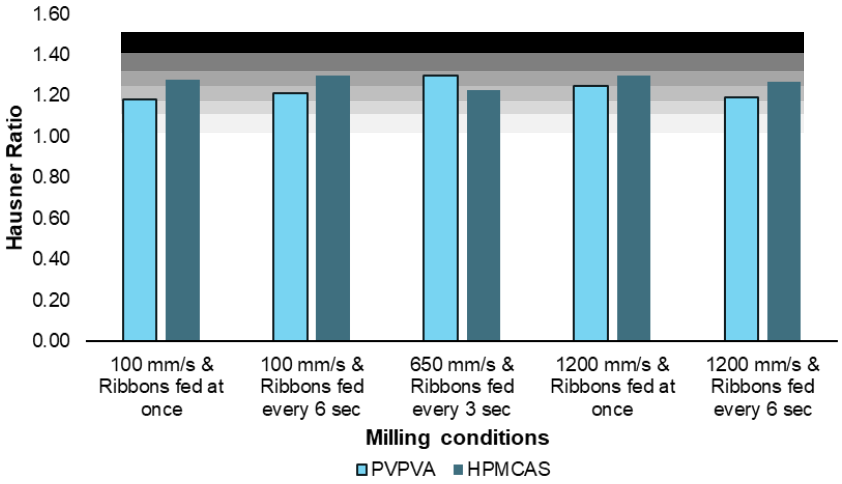

Figure 3.13 – Frewitt granules flow properties results.

3.4. Study 4: Lab tableting properties analysis

Round 7 mm diameter with convex cups tablets were manufactured from all the RC trials, as there was not a significant difference in terms of size distribution and flowability for the lab milling parameters assessment, only the compacts milled at 654 mm/s and fed every 3 seconds were used to manufacture tablets.

3.4.1. **Compactability – scale-up curve**

Six different compression thicknesses were tested each with n = 2, yielding a total 12 tablets per formulation. The Compactability analysis results are shown below.

For PVPVA, the RC conditions that produce the most robust tablets (higher tensile strength at zero porosity, σ_0) are 4 mm rolls' gap width and 3 kN/cm specific compaction force trial. This

was due to low both estimated and model predicted at gap SF resulting in a smaller loss of compactability when compared to the other trials, as can be seen by the SF at gap lines estimated and predicted in Figure 3.14 .

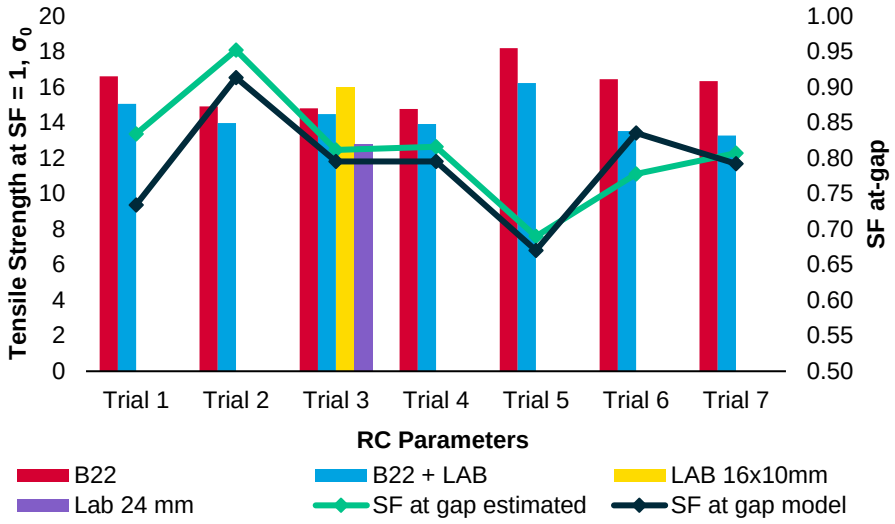

Figure 3.14 – Compactability analysis for PVPVA formulation.

For HPMCAS, the densest trial (trial #2 – 2 mm gap and 7 kN/cm force) resulted in the most robust tablets (Figure 3.15). For this particular trial it should be expected a higher degree of loss by compaction, however, this absence in loss of compaction may owe to the powder's high elastic recovery (Table 3.1) ending up having a SF out-of-gap of 0.69 that fits the ribbons typical range (0.55 – 0.80). [39]

Comparing the formulations, at a given solid fraction, PVPVA seem to produce more robust tablets, and also the tensile strength difference between formulations tends to be more significant as the SF out of die increases.

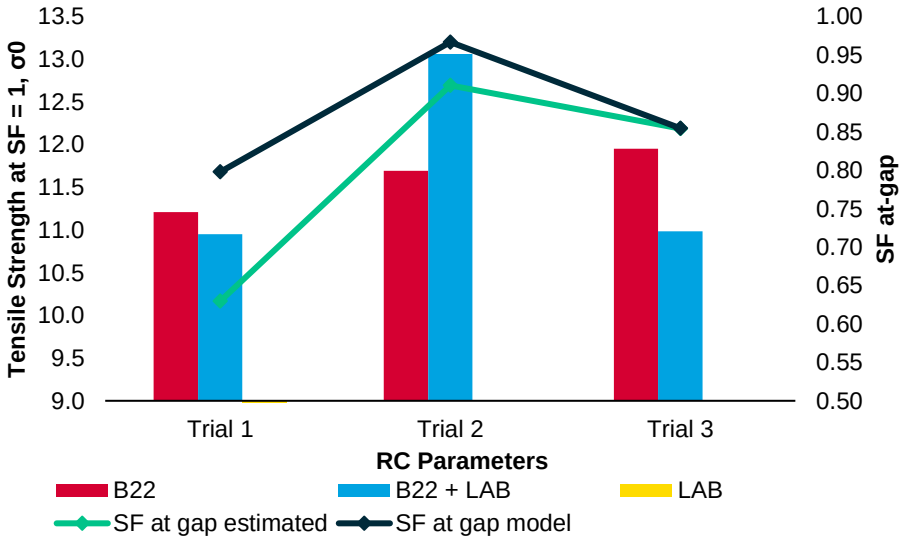

Figure 3.15 – Compactability analysis for HPMCAS formulation.

Since for HPMCAS the previous trial 2, yielded more material, it was simulated a "V-shaped" constant speed (30 mm/s) (no dwell time) compactability profile and further compared to a 30 RPM simulated rotary press. The aim was to understand the impact this would play in the tablet's tensile strength, for a given solid fraction. Dwell time effect in the compactability analysis[74] has been studied, and there should be no deviation between in Tensile strength at a given solid fraction with variable the dwell time which was also observed in this work as highlighted Figure 3.16.

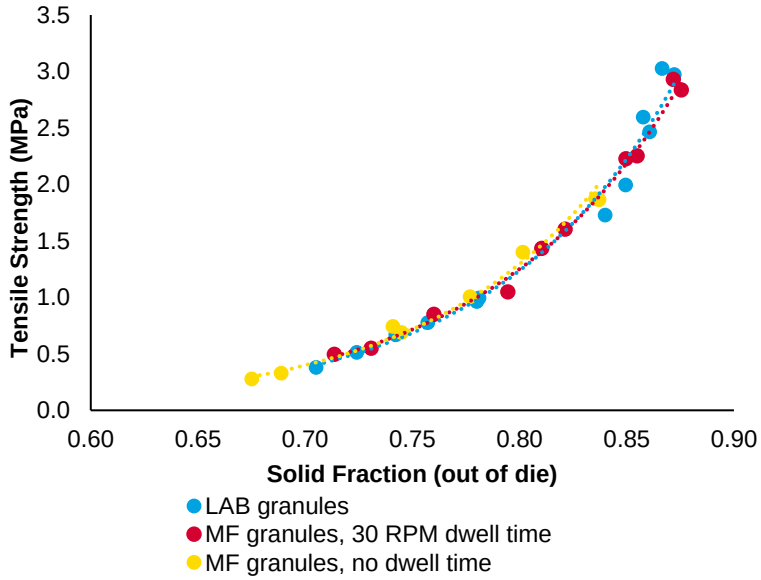

Figure 3.16 – HPMCAS RC trial 2 dwell time impact assessment.

As concluding remark, for all the RC trials, the B22 vs LAB milling impact was assessed and it was concluded that milling in the Frewitt produced comparable granules to those yielded by RC (Figure 3.17). Trial 7 has the higher deviation between B22 and LAB granules. Since this trial produced the highest throughput (hence area at gap) the probability of fines bypassing through the gap is higher (this trial yielded the higher fines content in the sieve-shaker analysis – Figure 3.8.

The RC trial with 3 mm gap and 5 kN/cm force (test 3 and 4) was the only test able to be mimicked at lab by targeting slugs SF out of die to that same test's SF out of gap. Since test 4 only differed in the milling speed from test 3, it should be expected tablets from milling in the Frewitt for both these tests reproducing similar characteristics. With this in mind, the Compactability curves from different processing routes are almost overlapping meaning that both lab milling and lab slugging was representative of the B22 milling when targeting SF out of die to the desired SF out of gap. This is an excellent dry granulation scale-up indicator.

Legend:

- HPMCAS - Lab granules
- HPMCAS - MF granules
- PVPVA - Lab granules I
- PVPVA - Lab granules II
- PVPVA - MF granules
- PVPVA - MF granules (70 RPM)
- PVPVA - Lab granules (Slugging 24mm)
- PVPVA - Lab granules (Slugging 16x10mm)

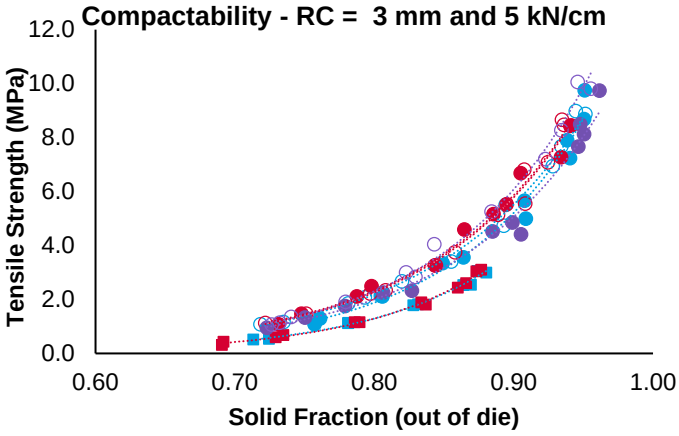

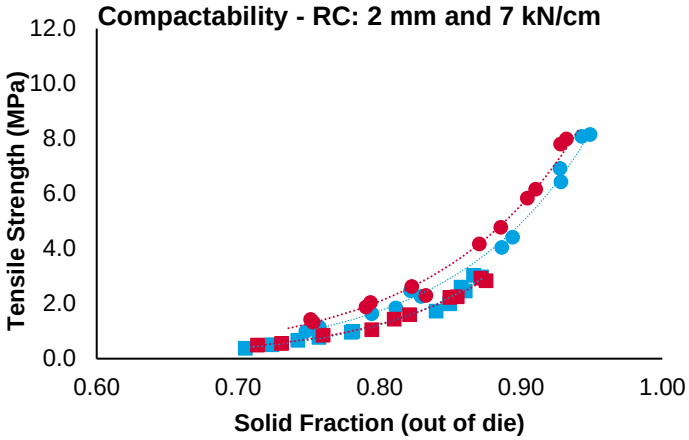

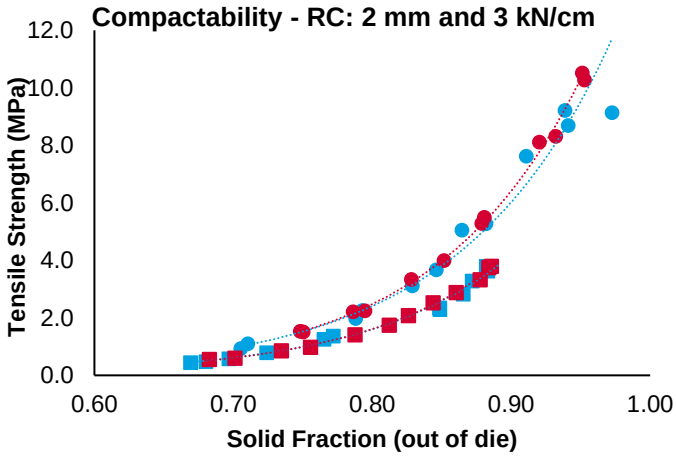

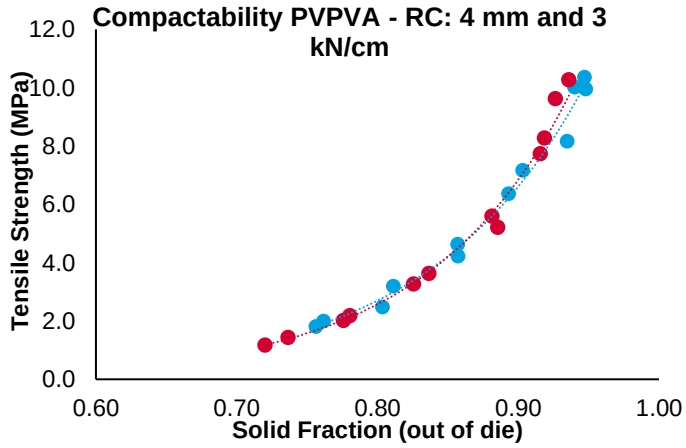

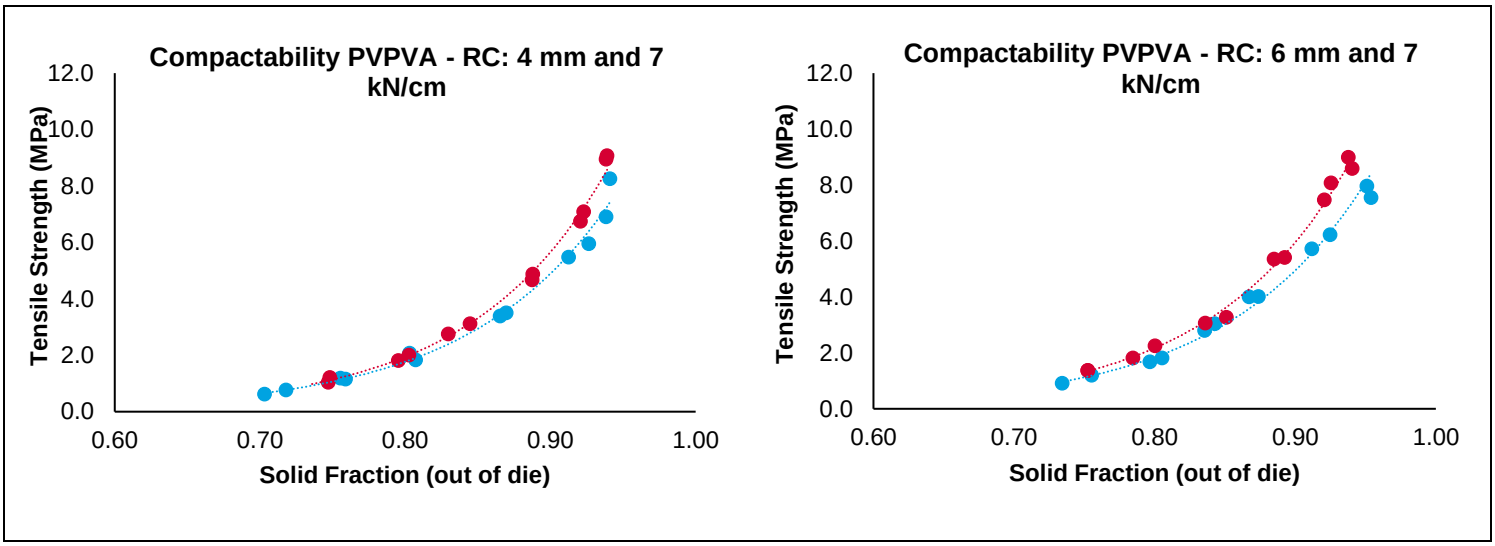

Figure 3.17 –Compactability results for HMPCAS and PVPVA formulations.

3.4.2. Tabletability

From a mechanical point of view, tabletability indicates when a certain blend achieves an overcompression plateau, meaning that the compacts are no longer “tabletable”, i.e. the critical compaction pressure during which no longer interparticle bonding takes place. To examine this better, all data was fitted with a second order polynomial regression as it displayed higher coefficient of determination, R^2, than linear regression fit.

The upper compaction pressure was limited to the selected tooling force security threshold of approximately 14.2 kN which, dividing by the punch’s specific area, corresponds to 370 MPa.

At the studied pressure range, the only trial that seemed not be tending to an overcompression plateau was trial 6 – 4 mm and 7 kN/cm, which was supported by its low estimated SF at gap (Table 3.1). Oppositely, trial 5 (4 mm and 3 kN/cm), which was estimated and model predicted to be the lowest SF at gap trial, both granules from MF and LAB tabletability profiles are reaching over compression, which should not be expected. Nevertheless, until overcompression was reached, the lab granules present higher tabletability, probably as a result of a broader size distribution of granules, as seen in the sieve-shaker results. At a given point, the compaction pressure (~300 MPa) was so high that the coarser granules fragmentation neutralized this higher tabletability effect seen at lower compaction pressures. However, the opposite trend was observed for trial 6 and 7, regardless the lab granules yielded a substantially lower fines content than the mf granules, similarly to trial 5. This way, the results demonstrate that tabletability was

independent of the granules size distribution. The difference between the granules origin tabletability was more evident when a larger gap was selected 2, 4 and 6 mm, regardless the MF granules size distribution always revealing significantly higher fines content.

The test from 2 mm gap and 7 kN/cm force was expected to be the first to achieve over compression for both formulations since it had the highest density at gap, which was observed. Furthermore, when compared to the compacts obtained from other RC conditions, these seems to be the less tabletable as a result of a lower tensile strength for a specific compaction pressure.

Regarding central conditions, 3 mm gap and 5 kN/cm force, over compression seems to be achieved. Also, the slugging performed with the 16x10 mm tooling seems to produce more robust tablets. Compared to the 24 mm, across the experimental pressure range.

By comparing both formulations, PVPVA reveals to be more tabletable than HPMCAS, for the reason that it produces more robust tablets, at the studied compaction pressure range as displayed in Figure 3.18.

Legend:

- HPMCAS - Lab granules
- HPMCAS - MF granules
- PVPVA - Lab granules I
- PVPVA - Lab granules II
- PVPVA - MF granules
- PVPVA - MF granules (70 RPM)
- PVPVA - Lab granules (Slugging 24mm)
- PVPVA - Lab granules (Slugging 16x10mm)

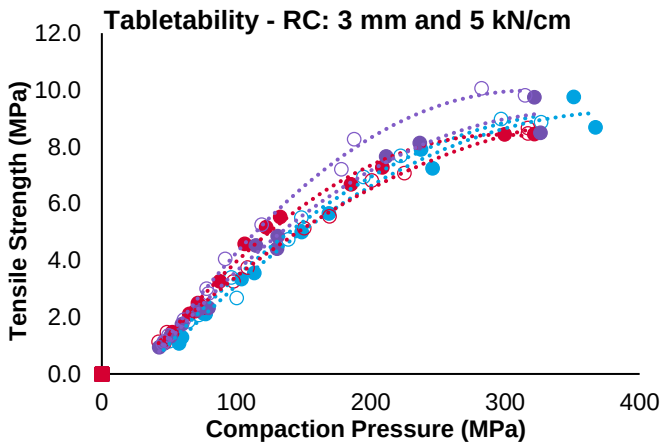

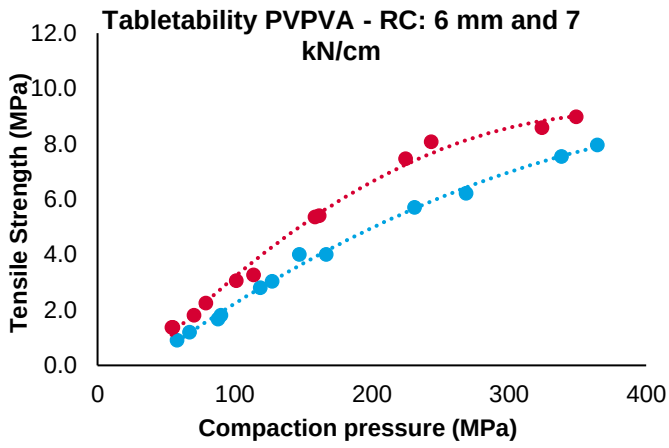

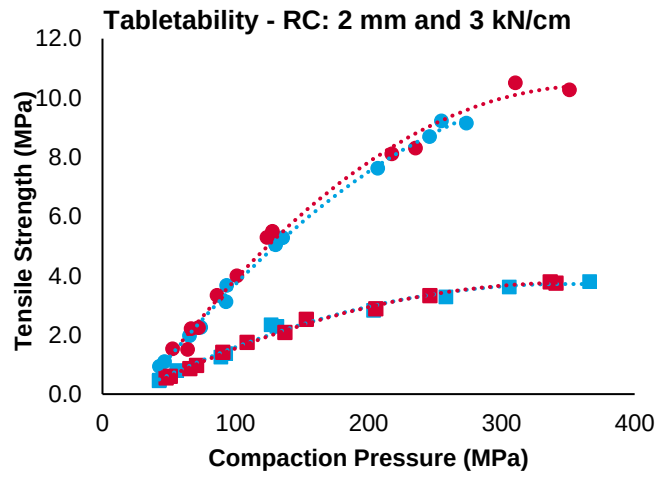

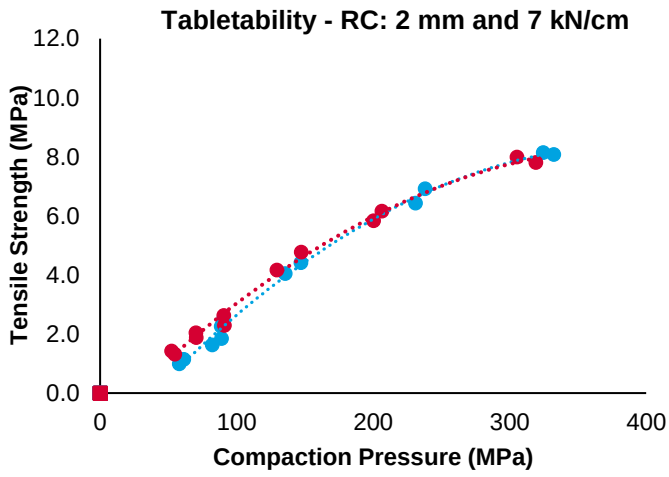

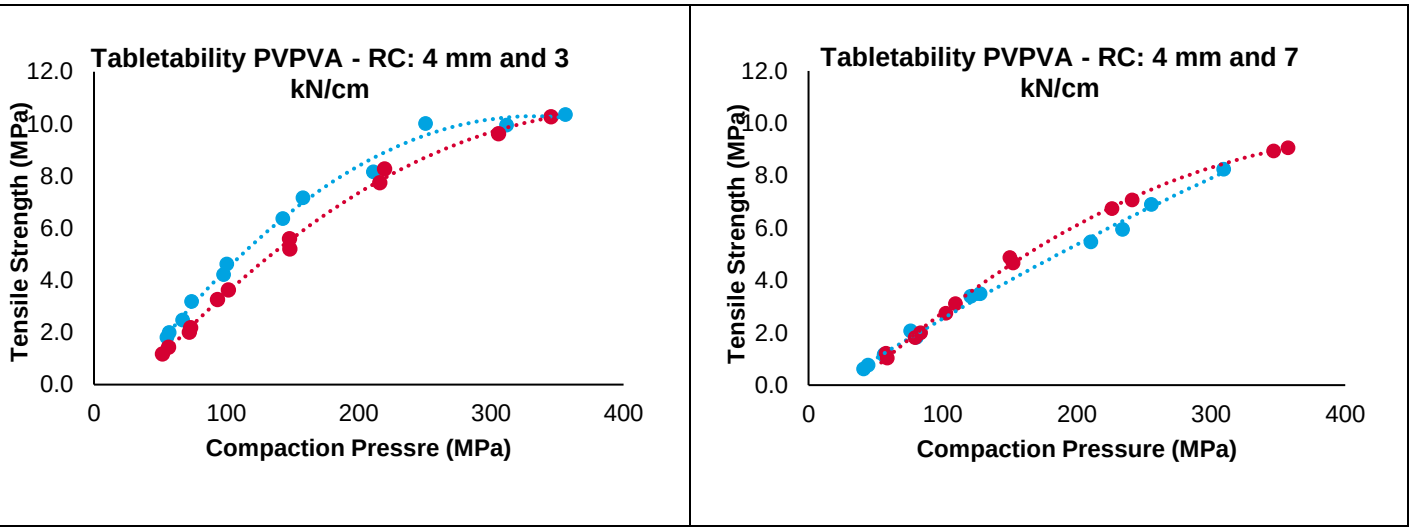

Figure 3.18 – Tabletability results for HMPCAS and PVPVA formulations.

3.4.3. Compressibility

Among polymers, HPMCAS represented higher yield strength values for the same RC conditions related to HPMCAS. Since HPMCAS presents higher elastic deformation behavior, it was expected to contain a higher yield pressure as it requires more force to overcome elastic deformation and begin to plastically deform. The compressibility differences between in die and out of die, in Figure 3.19, display that, during in die compaction, HPMCAS presents a higher compressibility, however, when the tablets are ejected from die, viscoelastic recovery acts and, out of die, PVPVA based formulation was more compressible.

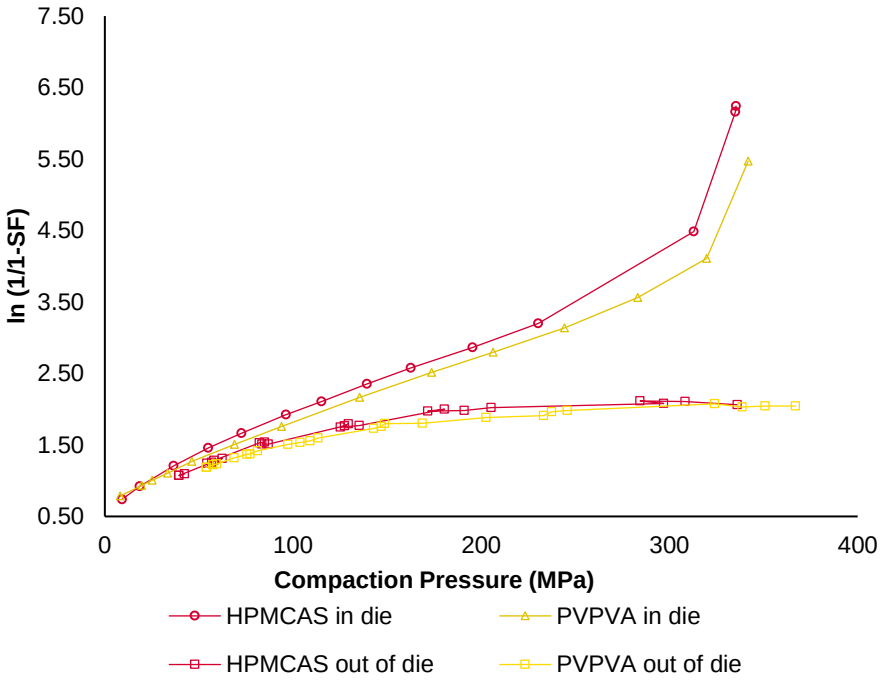

Figure 3.19 – Heckel in die and out of die plot for HPMCAS and PVPVA based formulations.

Yield pressure for both formulations was calculated according to Equation 1.12. The equation was applied on a pressure range between 60 and 100 MPa which should correspond to the linear phase, in order to normalize all the data and while not including data points near overcompression nor near rearrangement phase. The results are shown below in Figure 3.20.

PVPVA, which also acts like a tablet binder[28], was expected to present a lower yield pressure, suggesting it deforms similar to a brittle material, more by fracture than plastic deformation. In other words, tends to absorb the stress applied as plastic energy easier than HPMCAS, with increasing applied pressure. Although the pressure range used for yield pressure determination can be prone to error, these findings were verified, and thus, HPMCAS presents a higher compressibility.

Regarding RC conditions, for PVPVA and HPMCAS, RC force 5 kN/cm and gap 3 mm and force 7 kN/cm and gap 2 mm, respectively, generated the lowest variability in yield pressure, which was supported by the similar granule sizes distribution independently of the milling site, for this particular trial.

For trial 1, both polymers, show a decrease in yield pressure when comparing Lab granules to these from MF. The lower plastic deformation tendency (higher yield pressure) for larger granules compared to minor MF granules, at this pressure range, can be explained by opposition to dense packing (energy required to fragment larger granules), and therefore presenting a higher yield pressure.[95]

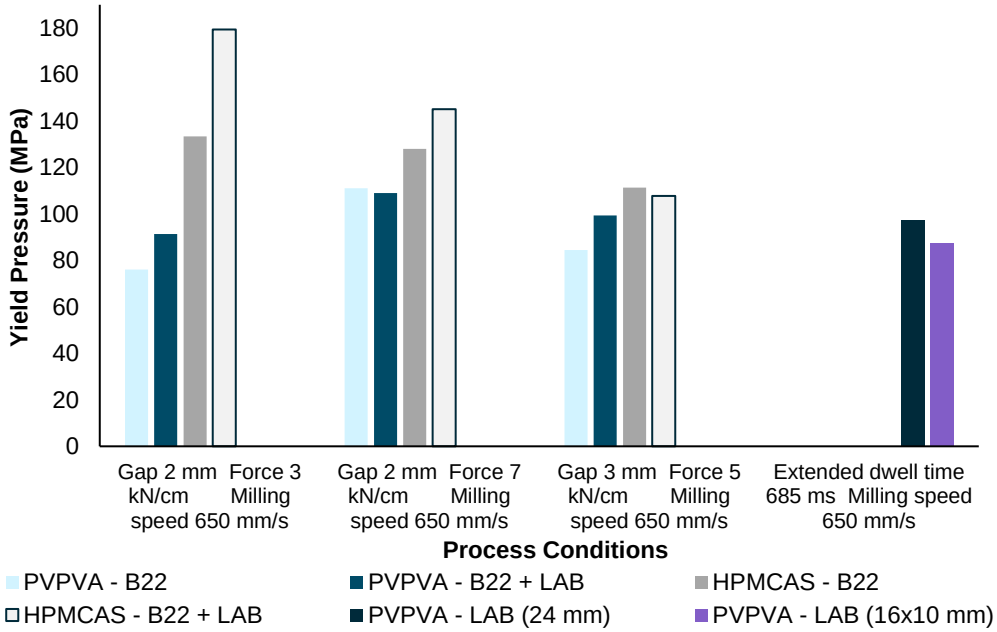

Figure 3.20 – Yield pressure estimation results.

3.4.3.1. *Strain rate sensitivity*

The impact of strain rate sensitivity was assessed for HPMCAS, in tablets yielded from RC 2 mm gap and 7 kN/cm force. A dwell time and a 30 RPM simulated rotary press versus no dwell time constant speed of 30 mm/s punch displacement profiles were compared. The results shown below in Figure 3.21, indicate that the dwell time allows particle to fragment and bond together for a fixed period of time, hence obtaining a higher compressibility for a specific compaction pressure compared to constant speed compaction, where no time is provided for the particles to deform and create new bonding areas.

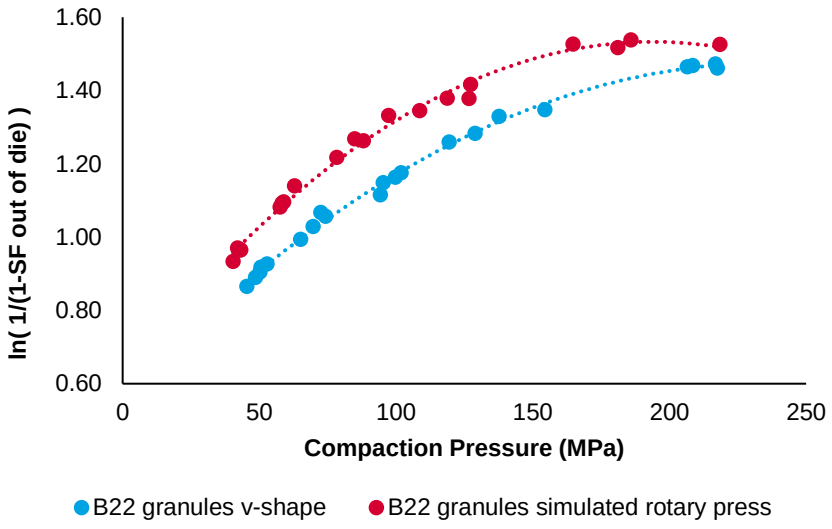

Figure 3.21 – Heckel plot: strain rate sensitivity analysis for HPMCAS: RC: 2 mm gap and 7 kN/cm force.

3.4.3.2. *Elastic recovery*

According to the results in Figure 3.22, from a mechanical point of view, the PVPVA based formulation displays substantially less elastic expansion than that of HPMCAS, which was also supported in having produced more robust tablets. This leads to the conclusion that formulations with PVPVA SDD may be more suitable when it is intended to achieve a specific SF in die, since the thicknesses deviation and, consequently, SF out of die vs out of gap after expansion will be less, compared to a polymer based SDD with a more elastic behavior, such as HPMCAS.

Among a specific polymer, the RC conditions or milling parameters, did not play a significant impact in terms of elastic recovery. The only exception, was for PVPVA, trial 7 (7 kN/cm force and 6 mm gap) that until ~175 MPa of compaction pressure seems to be the trial with the higher elastic recovery. A possible explanation was that this trial was yielded from the largest RC gap tested and consequently yielded larger granules. Furthermore, this trial was also milled at the lab, so it had a lower fines content, thus at low compaction stresses it is more hard to fragment larger granules. As compaction pressure continues to increase, these granules start to fragment and elastic recovery becomes independent of the particle size.

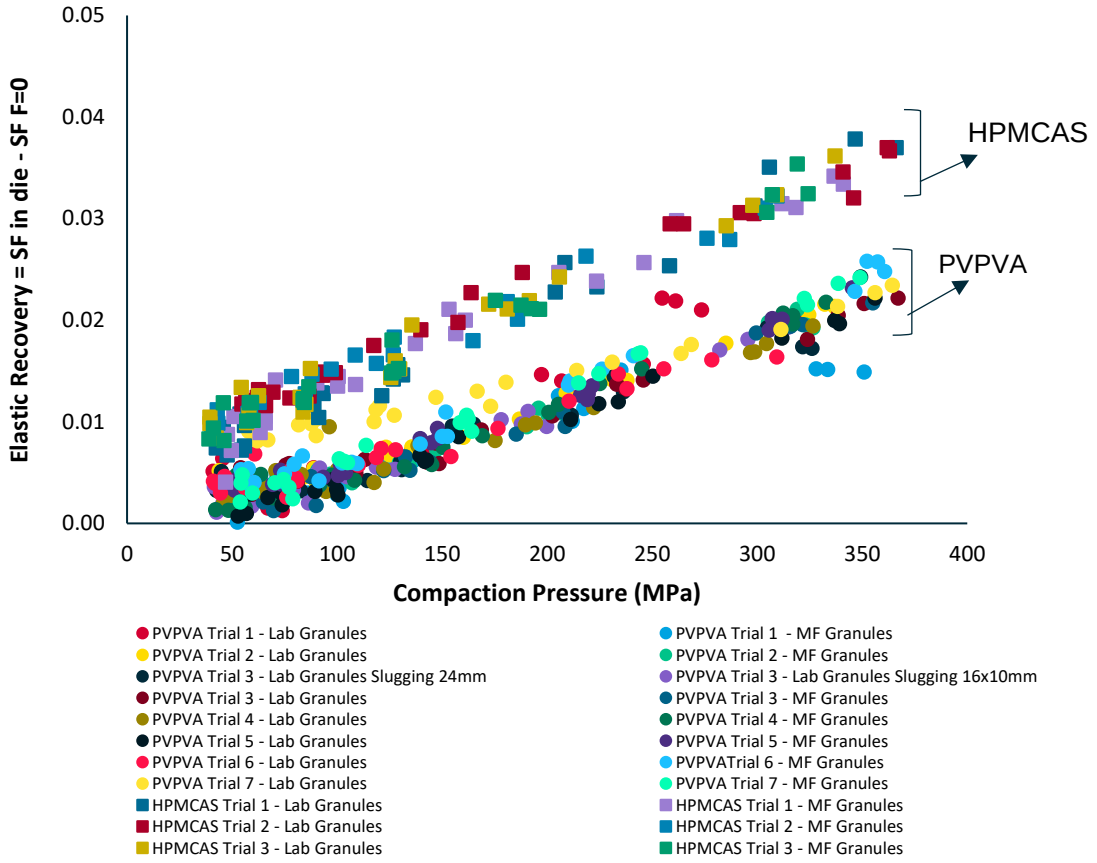

Figure 3.22 – Elastic recovery for 7 mm round convex tablets at 30 RPM simulated rotary press – PVPVA (o) and HPMCAS (□).

3.4.3.3. *Viscoelastic recovery*

Viscoelastic recovery was already studied in the past[72], for three different formulations with different physical properties, using both constant speed (no dwell time) and simulated rotary press (with dwell time) compaction profiles. Akin to that study, in this thesis (Figure 3.23), visco-elastic recovery revealed to have a decreasing tendency as a function of compaction pressure, however the correlation coefficients (R^2) in this thesis were not accurate enough to predict the viscoelastic recovery only based on a high and low compaction pressure tablets. The results for viscoelastic recovery in figure below, demonstrate that, similarly to elastic recovery, there was not a trend observed between viscoelastic recovery and RC parameters or milling parameters.

Additionally, the HPMCAS formulation (square data) tends to have a higher viscoelastic expansion related to PVPVA (circles data) at a given compaction pressure.

As compaction pressure increased, viscoelastic recovery decreases owing to elastic energy that was being absorbed into plastic energy, in other words, stress relaxation. Comparing the two polymers, PVPVA presents less expansion after being ejected from die due to a fewer elastic behavior, compared to HPMCAS based formulation.

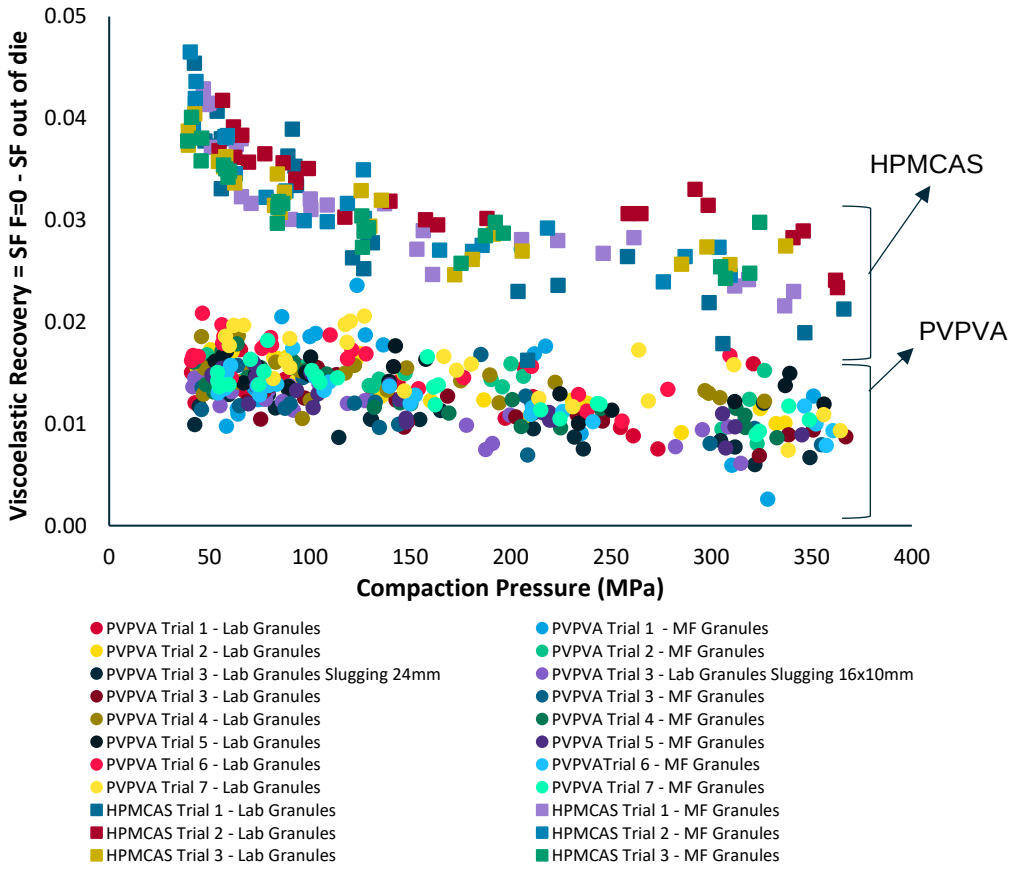

Figure 3.23 – Viscoelastic recovery, corrected from elastic recovery, using a set of 7 mm round concave punches at 30 RPM simulated rotary press – PVPVA (o) and HPMCAS (□).

3.4.4. Friability and disintegration

Friability and disintegration tests were only done for half of the blends obtained due to equipment usage time limitations (results are in Figure 3.24 and Figure 3.25). HPMCAS based formulation tablets were both more easily friable and faster disintegrating under the same conditions.

Since HPMCAS is an enteric polymer it explains its quick disintegration times. Also, for higher SFs it takes more to disintegrate, since there is less porosity it is more difficult for the

disintegration medium to penetrate and cause the disintegrant to swell. For PVPVA, swelling was observed for tablets with higher porosity in comparison to the denser tablets, however, as PVPVA is a non-enteric polymer it generated much longer disintegration times, comparing to HPMCAS.

Regarding HPMCAS friability results, less dense tablets individually overtook the friability limit of 1.00% weight loss. For PVPVA, all tablets did not lose >0.5% of its initial weight. In fact, some of the samples increased their weight after being submitted to the test drum which may be due to moisture absorbed into the tablets, since at 50% relative humidity, PVPVA can gain up to 10% weight.[28]

Typically, to select the optimal operational zone, the friability and disintegration data are normalized against tablets SF out of die and tensile strength in order to obtain a range where neither friable tablets (ideally less than 0.5% friability) nor high disintegration times are obtained.

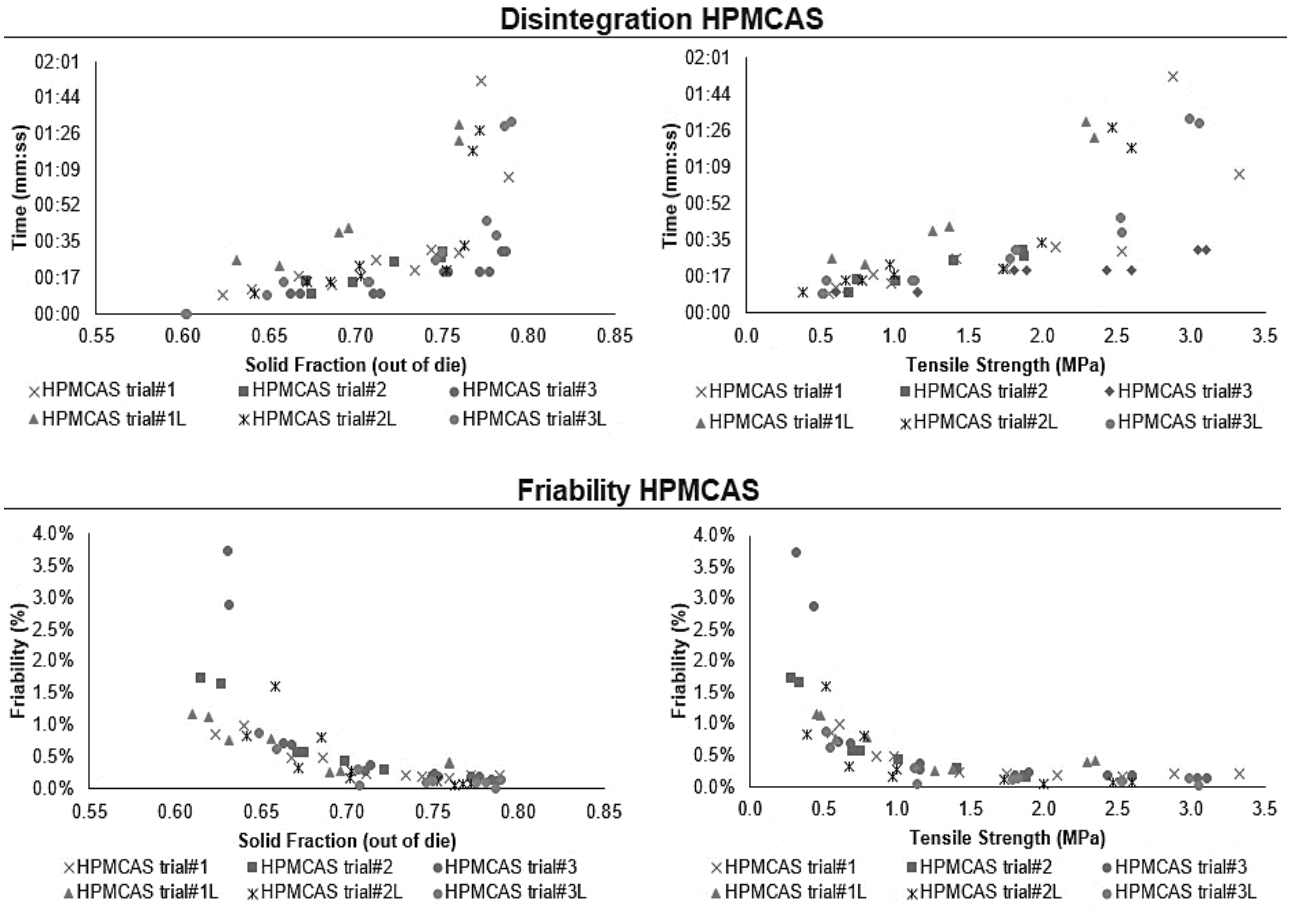

Figure 3.24 – Disintegration and Friability results for HPMCAS based formulation.

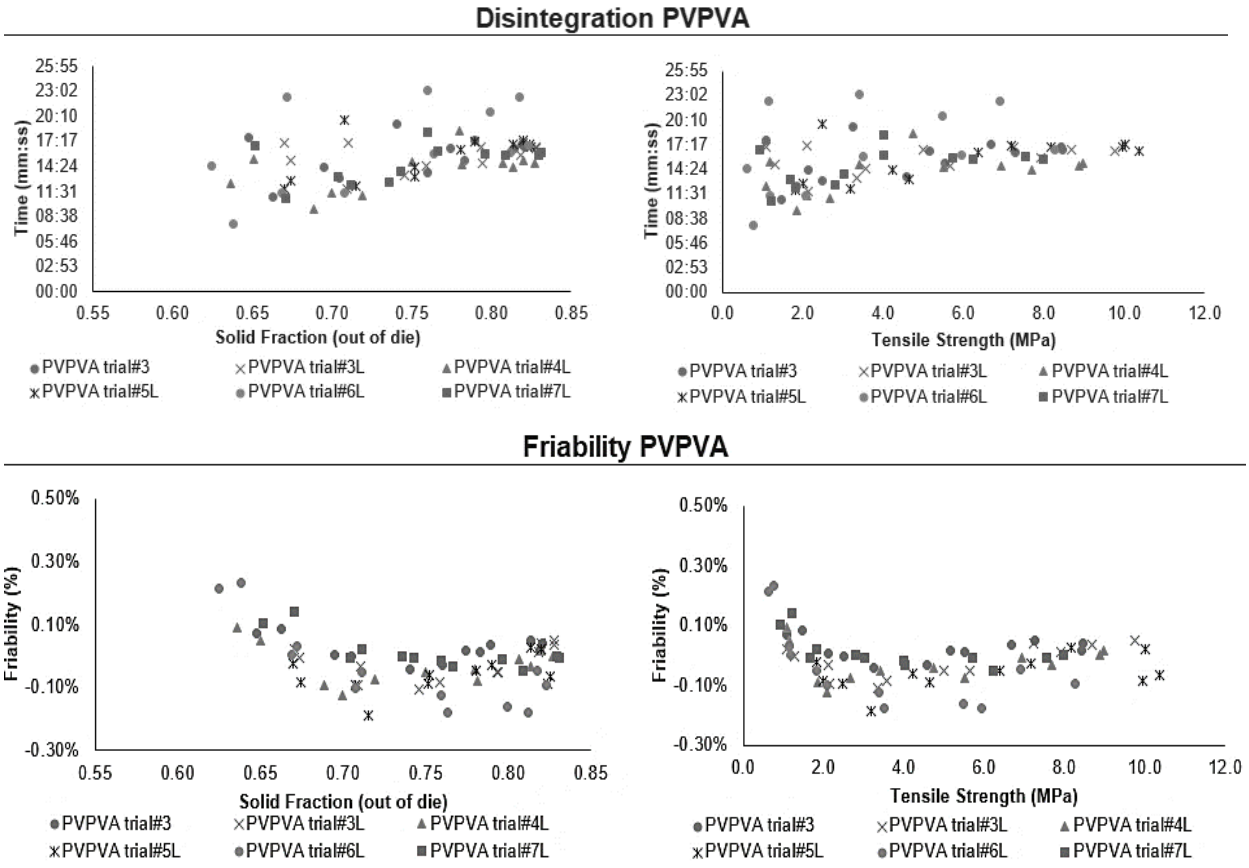

Figure 3.25 – Disintegration and Friability results for PVPVA based formulation.

3.5. Study 5: Pilot-plant tableting – study of the feeding parameters

3.5.1. Study of the feeding parameters

Feeder and Turret speed – Here, the goal was to identify until which point it was possible to maximize the productivity of tablets without compromising the content uniformity by having undesired weight variations. The tablets were further produced, using two different toolings, 7 mm round convex and 16x10 mm oval convex and the target weights were 125 and 800 mg, respectively.

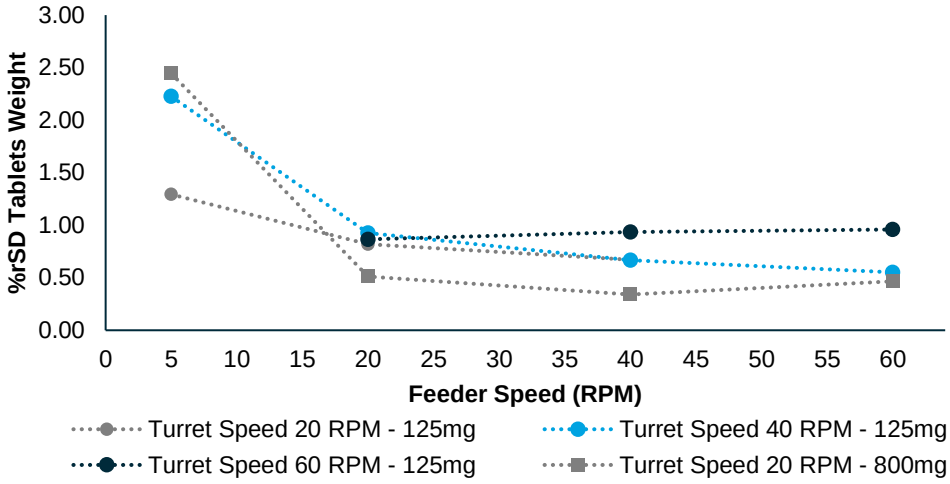

Figure 3.26 – Effect of turret and feeder speed on tablets' weight variation.

The goal was to assess 3 turret (20, 40 and 60 rotation per minutes (RPM)) and 4 feeder speeds (5, 20, 40 and 60 RPM) for each tooling, but due to insufficient material, only one turret speed was assessed for the 800 mg tablets. Figure 3.26 shows that the relative standard deviation was higher when the feeder speed is 5 RPM and tends to increase with turret speed. At 60 RPM turret speed the powder could not be uniformly fed into the die, hence the target weight was not achieved, which is in agreement with the work of Tang et al.[96], which also studied feeding parameters using a Korsch XL 100 Pro, as in this thesis.

When the feeder and turret speed were 5 and 20 RPM, respectively, the weight variability increased with tooling's size.

For Feeder Speeds above 5 RPM, the %RSD was below 1% in all experiments, showing less weight variations. For 125 mg tablets, turret 20 RPM and Feeder 60 RPM was not performed due to excessive powder feeding - the powder was projected from the feeder, due to the high feeding rate.

All the tablets weighed from each trial were within the European Pharmacopoeia weight variation test limits as displayed in Table 2.6.

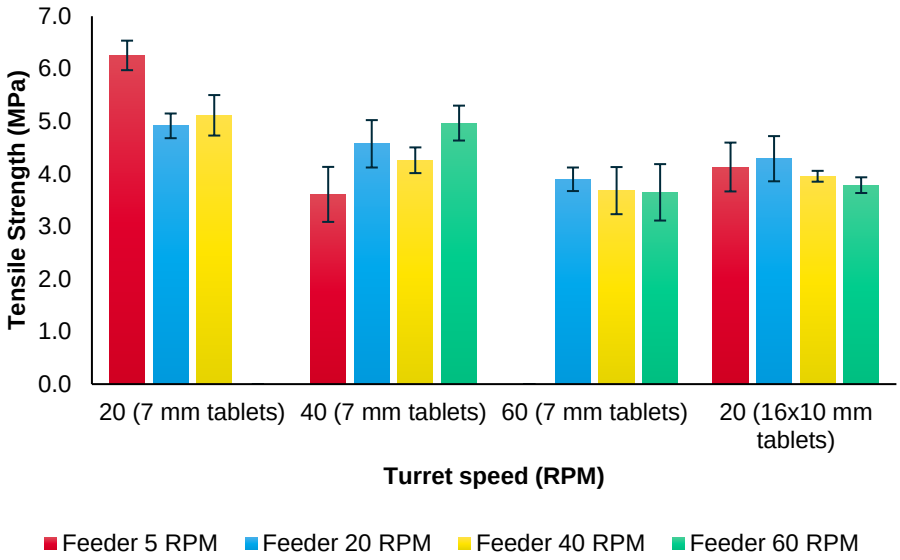

Figure 3.27 – Tensile strength as a function of feeding parameters.

Accordingly to [74], the results in Figure 3.27 demonstrate that, as the turret speed decreases so tensile strength for the reason that a higher turret speed causes a decrease in dwell time, assuming that the process was adjusted so that all tablets were produced at the same compaction force.

The set of feeder speeds studied for 60 RPM turret speed, present the tighter variability, however, yielding the less robust tablets as consequence of a reduced dwell time (higher turret speeds lead to shorter dwell time as discussed in section 1.6.3).

3.5.2. STYL'One NANO and Korsch XL-100 Pro – Compactability comparison

Amongst MF facilities tablets, the results display that tensile strength the 800 and 125 mg compactability data overlaps, independently on the tablets size. The curves were expected to be overlapping since it has been demonstrated that SF versus TS should be the blend's "footprint" as it does not depend on the dwell time nor the shape and size of the selected punches.[74]

Comparing the tablets yielded at MF versus LAB, using the same set of tooling 7 mm round convex tablets, the Lab tablets are more compactable. However, their hardness was measured on a different apparatus than the MF tablets (Figure 3.28). To assess this, 10 specimens from each trial were sampled for hardness and SF calculation in Lab. The results reinforce that, after normalizing the hardness by measuring on a single apparatus, it is crucial that the hardness testers both at lab and MF must be calibrated on a regular basis to avoid future significant deviations similar to the displayed above in Figure 3.28 and 3.29. Regarding the 800 mg tablets, the hardness could not be measured in the lab hardness tester since it overpassed the apparatus force limit and the tablets were not able to break.

Regarding feeding parameters, emphasis on 5 and 20 rotations per minute feeder and turret speeds, respectively that noticeably yielded the stronger tablets. This resulted from a combination of slower feeding and higher dwell times allowing an efficient homogeneous die filling and bonding area establishment, respectively, when compared to the other conditions tested. (Figure 3.29).

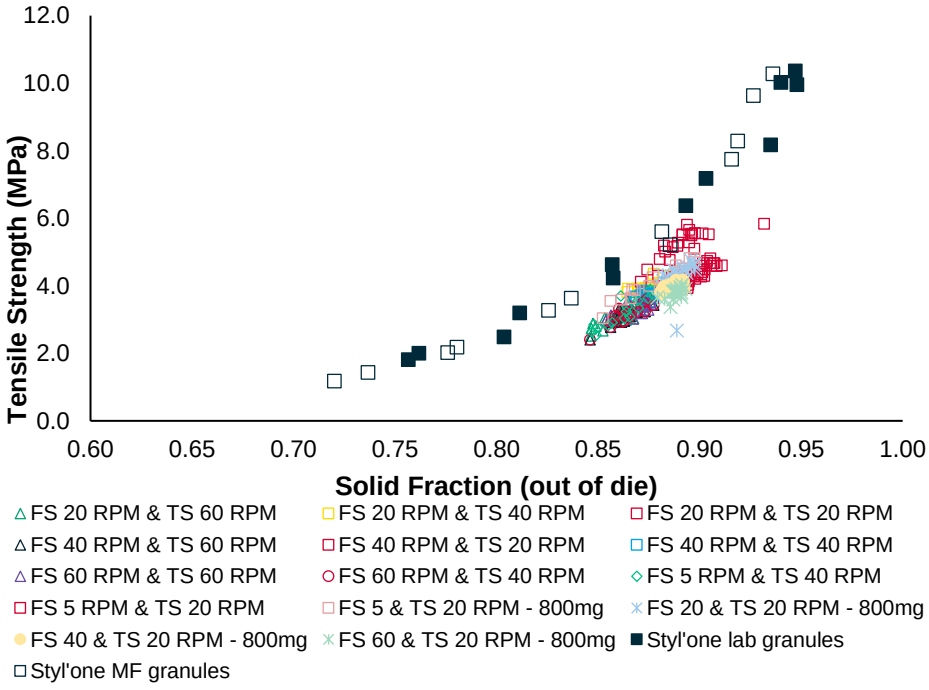

Figure 3.28 – Tablets comparison yielded from the same RC settings with hardness measured on different sites. FS denotes Feeder Speed and TS denotes Turret Speed.

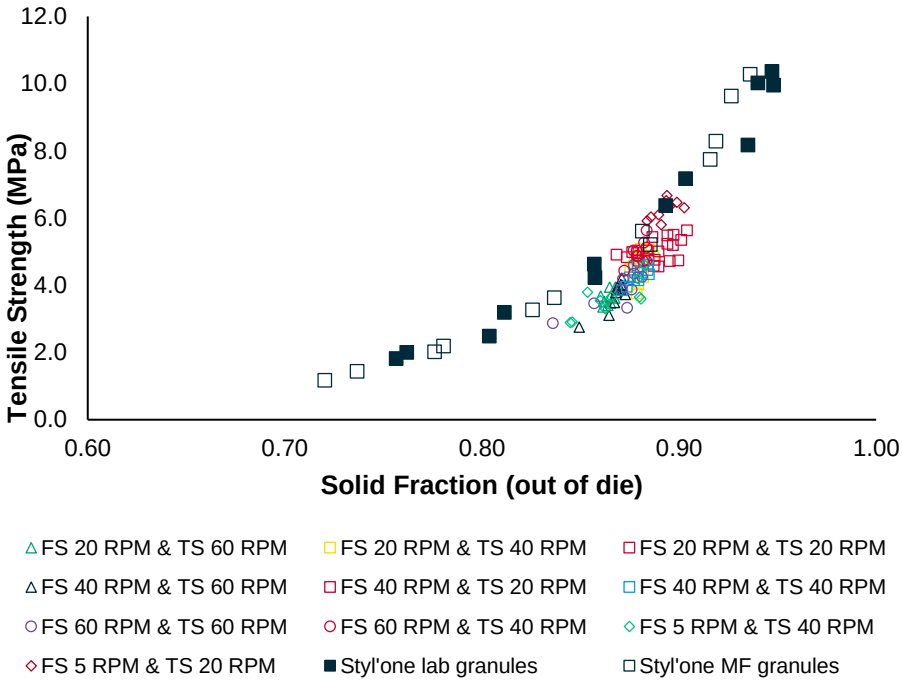

Figure 3.29 – Tablets comparison yielded from the same RC settings with hardness measured on Lab. FS denotes Feeder Speed and TS denotes Turret Speed.

Different feeding conditions were tested at the MF pilot scald rotary press. Figure 3.29 illustrates that a Feeder Speed and Turret speed of 5 and 20 RPM, respectively, are the more accurate representation of the die filling by hand at the lab. This was expected since this condition presents the slowest feeding speed, hence enabling the granules to uniformly flow and fill the die. Additionally, in terms of turret speed, the dwell time from 30 RPM simulated rotary press runs at the lab (~124 ms) was very similar to the calculated dwell time from 20 RPM turret speed (129.5 ms) (as in Table 2.5).

As for the other tested conditions the tensile strength for a specific SF was lower due to both faster die filling and lower dwell times, as a result of non-uniform die filling and less granules consolidation time.

The results demonstrate that MF tableting can be successfully mimicked at lab when a combination of 5 RPM feeder and 20 RPM turret speed at MF are selected.

3.5.3. SF estimation sensitivity analysis

Another source of deviation might be the assumed punch and die hole specific dimensions used in the SF calculations. After contacting the punches supplier, it was assessed that cup volumes were not accurate, when a value of 17.88 mm^3 and 94.87 mm^3 were being adopted instead of 13.44 mm^3 and 68.31 mm^3 for the 7 mm round convex and 16x10 mm oval convex toolings, respectively. This played a significant impact in both the smaller and larger toolings.

This was evaluated by varying the tablet's wall to cup height ratio, assuming a typical 125 mg weight for the 7 mm round concave punches and a 600 mg weight for the 16x10 mm oval concave punches, in Figure 3.30 and Figure 3.31, respectively. It was observed that:

- With varying wall to cup ratios, between the minimum dimensions and the maximum dimensions, provided by the supplier, a non-significant difference was found. Furthermore, increasing the wall to cup ratio to, decreases this impact;
- A major difference was found in SF estimation when using the previous and the current corrected cup volumes, especially if targeting to higher SF values.
- The difference was more substantial concerning larger tooling.

Impact on SF can be mitigated by selecting a flat tooling to compress, for R&D purposes. Once the compaction range is studied, further non-flat tooling can be used for studying tablet performance (*i.e.* bio relevant dissolution, disintegration, friability tests).

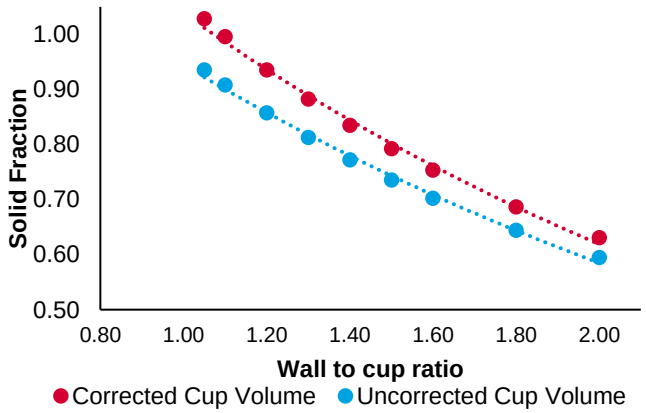

Figure 3.30 – Sensitivity analysis to tooling dimensions in SF calculation, for 7 mm round concave tooling.

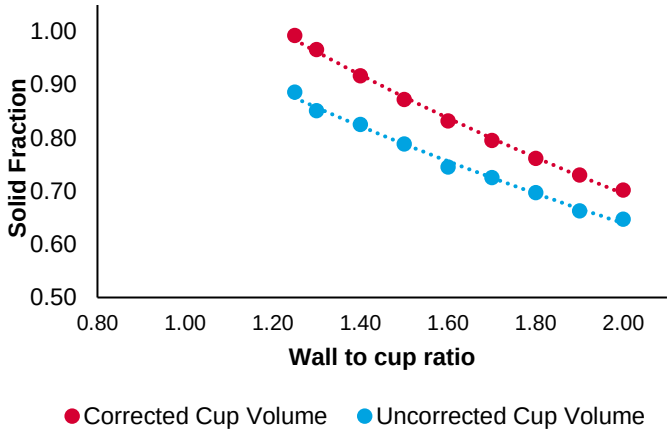

Figure 3.31 – Sensitivity analysis to tooling dimensions in SF calculation, for 16x10 mm oval concave tooling.

3.5.4. MF tablets: Disintegration and Friability results

Disintegration testing was done according to 0. The manufacturing tablets' friability was performed according to the USP Pharmacopoeia method as stated in 2.12.2. The results are displayed Figure 3.32, where 125 mg are represented in blue and red circles and 800 mg tablets in yellow circles.

The friability between MF and Lab tablets seems to be well aligned independently on the tooling used. On the other hand, for disintegration results, the 800 mg took longer to fully disintegrate due to a larger dosage size.

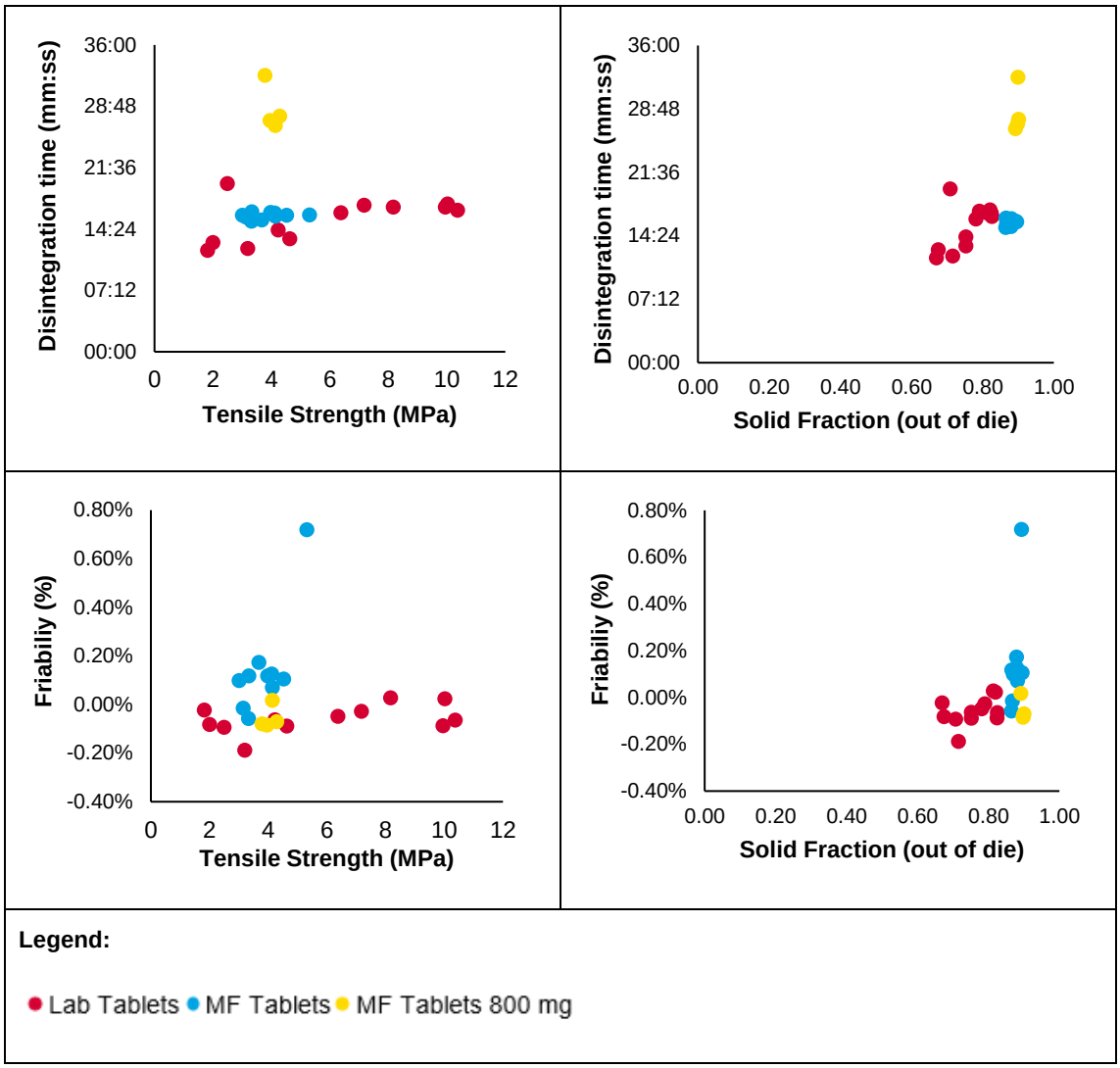

Figure 3.32 - Lab and MF tablets disintegration and friability results.

4

Conclusions

The experimental plan was successfully executed. Some trials were not performed due to material or time constraints. Nevertheless, the main goals of the work were addressed. The main conclusions were the following:

Regarding the RC studies, the ribbons SF at gap was estimated via throughput. By comparing the data with RC model predictions, calibrated using in die data from compaction simulation, the model was successfully validated. Although the model considers flat rolls to predict SF at gap, by correcting the area at gap, the relative deviation from the model decreased. The estimated SF at gap is overestimated, since some fines bypassed the compaction area. This was further confirmed by granules size distribution results, as granules from MF contained a higher fines fraction than those yielded from Lab.

The ribbon and slugs SF in-die/out-of-die data presented a similar off-set regardless of the polymer and SDD loading, using this thesis and project A data, even when correcting the compaction area from the rolls indentation's depth, which played a more significant impact at lower rolls gap.

By guaranteeing the same milling tip speed, Lab milling step can mimic the milling step in RC at MF – granules from lab and MF yielded the same size distribution and tableting CTC pro-

files. Additionally, changing lab milling tip speed and feed rate did not significantly affect the granules size distribution nor the Hausner ratio. Fixing the milling conditions, granules' size was found to increase with compaction force at a fixed gap, as a result of SF at gap increase. Nevertheless, regarding rheology, both formulations predominantly presented fairly/passable flow characteristics (typical dry granulation range), independently on the RC force and gap.

Concerning tableting, it was demonstrated that MF tableting can be mimicked at lab. Additionally, the PVPVA formulation yielded more robust tablets, owing to lower friability and higher tensile strength for a specific compaction pressure and SF. In terms of compressibility, out of die PVPVA delivered more compressible tablets indicating more deformation behavior through brittle facture than HPMCAS. In die, HPMCAS presented higher compressibility, representing easier plastic deformation. However, when compaction pressure was released (out of die), HPMCAS's elastic and viscoelastic recovery was higher than PVPVA tablets. For HPMCAS, a strain rate sensitivity analysis was carried out and it was concluded that tensile strength remained unchanged for a specific solid fraction, independently of the compaction time profile.

A scale-up methodology was proposed to enable right-first-time scale-up from lab to MF, based on out of die compressibility profiles, described by Heckel's equation, where negligible impact was found by varying dwell time.

5

Future Work

Based on this thesis work, some considerations concerning future work are presented below:

Predicting a formulation's elastic recovery can be key for scale-up from LAB to MF, since granules from slug and ribbons with the same SF out of die and SF out of gap, respectively resulted in tablets with similar tableting properties.

An additional proposal is to acquire a device to measure ribbons' tensile strength[39]. This would allow comparing compactability profiles of slugs and ribbons, regardless of the manufacturing conditions (*i.e.* dwell time, densification time, compaction pressure,). The aim would be that the slugs' tensile strength remains the same as the ribbons at a specific SF (ideally, both in and out of die).

Further, bio relevant dissolution profiles would be studied by incorporating a model API in the optimal trials.

Additionally, the use of flat rolls should be assessed, as it eliminates the need to correct the area term when estimating SF at gap via throughput and, thus, enabling a constant area at gap. However, caution should be made when changing to flat rolls, as this can hinder flowability to the gap and, therefore, yield non-uniform SF among ribbons.

Finally, in the future, new tests should be performed using a new RC sealing system, to assess if fines content visually bypassing the compaction zone persists. This is to be confirmed mainly by further comparing slugs and ribbons SF profiles and also by comparing lab granules with MF granules particle size distributions.

6

References

[1] Sousa, R., Valente, P. C., Nakach, M., Bardet, L., Wacquet, M., Midoux, N., Authelin, J.R., "Roller Compaction Scale-Up Made Simple: An Approximate Analytical Solution to Johanson's Rolling Theory," *J. Pharm. Sci.*, 2020, doi: 10.1016/j.xphs.2020.05.004.

[2] Drugs Development & Approval Process, "Through Innovation New Drug Therapy Approvals 2019," *U.S. Food Drug Adm.*, no. January, pp. 1–44, 2020.

[3] R. R. N. Teja Dasari, Sai Lakshmi Jyothirmai Kala, "In process quality control tests of solid dosage forms: a comprehensive review," *Sch. Acad. J. Pharm.*, vol. 6, no. 6, pp. 273–280, 2017, doi: 10.21276/sajp.

[4] FDA, "2017 New drug approvals," *U.S. Food Drug Adm.*, vol. 315, no. 7109, p. 689, 2017, doi: 10.1136/bmj.315.7109.689.

[5] Centre for Drug evaluation and Research (CDER), "Advancing Health Through Innovation New Drug Therapy Approvals 2018," 2019.

[6] I. Duarte, "Development of new screening methodologies and preparation methods with application in amorphous solid dispersions and pharmaceutical cocrystals," p. 3, 2016.

[7] I. Nikolakakis and I. Partheniadis, "Self-Emulsifying granules and pellets: Composition and formation mechanisms for instant or controlled release," *Pharmaceutics*, vol. 9, no. 4, 2017, doi: 10.3390/pharmaceutics9040050.

[8] Anne Newman, "Pharmaceutical Amorphous Solid Dispersions," in *Pharmaceutical Amorphous Solid Dispersions*, 2015, p. 488.

[9] F. Cao, J.-X. Guo, Q.-N. Ping, and Z.-G. Liao, "Prodrugs of scutellarin: Ethyl, benzyl and N,N-diethylglycolamide ester synthesis, physicochemical properties, intestinal metabolism and oral bioavailability in the rats," *Eur. J. Pharm. Sci.*, vol. 29, no. 5, pp. 385–393, 2006, doi: https://doi.org/10.1016/j.ejps.2006.07.007.

[10] S. Maragos, H. Archontaki, P. Macheras, and G. Valsami, "Effect of cyclodextrin complexation on the aqueous solubility and solubility/dose ratio of praziquantel," *AAPS*

PharmSciTech, vol. 10, no. 4, pp. 1444–1451, 2009, doi: 10.1208/s12249-009-9346-7.

[11] K. Čerpnjak, A. Z. Pobirk, F. Vrečer, and M. Gašperlin, “Tablets and minitablets prepared from spray-dried SMEDDS containing naproxen,” *Int. J. Pharm.*, vol. 495, no. 1, pp. 336–346, 2015, doi: https://doi.org/10.1016/j.ijpharm.2015.08.099.

[12] R. H. Müller, S. Gohla, and C. M. Keck, “State of the art of nanocrystals – Special features, production, nanotoxicology aspects and intracellular delivery,” *Eur. J. Pharm. Biopharm.*, vol. 78, no. 1, pp. 1–9, 2011, doi: https://doi.org/10.1016/j.ejpb.2011.01.007.

[13] R. Thakuria, A. Delori, W. Jones, M. P. Lipert, L. Roy, and N. Rodríguez-Hornedo, “Pharmaceutical cocrystals and poorly soluble drugs,” *Int. J. Pharm.*, vol. 453, no. 1, pp. 101–125, 2013, doi: https://doi.org/10.1016/j.ijpharm.2012.10.043.

[14] B. C. Hancock and M. Parks, “What is the True Solubility Advantage for Amorphous Pharmaceuticals?,” *Pharm. Res.*, vol. 17, no. 4, pp. 397–404, 2000, doi: 10.1023/A:1007516718048.

[15] K. Wlodarski, F. Zhang, T. Liu, W. Sawicki, and T. Kipping, “Synergistic Effect of Polyvinyl Alcohol and Copovidone in Itraconazole Amorphous Solid Dispersions,” *Pharm. Res.*, vol. 35, no. 1, 2018, doi: 10.1007/s11095-017-2313-1.

[16] A. Singh and G. Van den Mooter, “Spray drying formulation of amorphous solid dispersions,” *Adv. Drug Deliv. Rev.*, vol. 100, pp. 27–50, 2016, doi: 10.1016/j.addr.2015.12.010.

[17] D. Psimadas, P. Georgoulias, V. Valotassiou, and G. Loudos, “Molecular Nanomedicine Towards Cancer :,” *J. Pharm. Sci.*, vol. 101, no. 7, pp. 2271–2280, 2012, doi: 10.1002/jps.

[18] Í. Duarte, J. L. Santos, J. F. Pinto, and M. Temtem, “Screening methodologies for the development of spray-dried amorphous solid dispersions,” *Pharm. Res.*, vol. 32, no. 1, pp. 222–237, 2015, doi: 10.1007/s11095-014-1457-5.

[19] H. Sandhu, N. Shah, H. Chokshi, and W. A. Malick, “Overview of Amorphous Solid Dispersion Technologies,” in *Amorphous Solid Dispersions: Theory and Practice*, N. Shah, H. Sandhu, D. S. Choi, H. Chokshi, and A. W. Malick, Eds. Springer-Verlag New York, 2014, pp. 91–122.

[20] K. Masters, *Spray Drying in Practice*. SprayDryConsult, 2002.

[21] B. B. Patel, J. K. Patel, and S. Chakraborty, “Review of patents and application of spray drying in pharmaceutical, food and flavor industry.,” *Recent Pat. Drug Deliv. Formul.*, vol. 8, no. 1, pp. 63–78, Apr. 2014, doi: 10.2174/1872211308666140211122012.

[22] R. Vehring, “Pharmaceutical particle engineering via spray drying,” *Pharm. Res.*, vol. 25, no. 5, pp. 999–1022, 2008, doi: 10.1007/s11095-007-9475-1.

[23] J. Elversson and A. Millqvist-Fureby, “Particle size and density in spray drying-effects of carbohydrate properties.,” *J. Pharm. Sci.*, vol. 94, no. 9, pp. 2049–2060, Sep. 2005, doi: 10.1002/jps.20418.

[24] J. Elversson, A. Millqvist-Fureby, G. Alderborn, and U. Elofsson, “Droplet and particle size relationship and shell thickness of inhalable lactose particles during spray drying.,” *J. Pharm. Sci.*, vol. 92, no. 4, pp. 900–910, Apr. 2003, doi: 10.1002/jps.10352.

[25] S. Poozesh and E. Bilgili, “Scale-up of pharmaceutical spray drying using scale-up rules: A review,” *Int. J. Pharm.*, vol. 562, no. January, pp. 271–292, 2019, doi: 10.1016/j.ijpharm.2019.03.047.

[26] P. D. Hede, P. Bach, and A. D. Jensen, “Two-fluid spray atomisation and pneumatic nozzles for fluid bed coating/agglomeration purposes: A review,” *Chem. Eng. Sci.*, vol. 63, no. 14, pp. 3821–3842, 2008, doi: 10.1016/j.ces.2008.04.014.

[27] P. Walzel, “Influence of the spray method on product quality and morphology in spray drying,” *Chem. Eng. Technol.*, vol. 34, no. 7, pp. 1039–1048, 2011, doi: 10.1002/ceat.201100051.

[28] R. C. Rowe, P. J. Sheskey, and et al, *Handbook of Pharmaceutical Excipients Fifth edition*. 2006.

[29] F. Alanazi and A. A. Sakr, “Oral Solid Dosage Forms,” in *Remington Essentials of Pharmaceutics*, 2013, pp. 581–610.

[30] G. Sri Divya, K. Geetha, A. Pratyusha, and V. Uma Maheshwar Rao, “Development of Suitable Pharmaceutical Dosage forms through Herbal Plant Extract,” *Icjpir*, vol. 2, no. 3, pp. 49–58, 2015.

[31] S. Page and R. Maurer, “Downstream Processing Considerations,” in *Amorphous Solid Dispersions: Theory and Practice*, N. Shah, H. Sandhu, D. S. Choi, H. Chokshi, and A. W. Malick, Eds. Springer-Verlag New York, 2014, pp. 395–417.

[32] S. Patel, A. M. Kaushal, and A. K. Bansal, “Compression physics in the formulation development of tablets,” *Crit. Rev. Ther. Drug Carrier Syst.*, vol. 23, no. 1, pp. 1–65, 2006, doi: 10.1615/critrevtherdrugcarriersyst.v23.i1.10.

[33] S. A. Howard, “Solids : Flow Properties,” no. June, 2016, doi: 10.1081/E-EPT3-100200005.

[34] Barjat, H. Checkley, S. Chitu, T., Dawson, N., Farshchi, A., Ferreira, A., Gamble, J., Leane, M., Mitchell, A., Morris, C., Pitt, K., Storey, R., Tahir, F., Tobyn, M., “Demonstration of the Feasibility of Predicting the Flow of Pharmaceutically Relevant Powders from Particle and Bulk Physical Properties,” *J. Pharm. Innov.*, 2020, doi: 10.1007/s12247-020-09433-5.

[35] W. J. Sun, J. Rantanen, and C. C. Sun, “Ribbon density and milling parameters that determine fines fraction in a dry granulation,” *Powder Technol.*, vol. 338, pp. 162–167, 2018, doi: 10.1016/j.powtec.2018.07.009.

[36] S. Shanmugam, “Granulation techniques and technologies: recent progresses,” *Bioimpacts*, vol. 5, no. 1, pp. 55–63, 2015, doi: 10.15171/bi.2015.04.

[37] E. Jannat, A. Al Arif, M. Mehdi Hasan, A. Bin Zarziz, H. Ar Rashid, and C. Md Mehdi Hasan, “Granulation techniques & its updated modules,” *Pharma Innov. J.*, vol. 5, no. 10, pp. 134–141, 2016.

[38] B. M. J. Hall, B. D. Koblinski, H. W. Bernthal, K. V Jacob, and K. B. Ender, “A New Hypromellose Excipient for Direct-Compression , Controlled-Release Applications,” pp. 1–7, 2009.

[39] A. V. Zinchuk, M. P. Mullarney, and B. C. Hancock, “Simulation of roller compaction using a laboratory scale compaction simulator,” *Int. J. Pharm.*, vol. 269, pp. 403–415, 2004, doi: 10.1016/j.ijpharm.2003.09.034.

[40] P. Kleinebudde, “Roll compaction/dry granulation: Pharmaceutical applications,” *Eur. J. Pharm. Biopharm.*, vol. 58, no. 2, pp. 317–326, 2004, doi: 10.1016/j.ejpb.2004.04.014.

[41] J. Clayton, T. Freeman, H. Vom Bey, M. Hanisch, and K. Brockbank, “The influence of roller compaction processing variables on the rheological properties of granules,” *Part. Technol. Forum 2016 - Core Program. Area 2016 AIChE Annu. Meet.*, vol. 11, pp. 115–121, 2016.

[42] Y. Teng, Z. Qiu, and H. Wen, “Systematical approach of formulation and process development using roller compaction,” *Eur. J. Pharm. Biopharm.*, vol. 73, no. 2, pp. 219–229, 2009, doi: 10.1016/j.ejpb.2009.04.008.

[43] S. Peter, R. F. Lammens, and K. J. Steffens, “Roller compaction/Dry granulation: Use of

the thin layer model for predicting densities and forces during roller compaction," *Powder Technol.*, vol. 199, no. 2, pp. 165–175, 2010, doi: 10.1016/j.powtec.2010.01.002.

[44] H. Lim, V. S. Dave, L. Kidder, E. Neil Lewis, R. Fahmy, and S. W. Hoag, "Assessment of the critical factors affecting the porosity of roller compacted ribbons and the feasibility of using NIR chemical imaging to evaluate the porosity distribution," *Int. J. Pharm.*, vol. 410, no. 1–2, pp. 1–8, 2011, doi: 10.1016/j.ijpharm.2011.02.028.

[45] H. L. Keizer and P. Kleinebudde, "Elastic recovery in roll compaction simulation," *Int. J. Pharm.*, vol. 573, no. July 2019, p. 118810, 2020, doi: 10.1016/j.ijpharm.2019.118810.

[46] Leane, M., Pitt, K., Reynolds, G., Anwar, J., Charlton, S., Crean, A., Creekmore, R., Davies, C., DeBeer, T., De-Matas, M., Djemai, A., Douroumis, D., Gaisford, S., Gamble, J., Stone, E., H., Kavanagh, A., Khimyak, Y., Kleinebudde, P., Moreton, C., Paudel, A., Storey, R., Toschkoff, G., Vyas, Kiren, "A proposal for a drug product Manufacturing Classification System (MCS) for oral solid dosage forms," *Pharm. Dev. Technol.*, vol. 20, no. 1, pp. 12–21, 2015, doi: 10.3109/10837450.2014.954728.

[47] Toson, P.,Lopes, D. G.,Paus, R.,lKumar, A.,Geens, J.,Stibale, S.,Quodbach, J.,Kleinebudde, P.,Hsiao, W. K., Khinast, J., "Model-based approach to the design of pharmaceutical roller-compaction processes," *Int. J. Pharm. X*, vol. 1, no. October 2018, p. 100005, 2019, doi: 10.1016/j.ijpx.2019.100005.

[48] V. V. Nesarikar, C. Patel, W. Early, N. Vatsaraj, O. Sprockel, and R. Jerzweski, "Roller compaction process development and scale up using Johanson model calibrated with instrumented roll data," *Int. J. Pharm.*, vol. 436, no. 1–2, pp. 486–507, 2012, doi: 10.1016/j.ijpharm.2012.06.027.

[49] C. F. Gurnham and H. J. Masson, "Expression of Liquids from Fibrous Materials.," *Ind. Eng. Chem.*, vol. 38, no. 12, pp. 1309–1315, Dec. 1946, doi: 10.1021/ie50444a026.

[50] D. Zhou, W. R. Porter, and G. G.Z. Zhang, "Chapter 5 - Drug Stability and Degradation Studies," Y. Qiu, Y. Chen, G. G. Z. Zhang, L. Liu, and W. R. B. T.-D. S. O. D. F. Porter, Eds. San Diego: Academic Press, 2009, pp. 87–124.

[51] W. Jiang and L. X. Yu, "Chapter 38 - Modern Pharmaceutical Quality Regulations: Question-based Review," Y. Qiu, Y. Chen, G. G. Z. Zhang, L. Liu, and W. R. B. T.-D. S. O. D. F. Porter, Eds. San Diego: Academic Press, 2009, pp. 885–901.

[52] S. Mangal, F. Meiser, D. Morton, and I. Larson, "Particle Engineering of Excipients for Direct Compression: Understanding the Role of Material Properties," *Curr. Pharm. Des.*, vol. 21, Oct. 2015, doi: 10.2174/1381612821666151008125117.

[53] S. Schiano, C. Y. Wu, A. Mirtic, and G. Reynolds, "A novel use of friability testing for characterising ribbon milling behaviour," *Eur. J. Pharm. Biopharm.*, vol. 104, pp. 82–88, 2016, doi: 10.1016/j.ejpb.2016.03.034.

[54] K. Csordas, R. Wiedey, and P. Kleinebudde, "Impact of roll compaction design, process parameters, and material deformation behaviour on ribbon relative density," *Drug Dev. Ind. Pharm.*, vol. 44, no. 8, pp. 1295–1306, 2018, doi: 10.1080/03639045.2018.1446444.

[55] J. C. Cunningham, "Experimental studies and modeling of the roller compaction of pharmaceutical powders," 2005.

[56] G. E. Peck, *Pharmaceutical powder compaction technology*, vol. 42, no. 3. 1996.

[57] D. W. Green and R. H. Perry, *Perry's Chemical Engineers' Handbook, Eighth Edition*, 8th ed. /. New York: McGraw-Hill Education.

[58] Mazor, A.,Perez-gandarillas, L.,Ryck, A. D.,Michrafy, A., "Effect of roll compactor sealing system designs : A finite element analysis To cite this version : HAL Id : hal-01609015 Effect of roll compactor sealing system designs : A fi nite element analysis," 2019.

[59] M. Allesø, R. Holm, and P. Holm, “Roller compaction scale-up using roll width as scale factor and laser-based determined ribbon porosity as critical material attribute,” *Eur. J. Pharm. Sci.*, vol. 87, pp. 69–78, 2016, doi: 10.1016/j.ejps.2015.11.001.

[60] H. L. Reimer and P. Kleinebudde, “Hybrid modeling of roll compaction processes with the Styl’One Evolution,” *Powder Technol.*, vol. 341, pp. 66–74, 2019, doi: 10.1016/j.powtec.2018.02.052.

[61] C. C. Sun and P. Kleinebudde, “Mini review: Mechanisms to the loss of tabletability by dry granulation,” *Eur. J. Pharm. Biopharm.*, vol. 106, pp. 9–14, 2016, doi: 10.1016/j.ejpb.2016.04.003.

[62] H. Nyqvist and A. Brodin, “Ring shear cell measurements of granule flowability and the correlation to weight variations at tableting.,” *Acta Pharm. Suec.*, 1982.

[63] C. C. Sun, “Setting the bar for powder flow properties in successful high speed tableting,” *Powder Technol.*, vol. 201, no. 1, pp. 106–108, 2010, doi: 10.1016/j.powtec.2010.03.011.

[64] M. K. Taylor, J. Ginsburg, A. J. Hickey, and F. Gheyas, “Composite method to quantify powder flow as a screening method in early tablet or capsule formulation development,” *AAPS PharmSciTech*, vol. 1, no. 3, 2000, doi: 10.1208/pt010318.

[65] United States Pharmacopeia, “USP Powder Flow,” *Stage 6 Harmon.*, vol. 30(60), no. 6, p. 7, 2016.

[66] R. L. Carr, “Classifying flow properties of solids,” *Chem. Eng.*, 1965, doi: 10.5897/AJFS2015.1279.

[67] T. v. Kármán, “8. Beitrag zur Theorie des Walzvorganges,” *ZAMM - J. Appl. Math. Mech. / Zeitschrift für Angew. Math. und Mech.*, vol. 5, no. 2, pp. 139–141, Jan. 1925, doi: 10.1002/zamm.19250050213.

[68] J. R. Johanson, “A Rolling Theory for Granular Solids,” *J. Appl. Mech.*, vol. 32, no. 4, pp. 842–848, Dec. 1965, doi: 10.1115/1.3627325.

[69] G. Reynolds, R. Ingale, R. Roberts, S. Kothari, and B. Gururajan, “Practical application of roller compaction process modeling,” *Comput. Chem. Eng.*, vol. 34, no. 7, pp. 1049–1057, 2010, doi: 10.1016/j.compchemeng.2010.03.004.

[70] J. M. Katz, R. Roopwani, and I. S. Buckner, “A material-sparing method for assessment of powder deformation characteristics using data collected during a single compression-decompression cycle,” *J. Pharm. Sci.*, vol. 102, no. 10, pp. 3687–3693, 2013, doi: 10.1002/jps.23676.

[71] S. Paul and C. C. Sun, “Gaining insight into tablet capping tendency from compaction simulation,” *Int. J. Pharm.*, vol. 524, no. 1–2, pp. 111–120, 2017, doi: 10.1016/j.ijpharm.2017.03.073.

[72] J. M. Katz and I. S. Buckner, “Full Out-of-Die Compressibility and Compactibility Profiles From Two Tablets,” *J. Pharm. Sci.*, vol. 106, no. 3, pp. 843–849, 2017, doi: 10.1016/j.xphs.2016.11.005.

[73] E. N. Hiestand, J. E. Wells, C. B. Peot, and J. F. Ochs, “Physical processes of tableting,” *J. Pharm. Sci.*, vol. 66, no. 4, pp. 510–519, 1977, doi: 10.1002/jps.2600660413.

[74] C. K. Tye, C. Sun, and G. E. Amidon, “Evaluation of the effects of tableting speed on the relationships between compaction pressure, tablet tensile strength, and tablet solid fraction,” *J. Pharm. Sci.*, 2005, doi: 10.1002/jps.20262.

[75] I. Holand, “Dwelling on it —how does dwell time impact tablet manufacturing?,” 2017.

[76] E. Peeters, A. F. T. Silva, M. Fonteyne, T. De Beer, C. Vervaet, and J. P. Remon, “Influence of extended dwell time during pre- and main compression on the properties of

ibuprofen tablets," *Eur. J. Pharm. Biopharm.*, vol. 128, no. May, pp. 300–315, 2018, doi: 10.1016/j.ejpb.2018.05.007.

[77] R. W. Heckel, "Density-Pressure Relationships in Powder Compaction," *Trans Met Soc AIME*, vol. 22, pp. 671–675, 1961, doi: 10.1007/978-3-642-16416-3_17.

[78] S. Paul and C. C. Sun, "The suitability of common compressibility equations for characterizing plasticity of diverse powders," *Int. J. Pharm.*, vol. 532, no. 1, pp. 124–130, 2017, doi: 10.1016/j.ijpharm.2017.08.096.

[79] Dai, S.,Xu, B.,Zhang, Z.,Yu, J.,Wang, F.,Shi, X.,Qiao, Y., "A compression behavior classification system of pharmaceutical powders for accelerating direct compression tablet formulation design," *Int. J. Pharm.*, vol. 572, no. 11, p. 118742, 2019, doi: 10.1016/j.ijpharm.2019.118742.

[80] D. Hooper, F. C. Clarke, J. C. Mitchell, and M. J. Snowden, "A Modern Approach to the Heckel Equation: The Effect of Compaction Pressure on the Yield Pressure of Ibuprofen and its Sodium Salt," *J. Nanomed. Nanotechnol.*, vol. 7, no. 3, 2016, doi: 10.4172/2157-7439.1000381.

[81] C. Sun and D. J. W. Grant, "Influence of Elastic Deformation of Particles on Heckel Analysis," vol. 6, no. 2, pp. 193–200, 2001.

[82] M. Kuentz and H. Leuenberger, "Pressure susceptibility of polymer tablets as a critical property: A modified heckel equation," *J. Pharm. Sci.*, vol. 88, no. 2, pp. 174–179, 1999, doi: https://doi.org/10.1021/js980369a.

[83] K. Kawakita and Y. Tsutsumi, "BULLETIN OF THE CHEMICAL SOCIETY OF JAPAN A Comparison Compression of Equations for Powder By Kimio KAWAKITA and Yuhbun TSUTSUMI of Chemistry , Faculty of Engineering , Hosei University , Tokyo," vol. 71, no. 1963, pp. 1364–1368, 1966.

[84] G. Frenning, J. Nordström, and G. Alderborn, "Effective Kawakita parameters for binary mixtures," *Powder Technol.*, vol. 189, no. 2, pp. 270–275, 2009, doi: 10.1016/j.powtec.2008.04.016.

[85] A. S. Persson and G. Alderborn, "A hybrid approach to predict the relationship between tablet tensile strength and compaction pressure using analytical powder compression," *Eur. J. Pharm. Biopharm.*, vol. 125, no. October 2017, pp. 28–37, 2018, doi: 10.1016/j.ejpb.2017.12.011.

[86] E. RYSHKEWITCH, "Compression Strength of Porous Sintered Alumina and Zirconia: 9th Communication to Ceramography," *Journal of the American Ceramic Society*, vol. 36, no. 2. pp. 65–68, 1953.

[87] C. Y. Wu, S. M. Best, A. C. Bentham, B. C. Hancock, and W. Bonfield, "Predicting the tensile strength of compacted multi-component mixtures of pharmaceutical powders," *Pharm. Res.*, vol. 23, no. 8, pp. 1898–1905, 2006, doi: 10.1007/s11095-006-9005-6.

[88] C. Sun and D. J. W. Grant, "Influence of crystal structure on the tableting properties of sulfamerazine polymorphs," *Pharm. Res.*, vol. 18, no. 3, pp. 274–280, 2001, doi: 10.1023/A:1011038526805.

[89] B. HANCOCK, J. COLVIN, M. MULLARNEY, and A. ZINCHUK, "The relative densities of pharmaceutical powders, blends, dry granulations, and immediate-release tablets," *Pharm. Technol.*, vol. 27, no. 4, pp. 64–80, 2003.

[90] United States Pharmacopeial Convention, "<786> Particle Size Distribution Estimation by Analytical Sieving," *United States Pharmacop. Natl. Formul. 41*, vol. 30, no. 6, pp. 6970–6975, 2017.

[91] EUROPEAN PHARMACOPOEIA, "2.9.5. Uniformity of Mass of Single-Dose Preparations

Single-Dose Preparations," *European Pharmacopoeia 9.0*. pp. 265–266, 2015.

[92] FDA, "⟨ 1217 ⟩ Tablet Breaking," *Food Drug Adm.*, no. c, pp. 2011–2013, 2012.

[93] United States Pharmacopeia, "⟨ 1216 ⟩ Tablet Friability," *United States Pharmacop.*, vol. 38, pp. 1432–1433, 2015.

[94] J. Al-Gousous and P. Langguth, "Oral Solid Dosage Form Disintegration Testing - The Forgotten Test," *J. Pharm. Sci.*, vol. 104, no. 9, pp. 2664–2675, 2015, doi: 10.1002/jps.24303.

[95] S. Patel, A. M. Kaushal, and A. K. Bansal, "Effect of particle size and compression force on compaction behavior and derived mathematical parameters of compressibility," *Pharm. Res.*, vol. 24, no. 1, pp. 111–124, 2007, doi: 10.1007/s11095-006-9129-8.

[96] X. Tang, A. Zakhvatayeva, L. Zhang, Z. F. Wu, P. Sun, and C. Y. Wu, "Flow behaviour of pharmaceutical powders during rotary die filling with a paddle feeder," *Int. J. Pharm.*, vol. 585, no. June, p. 119547, 2020, doi: 10.1016/j.ijpharm.2020.119547.

Appendix A – True Density results

As expected, since SDDs are generally hollow materials, the true density values were lower for single SDD than when blended with excipients. This was additionally confirmed by comparing the intragranular with the extragranular phase true density in both blends, as it is observed in Table A.1.

Table A.1 - True Density measurement results.

	Product type	True density (g/cm^3)	rSD (%)
HPMCAS	SDD	1.295	0.17%
	SDD + intragranular	1.368	0.01%
	SDD + extragranular low density	1.409	0.02%
	SDD + extragranular high density	1.401	0.03%
PVPVA	SDD	1.216	0.08%
	SDD + intragranular	1.313	0.02%
	SDD + extragranular low density	1.360	0.09%
	SDD + extragranular high density	1.379	0.07%